

 **JUNE** 2017

QUALITY CONTROL IN ADDITIVE MANUFACTURING

CAPACITY ASSESSMENT OF NON-TOUCHING METHODS

JOÃO TOMÁS F. G. AFONSO

MASTERS DISSERTATION PRESENT TO
FACULDADE DE ENGENHARIA DA UNIVERSIDADE DO PORTO IN
ENGENHARIA METALÚRGICA E DE MATERIAIS

SUPERVISOR

ELSA WELLENKAMP DE SEQUEIROS

INSTITUCIONAL SUPERVISOR

ELENA LOPEZ

<i>CANDIDATO</i>		<i>Código</i>
<i>TÍTULO</i>		
<i>DATA</i>	__ de _____ de _____	
<i>LOCAL</i>	Faculdade de Engenharia da Universidade do Porto - Sala _____ - __:__h	
<i>JÚRI</i>	<i>Presidente</i>	DEMM/FEUP
	<i>Arguente</i>	DEM/FEUP
	<i>Orientador</i>	DEMM/FEUP

Abstract

This work was developed within the scope of the dissertation for the conclusion of the Integrated Master's Degree in Metallurgical and Materials Engineering and was elaborated during the curricular internship at Fraunhofer Institute IWS.

Additive manufacturing (AM) promises to revolutionize the way parts are made, by allowing the production of parts layer by layer directly from digital data. This unique ability has tremendous potential, which cannot be matched by conventional manufacturing technologies. This leads to a growth of AM parts for structurally critical components, where the need for qualification and quality control is paramount. In this field, work has been done in the qualification of processes. However, there is still a need for qualification of final parts after production. This dissertation gives a closer look on the application of non-touching methods for nondestructive testing of AM metal parts. 3D scanning and X-ray computed tomography (CT) were used to evaluate parts made through laser powder bed fusion (LPBF), electron beam melting (EBM) and direct energy deposition (DED). It was performed geometrical comparison against the CAD model and porosity analysis. The results show the limitation of AM processes in manufacturing features with dimensions below 0.5 mm and without porosity. It was also highlighted the unique capacity of CT to provide the required inspection for AM parts, while pointing out the limitations and precautions needed when using these methods.

Keywords

Additive Manufacturing (AM); Laser Powder Bed Fusion (LPBF); Electron-Beam Melting (EBM); Quality control; 3D Scan; Computer Tomography (CT); Porosity analysis

Resumo

Este trabalho foi desenvolvido no âmbito da dissertação para a conclusão do curso de Mestrado Integrado em Engenharia Metalúrgica e de Materiais e foi elaborado durante o estágio curricular no Instituto Fraunhofer IWS.

O fabrico aditivo (AM) promete revolucionar o modo como as peças são feitas, permitindo a produção por camadas diretamente a partir de dados digitais. Essa possibilidade única tem enorme potencial que não consegue ser igualada por tecnologias de fabrico convencional. Devido a isto, regista-se um crescimento na aplicação de peças de fabrico aditivo em componentes estruturais, onde a qualificação e controlo de qualidade são primordiais. Nesta área, têm sido feito progressos na qualificação de processos. Contudo, existe a necessidade de qualificação final de peças antes da aplicação. Esta dissertação explora a aplicação de métodos não destrutivos e sem contacto no controlo de peças metálicas de fabrico aditivo. São utilizadas digitalização 3D e tomografia computadorizada (CT) para examinar peças fabricadas por fusão seletiva por laser (LPBF), fusão por feixe de eletrões (EBM) e deposição por energia direta (DED). Foi estabelecida comparação geométrica em relação ao modelo CAD e análise de porosidade. Os resultados demonstram a limitação dos processos de fabrico aditivo em reproduzir detalhes com dimensões inferiores a 0,5 mm e sem porosidade. Também se destacou a capacidade única da tomografia computadorizada em realizar a inspeção necessária a peças produzidas por fabrico aditivo, além de se apontarem as limitações e precauções necessárias ao usar este método de inspeção.

Zusammenfassung

Diese Dissertation entstand zum Abschluss des integrierten Masterabschlusses „Metallurgical and Materials Engineering“ im Rahmen eines Forschungsaufenthalts am Fraunhofer IWS.

Im Zuge des zunehmenden Einflusses von generativen Fertigungsverfahren in der Produktion von strukturellen Bauteilen entsteht die Notwendigkeit der Produktqualifizierung und Qualitätskontrolle.

Aufgrund der einzigartigen Fähigkeiten dieser Fertigungsverfahren müssen neue Methoden und Strategien der Qualitätskontrolle eingesetzt werden, wobei insbesondere auf dem Feld der Prozessqualifizierung Fortschritte gemacht werden. Darüber hinaus bleibt die Notwendigkeit der Qualitätskontrolle der finalen Bauteile bevor diese zum Einsatz kommen.

Diese Arbeit behandelt integritätserhaltende Methoden zur Untersuchung mittels generativer Fertigungsverfahren hergestellter Metallbauteile. Die Arbeit konzentriert sich hierbei auf die 3-dimensionale Bildgebung mit einem speziellen Fokus auf die Computertomographie (CT). Untersucht wurden mit den Verfahren der selektiven Laserschmelze (LPBF), der Elektronenstrahlschmelze (EBM) und der direkten Energiedeposition (DED) hergestellte Bauteile. Diese wurden hinsichtlich ihrer Porosität analysiert und zur Untersuchung der geometrischen Originaltreue mit „computer-aided design“- Modellen (CAD) verglichen.

Die Ergebnisse dieser Studie zeigen die Grenzen generativer Fertigungsverfahren insbesondere im Rahmen der Produktion von kleineren Strukturen unter 0.5 mm Größe und hinsichtlich des Qualitätskriterium Porosität. Außerdem werden Kapazitäten wie auch Grenzen der 3-dimensionalen Bildgebung für die Qualitätskontrolle generativ erzeugter Bauteile beleuchtet. Auf Basis der CT-Untersuchungstechnik wird auf den Einfluss unterschiedlicher Parameter für die Volumen- und Porositätsbestimmung und die Notwendigkeit der Standardisierung von Untersuchungsparametern eingegangen.

Acknowledgements

The author would like to thank the supervisor Elsa Sequeiros for the careful, thoughtful and supportive orientation during the development of this master thesis in which culminated the curricular internship at Fraunhofer Institute IWS.

To Fraunhofer Institute IWS, in particular to the institutional supervisor Elena Lopez for the guidance, opportunities and thrust bestowed during the curricular internship. I would also like to thank Axel Marquardt for the formation on the computer tomography, the support and guidance through the tantrums of that machine. To Christian Grunert for the formation on the 3D scanner and the data provided on the demonstrators. To Dorit Linaschke for the samples, the insightful questions about the processes and contact with Fraunhofer Institute IPK and IWU. To all the colleagues at Fraunhofer Institute IWS for their kind support.

To Fraunhofer Institute IPK for the cooperation with the fabrication of the LPBF Ti6Al4V demonstrators and especially, Angelina Marko and Julius Raute for the fabrication and analysis of the DED Inconel 718 cubes.

To Fraunhofer Institute IWU for the fabrication of the LPBF AISI10Mg demonstrator.

To Maria Barbosa for the contact with Fraunhofer Institute IWS, the guidance and support during the first steps at Fraunhofer Institute IWS.

And last but not least to my family and friends which supported me during the course of my academic studies, in particular during my stay in Dresden. A special thanks to my parents and sister that always advised me during the direst moments.

Index

ABSTRACT I

KEYWORDS I

RESUMO II

ZUSAMMENFASSUNG..... III

ACKNOWLEDGEMENTS..... IV

FIGURE INDEX IV

TABLE INDEX VII

LIST OF ABBREVIATIONS VIII

1. INTRODUCTION 1

2. ADDITIVE MANUFACTURING..... 1

2.1. APPLICATIONS..... 3

3. METAL ADDITIVE MANUFACTURING TECHNIQUES..... 4

3.1. POWDER/WIRE FEED 5

3.2. POWDER BED FUSION (PBF) 7

 3.2.1. LASER POWDER BEAM MELTING (LPBF) AND ELECTRON-BEAM MELTING (EBM) 8

4. METALLIC POWDERS..... 10

5. QUALITY CONTROL IN ADDITIVE MANUFACTURING..... 12

5.1. APPROACHES FOR QUALITY CONTROL OF AM PARTS 12

5.2. X-RAY COMPUTED TOMOGRAPHY (CT) 14

 5.2.1. WORKING MECHANISM AND PARAMETERS..... 15

5.3. 3D SCANNING 20

5.4. DEMONSTRATORS 22

6. EXPERIMENTAL PROCEDURES 24

6.1 COMPUTER TOMOGRAPHY 24

 6.1.1. EQUIPMENT..... 24

 6.1.2. SOFTWARE 27

6.2. 3D SCANNING 32

 6.2.1. EQUIPMENT..... 32

 6.2.2. SOFTWARE 33

6.3. MEASUREMENTS 33

6.3.1. GEOMETRIC ANALYSIS 33

 6.3.1.1 LPBF DEMONSTRATORS..... 34

 6.3.1.2. EBM DEMONSTRATORS..... 34

 6.3.1.3. CT ANALYSIS OF THE DEMONSTRATORS 35

6.3.2. COMPARISON OF CT AGAINST 3D SCANNING 35

6.3.3. POROSITY ANALYSIS..... 36

6.3.4. RECONSTRUCTION SETTINGS ASSESSMENT 38

7. RESULTS AND DISCUSSION 39

7.1 GEOMETRIC ANALYSIS 39

 7.1.1. LPBF DEMONSTRATORS..... 39

 7.1.2. EBM DEMONSTRATORS..... 42

 7.1.3. OVERVIEW OF LPBF AND EBM..... 45

7.2. COMPARISON OF CT AGAINST 3D SCANNING 45

7.3. POROSITY ANALYSIS 49

7.4. RECONSTRUCTION SETTINGS ASSESSMENT 54

8. CONCLUSIONS AND OUTLOOK 58

REFERENCES..... 61

ANNEXES 68

Figure index

Figure 1 - Relationship between build rate, power and definition of AM processes [5].	4
Figure 2- Schematics of a generic AM powder feed system [5].	5
Figure 3 - Schematics of a generic AM powder bed system [5].	7
Figure 4 a) - Process parameter map for single track scans of AlSi10Mg [39]. b) - Five tests tracks made in M2 steel in argon atmosphere with CO2 laser and 1,1 mm spot size [7].	7
Figure 5 - Optical absorption of metals versus wavelength (micrometers) [7].	8
Figure 6 - AM quality pyramid, adapted [50].	12
Figure 7 - Results of feedback control on LPBF of a closed overhand with 5mm leght or diamter. Left - no feedback control, Right - With feedback control [50].	14
Figure 8 -a) Projection reconstruction principle [77]. b) Flat panel CT working principle [78].	16
Figure 9 - Typical reflection X-ray tube [78].	16
Figure 10 - Image magnification and blurring by moving the object towards the source having a finite X-ray spot. FOD- Focus object distance; FDD - Focus detector distance [78].	17
Figure 11 - CT artifacts examples. a) Effect of beam hardening without and with a physical filtering of the X-ray [78]. b) Ring artifact.	19
Figure 12 - Example of image noise [87].	19
Figure 13 - Influence factors CT [81].	20
Figure 14 - Working mechanism of structured light 3D scanner devices [97].	21
Figure 15 - Positioning system using markers [99].	22
Figure 16 - Proposed demonstrator by the National Institute of Standards and Technology (NIST) [105].	23
Figure 17 - Fraunhofer IWS demonstrator developed to evaluate different challenging geometrical features.	23
Figure 18 - Horizontal cut of the demonstrator highlighting the internal channels.	23
Figure 19 - Steps performed on the CT inspection with focus on the machine and software used and parameters needed to define in each stage.	24
Figure 20 - Used Computer tomppgraph YXLON FF35 CT.	25

Figure 21 - Placement of the demonstrator inside the CT..... 25

Figure 22 - YXLON FF35 CT live menu. 26

Figure 23 - 2D and 3D views of a part in VGStudio Max 3.0. a) Incorrectly registered; b) Correctly registered with the back plane of the sample through *Simple 3-2-1 Registration*. 28

Figure 24 - Histogram. a) VGStudio MAX 3.0 histogram; b) Histogram illustration and correspondence. 29

Figure 25 - Surface determination process through gray value means [108]..... 29

Figure 26 - Detail of the advance surface determination on an object corner with different gray values due to an edge artifact. 29

Figure 27 - Pore detection process, from seed to neighborhood analysis[109]..... 31

Figure 28 - Steps followed for 3D scanning. 32

Figure 29- Scan of a part with GOM ATOS 135. Scanned area and live cam on the computer screen. 33

Figure 30 - EBM Ti6Al4V demonstrators made on Arcam A2X with different square base sizes: a) 6x6 mm square size; b) 5x5 mm square size; c) 4x4 mm square size; d) 3x3 mm square size..... 34

Figure 31 - a) Nozzle made by EBM with Ti6Al4V b) Scanning of the nozzle using the GOM ATOS 135 and an inclinable turning table..... 36

Figure 32 - Inconel 718 cubes made by DED process on TruLaser Cell 7020. 37

Figure 33 - Digitized Ti6Al4V LPBF demonstrator. 39

Figure 34 - Demonstrator comparison at ± 0.5 mm tolerance with CAD file. a) Ti6Al4V LPBF demonstrator; b) Inconel 718 LPBF demonstrator; c) AlSi10Mg LPBF demonstrator. 40

Figure 35 - Internal channels deviation at ± 0.5 mm. a) Ti6Al4V LPBF demonstrator; b) Inconel 718 LPBF demonstrator; c) AlSi10Mg LPBF demonstrator. 41

Figure 36 - Deviation values at different tolerances of the LPBF demonstrators. 42

Figure 37 - EBM demonstrator with 3x3 mm base square size. 42

Figure 38 - Comparison of the EBM demonstrators against the CAD file at ± 0.5 mm tolerance. A) 6x6 mm; b) 5x5 mm; c) 4x4 mm; d) 3x3 mm square size. 43

Figure 39 - Comparison against the CAD at ± 0.5 mm tolerance with a perpendicular cut of the EBM demonstrators. a) 6x6 mm; b) 5x5 mm; c) 4x4 mm; d) 3x3 mm square size. 44

Figure 40 - Deviation of the EBM demonstrators at different tolerances..... 44

Figure 41 - Comparison of deviation of the EBM demonstrator 3x3 mm and the LPBF demonstrators at different tolerances. 45

Figure 42 - EBM nozzle scanned by CT and 3D scanner. a) CT reconstruction front view; b) 3D scanner, front view; c) CT half cut; d) 3D scanner half cut. 46

Figure 43 - Nominal/actual comparison of the nozzle at ± 0.5 mm tolerance. a) Comparison against the CT object; b) Comparison against the 3D scanned object..... 46

Figure 44 - Comparison of the CT and 3D scanning against the same CAD file at different tolerances..... 47

Figure 45 - 3D scanned nozzle. a) Detail of the marker used on the nozzle; b) Comparison of the 3D scanned nozzle with the CAD file at ± 0.1 mm tolerance..... 47

Figure 46 - a) 3D scan of the LPBF demonstrator made of inconel 718; b) Detail of the compact volumes. 48

Figure 47 - Horizontal cut of the Ti6Al4V LPBF demonstrator and comparison with CAD. .. 49

Figure 48 - Porosity analysis of cube n°2 with interpolation factor 1 and probability filter 1. a) 3D front view with 70% transparency; b) 3D side view with 70% transparency; c) 2D front view; d) 2D front view without analysis. 50

Figure 49 - Porosity analysis of cube n°14. a) Interpolation factor 1, probability 1; b) Interpolation factor 1.4, probability 0.3. 50

Figure 50 - Front view of a pore on cube n°3. a) Analysis of the pore with different parameters. Green - interpolation factor 1.4 and probability 0.3; blue- interpolation factor 1, probability 1; b) Pore without analysis..... 51

Figure 51 - Side view of a pore on cube n°3 with different parameters. a) Interpolation factor 1, probability 1; b) Interpolation factor 1.4, probability 0.3. 51

Figure 52 - Relative density obtained by CT with different analysis parameters and Archimedes. 53

Figure 53 - Total volume for each Inconel cube done by CT and through Archimedes method. 53

Figure 54 - Total volume of cube n°3 measured through CT with different deactivated reconstruction parameters and Archimedes method. 55

Figure 55 - Total porosity volume detected through CT with different reconstruction parameters and Archimedes method. 56

Figure 56 - Front view 2D projection of cube n°3 with all filters disable. 57

Figure 57 - Front view 2D projection of cube n°3 with reconstruction volume size set to ISO voxel - 2166 hps..... 57

Table index

Table 1 - Various sensing equipment used in AM ,adapted [50].	13
Table 2 - Geometric features and their intended purpose [101].	22
Table 3 - Performed experiments.	24
Table 4 - Different specification of the GOM ATOS CORE 45 and GOM ATOS CORE 135 [96].	32
Table 5 - LPBF demonstrators used for the geometrical analysis.....	34
Table 8 - Deviation of the measured features through 3D scan on the LPBF demonstrator made of Inconel 718.....	48
Table 9 - Average of different characteristics detected through different parameters. ...	52

List of Abbreviations

.amf	Additive Manufacturing Format
.stl	Stereolithography File Format
AM	Additive Manufacturing
CAD	Computer-Aided Design
CAGR	Compound Annual Growth Rate
CAM	Computer Aided-Manufacturing
CNC	Computer Numerical Control
CT	X-ray Computed Tomography
DED	Direct Energy Deposition
EBM	Electron Beam Melting
FDD	Focus Detector Distance
FDM	Fused Deposition Modeling
FOD	Focus Object Distance
HIP	Hot Isotactic Pressing
hpc	Horizontal Pixel Count
LOM	Laminated Object Manufacturing
LPBF	Laser Powder Bed Fusion
NDT	Non-Destructive Techniques
PBF	Powder Bed Fusion
ROI	Region of Interest
RP	Rapid Prototyping
SL	Stereolithography
SLM	Selective Laser Melting
SLS	Selective Laser Sintering

1. Introduction

The materials and methods used in the production of products have always been a key point in the history of humankind, defining major turning points in its evolution. Additive manufacturing (AM) technologies have been coined as “the third industrial revolution” by the *Economist* magazine [1], in which states that it will revolutionize the production of goods, changing the actual general paradigm of large centralized production to reduce cost and with little customization, to a more customized, made by demand, and with a simplified supply chain [2]. These technologies have unlocked new methods of creating new products, allowing a wide range of geometric shapes that were impossible or extremely costly through more conventional manufacturing methods (casting, machining, forging, among others), along with a high efficiency usage of raw material and energy, making it also a more environmentally friendly process due to the efficient use of material [2, 3].

Despite the optimism surrounding AM technology, and its rapid evolution since it emerged thirty years ago, it has still challenges to overcome. One of the major barriers to its widespread application, is the qualification of parts for final application, where it must be ensured the repeatability, dimensional precision, surface finish, mechanical properties, among others [4-6]. This leads to the use of quality control systems to quantify, control, identify and plan new strategies to deal with these issues. Ensuring quality in final applications, turning AM into a reliable and mainstream manufacturing process [4-7].

2. Additive Manufacturing

AM technology emerged in the late eighties through the stereolithography process from *3D Systems* that solidifies layers of liquid polymer sensitive to ultraviolet lights. This also gave birth to the .stl file format that is still used today in Computer Aided-Manufacturing (CAM) [8, 9]. Formerly, AM was known as rapid prototyping (RP) and used to quickly create prototypes directly from digital data. This allowed the reduction of time during design, concept testing, client approval and feedback during development [7, 8, 10]. However, with further progress in the technology, the parts that were produced were closer to an end product than a prototype, making the designation of RP unfitting, requiring a new and more suitable designation of additive

manufacturing. With this transition, AM changed its main field of application to areas with special interest like the aerospace, automotive and biomedical industries [6, 7, 10, 11].

Nowadays, AM has diverged in many different manufacturing approaches like powder and wire feed, powder bed, laminates etc.; and diverse processes, like fused deposition modeling (FDM), selective laser sintering (SLS), electron beam melting (EBM), etc. This has led AM to move on from its original polymeric materials and widen the material possibilities. The broader offer of materials available now ranges from polymers, ceramics, composites and various alloys of metals, even reaching food and biologic materials like tissue and cells [2, 7, 11-15].

With all this variety came the necessity of an official definition and standardization by ISO and ASTM, which defines AM as “A process of joining materials to make objects from 3D model data, usually layer upon layer, as opposed to subtractive manufacturing methodologies” [5, 16]. In AM, the production of a part is made through a 3D Computer-Aided Design (CAD) model, where the 3D model is sliced and each layer is a cross-section of the 3D part, then the AM machine creates the part layer by layer until the final part is achieved. This allows a direct fabrication of complex forms, transforming a 3D problem in 2D layers, making the design not being constrained by the manufacturing process, dismissing the use of additional tools and fixtures like in subtractive manufacturing [7, 10, 17].

AM machines work under a layer-based approach, where the thinner each layer is, closer it will be to the original 3D model. AM machines differ predominantly on the way that the layers are created, bonded and materials that can be used, affecting aspects like mechanical properties, accuracy, velocity, among others [7].

Generally, AM process can be divided in three basic core procedures, pre-processing, processing and post-processing [7, 12, 18, 19]. Pre-processing are activities related to design and conceptualization in the 3D CAD software. Parts can also be scanned from existing physical parts, being later corrected in the CAD software [7, 12]. Once the 3D model is created, it is then transformed in .stl/.amf, which is a triangulated representation of the model, being the .amf format the international standard by ASTM/ISO, contemplated in the ISO/ASTM 52915:2016 standard [7, 9, 12, 20, 21]. Then it's loaded into the machine software, here is defined the position, orientation

and number of the same part to be made, with the possibility for scaling to account for shrinkage, coatings or machining. The second step is processing, where are defined the machine setup with features like layer thickness, passage velocity, deposition rate, atmosphere, etc. And then the part is built, which is mainly an automated process. Finally comes post-processing, that involves collecting of surplus material, removal of supports, surface finish like sanding, polishing, sand blasting, painting, etc. or even machining to final dimensions. Parts might also require further treatments to achieve the desired mechanical properties, like heat treatment, hot isostatic pressing (HIP) or impregnation by another material [5, 7].

2.1. Applications

The applications of AM are very broad, ranging from simple hobbyist type FDM printer to make simple models to industrial applications. One of the first examples of tool making was in the foundry to make wax patterns and later, for sand moulds [7, 17]. Besides final parts AM is also used to make tools for: assemble, inspect and ship parts. These are used for example as: forming tools, quality control jigs, fixtures for components in assembly lines, alignment guides, supports for packing, etc. [6, 7, 10, 11, 22]. The production of AM parts is required when the requirements are:

- High product complexity - impossible or very complicated to make in other way (like milling or moulding) due to geometrical constrains [7, 23];
- Simplifying components - that require the joining of several parts in one simpler, more efficient, better performing and lighter part [6, 7, 24];
- Small scale production - replacing parts (for example due to the bankruptcy of the company that produced it), for maintenance of machines or repair of moulds [6, 7, 11, 23];
- High demand for product customization - like in the biomedical field for prosthetics, due to the need to be adjusted to each patient [7, 11, 23];
- Material processing - making parts of materials that are expensive and/or costly to process like Inconel or titanium alloys [5-7, 25].

Due to AM's amazing potentialities, it has been growing as an industry itself, with the *Wohlers Report of 2016* reporting an impressive compound annual growth rate (CAGR) of 31.5%, representing a total of 5.165 billion dollars in all AM products and

services worldwide [26-28]. Its expectations of growth and predicted impact in industry drew several research institutes and governments' attention, spanning many strategic investments plans and funded projects for research and development. Like European Union plan Horizon 2020 where AM falls within the Key Enabling Technologies category [29, 30], United Kingdom innovation plan [31] or United States of America [27, 32].

3. Metal Additive Manufacturing Techniques

AM applied to metals is an area that has received a lot of attention recently, mainly because of its capacity to create complex parts with an excellent buy-to-fly ratio (relation between weight of material used to make the component and the weight of the component made). AM enables the processing of metals that are difficult to process by other more conventional means [5, 7, 33].

Metal AM techniques produce metallic parts using indirect or direct methods. Indirect methods uses polymer based binders and coated powders that require further processing like impregnation with metals or sintering of the part [6, 7, 11]. The direct methods produce parts through melting or sintering of metal powders. This work will focus in techniques that produce usable metal parts directly from the machine through full melting. These techniques have their own advantages/disadvantages and typical defects, but there is a link between build rate, power and quality/resolution. Also, it can be expected a decrease of feature quality/resolution as the build rate increases (Figure 1). This is an important aspect to retain because it will manage the expectations of what can be anticipated by the techniques addressed next [5, 7, 12].

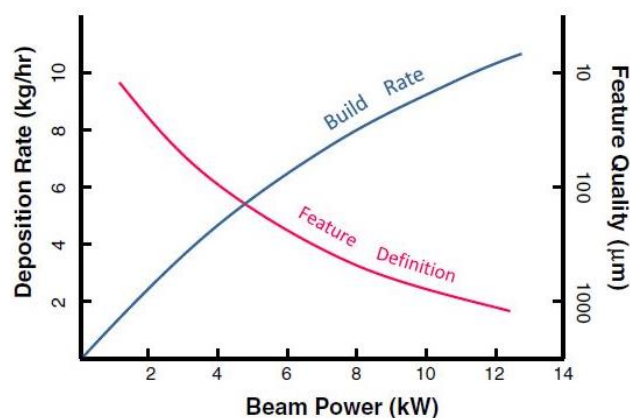


Figure 1 - Relationship between build rate, power and definition of AM processes [5].

3.1. Powder/Wire feed

Feed systems are typically designed as direct energy deposition (DED). This process uses a moving deposition head with a focused heat source to melt feedstock material under a protective atmosphere (Figure 2). Each pass creates a track of solidified metal to make up the layers and build up three-dimensional objects. Deposition is made by moving the deposition head, substrate or a combination of both [5, 11].

In DED with powders the typical deposition rates are between 25-40 g/h, using a laser or electron beam as heat source. The melting forms a small molten pool (0.25-1 mm diameter and 0.1- 0.5 mm depth) where the powder is transported by the protective atmosphere gas (typically argon). Each layer has a typical thickness of 0.25-0.5 mm and is generated by consecutive overlapping tracks, with overlap usually being 25% of the track width. This results in a re-melting of previously deposited material and welding to the layer below, making dimensional control in the building direction (Z axis) challenging. This can be attenuated by employing a close loop feedback system to correct thickness variations during building [7, 34].

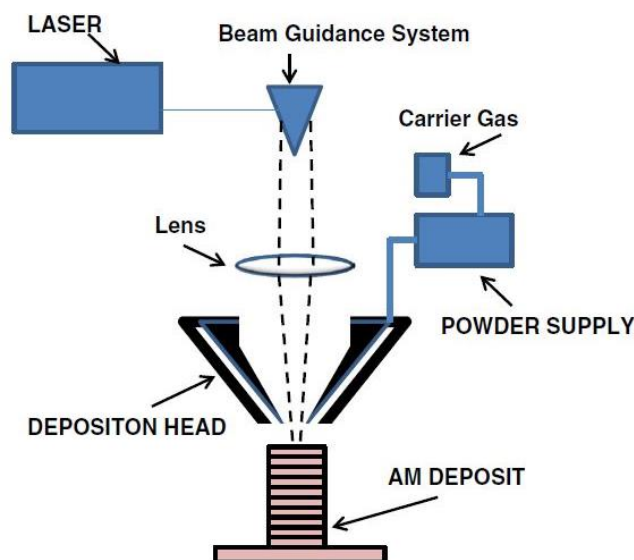


Figure 2- Schematics of a generic AM powder feed system [5].

The kinetic energy of powder particles being fed from the nozzle into the melt pool is greater than the effect of gravity on powders during flight, which allows non-vertical deposition to be just as effective as vertical deposition. However, there is a delicate balance between pressure to protect the melt from oxidization and powder delivery without causing excessive disturbance to the melt pool. Whatever the case,

not all powder is captured by the melt pool, which requires precautions for the recovery of the unused powders in a clean state for recycling [7, 35].

Coaxially supplied powder feedstock allows the ability of tailoring compositions and microstructure during deposition, due to the very high cooling rates (10^3 - 10^5 °C/s) and by adding different composition powders into the molten pool in specific locations of the part. This capacity creates parts with technologically unique properties, like negative Poisson ratio (physically unusual) or ductile metals with negative thermal expansion (unavailable in nature) [7, 35].

In wire feed DED the process is similar, with wire being feed instead of powder. Using wire allows almost 100% feedstock capture efficiency (minus the splatter from the melt pool) and higher deposition rates of 0.7 kg/h. This makes wire feed more adequate for simple geometries, larger size components, with less contamination, lower porosity and lower material costs. Wire is readily available and cheaper than metal powders thus making it very cost-competitive [7, 36, 37].

DED is mainly used for build geometrically complex large parts, repair of worn or damaged components and add value to simple parts where small features protrude, which, through traditional milling, would require a lot of machining from the block, originating a significant volume of waste material. Most AM machines come with pre-programmed parameters for the materials sold by machine manufactures. However, DED is highly dependent of the material, application and geometry, leading them to be sold frequently as flexible platforms, which imposes users to discover the correct parameters for their specific situation. This process of experience gaining can be costly and time consuming [7, 34, 35].

The main limitations of DED processes are the poor resolution and surface finish, being the lowest comparatively with other AM processes, with accuracy's better than 0.25 mm in the Z axis and a roughness of less than 25 μ m difficult to obtain. For those reasons DED is commonly found associated with Computer Numerical Control (CNC) milling machines in order to mill the part to final dimensions. Another drawback is the difficulty to make overhanging structures like internal channels. This is due to the lack of support during the build, which might require support structures, that need to be removed after build, adding cost to production and affecting the final part quality [7, 38].

3.2. Powder bed fusion (PBF)

Powder bed fusion processes are carried in a chamber under controlled atmosphere where the power source scans the powder bed according to the CAD model and melts layer after layer (Figure 3). In each layer the powder bed moves down and a roller/rake adds a new layer of powder. The thermal energy of subsequent scans is sufficient to re-melt a portion of the previous layer and bond the layers to each other, forming layers with thicknesses ranging from 0.02 to 0.15 mm [5, 7, 35, 39]. In these processes the accuracy is typically higher in the X and Y axis than in the Z, because this last is governed by less controllable variables like powder deposition layer and melting thickness between layers [7, 39].

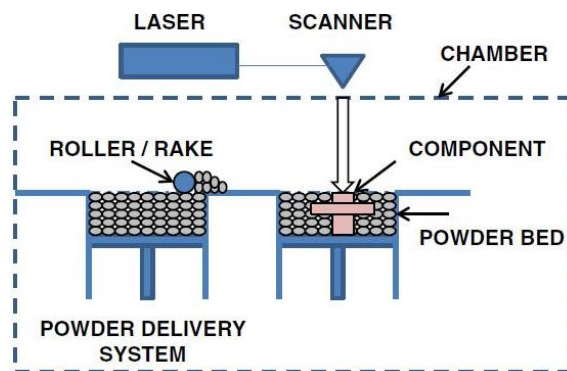


Figure 3 - Schematics of a generic AM powder bed system [5].

One typical phenomenon's that occurs in this kind of system is balling. This effect happens because of poor selection of scanning speed and power input of the power source, making the surface tension forces overcome the gravitational and adhesion forces (Figure 4- a). It can be highly detrimental for part quality, leading to porous parts, weak bonding between layers, inefficient spreading of powder and delamination. A way to avoid the problem is to select correctly the parameters by making a process parameter (Figure 4- b) [7, 35, 39, 40].

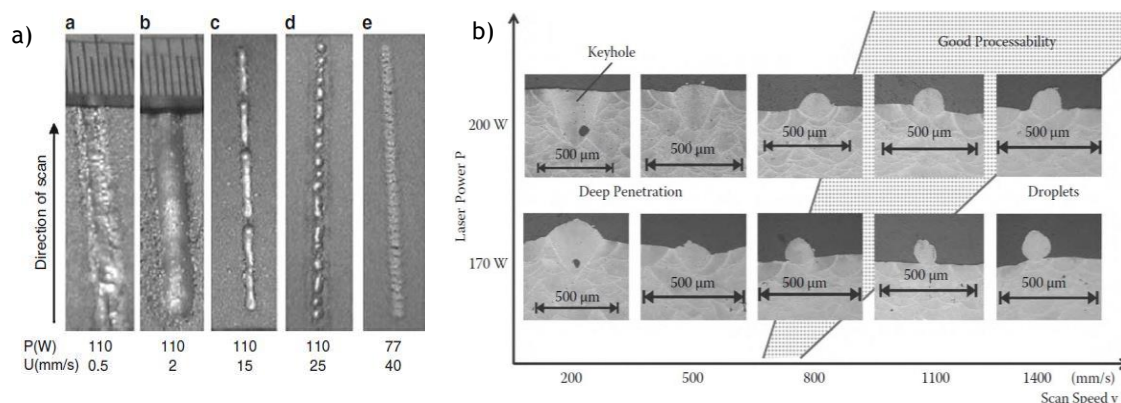


Figure 4 a) - Process parameter map for single track scans of AlSi10Mg [39]. b) - Five tests tracks made in M2 steel in argon atmosphere with CO₂ laser and 1.1 mm spot size [7].

3.2.1. Laser Powder Beam Fusion (LPBF) and Electron-Beam Melting (EBM)

LPBF and EBM are the two main techniques used in powder bed fusion method, where the main differences between them is the power source and atmosphere used.

LPBF is also commonly known by selective laser melting, although this is a name of a machine manufacturer. In LPBF the power source is a laser which is guided and controlled by galvanometers. There are different types of lasers used, CO₂, Nd:YAG and fiber lasers. Each one has different ranges of energies, laser modes (continuous wave, pulsed) and wavelengths that have different absorptivity by materials used (Figure 5). For atmosphere, LPBF uses inert gas like argon or nitrogen to avoid metal oxidation during processing [7, 12, 35, 41].

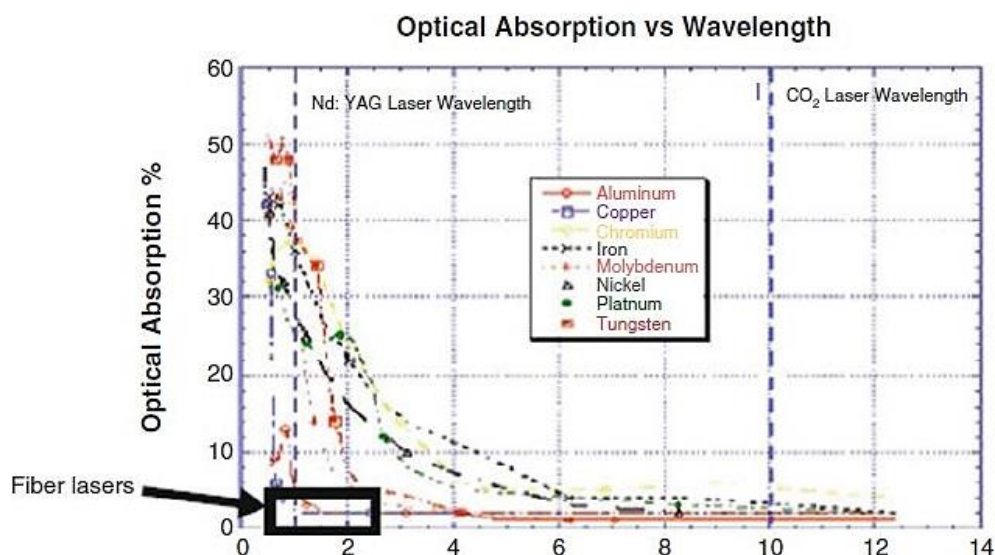


Figure 5 - Optical absorption of metals versus wavelength (micrometers) [7].

LPBF is used for production of small parts that are limited to the build volume of the machine, with the largest build volume of 630 x 400 x 500 mm [42]. The minimum feature size reported is 0.04-0.2 mm and an accuracy of 0.05-0.2 mm. It suffers from some typical imperfections, like melt pool instabilities, that lead to low quality of down facing surfaces and upper surfaces roughness, risk of internal pores, possibility of delamination and high residual stresses. It might also require the build of anchoring supports to avoid warpage, but add the risk of distortion of small features when removing them. However, LPBF has the advantages: of producing full dense parts (even over 99.9%) in a direct way without the need of post-processing, like sintering or HIPing; has one of better surface finish in AM metal processing

techniques; can reproduce fine details and make small parts; suited to process a large array of metals and can be used for polymers [7, 25, 40, 43].

In other hand, EBM power source is a high-energy electron beam powered by high voltage, typically 30 to 60 kV, under vacuum atmosphere ($<10^{-1}$ Pa) [12, 41, 44]. The beam is guided by electromagnetic lenses and heating is made through the absorption of kinetic energy from incoming electrons [7, 41].

This leads to absorption of electrons by the powder and an increase in negative charges which may cause two negative effects. First, if the repulsive force on the negatively charged particles overcomes the gravitational and frictional forces holding them in place, a rapid ejection of powder particles from the powder bed will occur, originating a powder cloud that will block the beam. Secondly, the increasingly negative charges in the powder bed particles will repel the incoming negative charged electrons, creating a more diffuse beam [7].

This phenomenon's dictate that the powders must be highly conductive and scan strategies must avoid the build-up of regions with negative charged particles. The repelling effect leads to a larger diameter beam, thus resulting in a bigger melt pool size and larger heat-affected zone. This leads to a larger minimum feature size, larger powder particles, thicker layers, lower resolution and surface finish when compared with LPBF [7, 41].

However, the use of electron beam has also advantages, for example:

- Is more energetically efficient and cheaper than lasers with comparable energies;
- Is particularly suited for processing highly reflective metals such as aluminum;
- Since the process is held under vacuum, it allows some removal of gases that normally occur in metal castings, being well suited for metals with a high affinity to oxygen, such as titanium;
- The scanning speed is also much higher than LPBF, which is limited by the inertia of the galvanometers, since EBM uses electromagnetic lenses that can almost instantaneously change beam direction, being highly beneficial when building nonsolid parts with designed porosity;

- The temperature in EBM is also more uniform throughout the build. This is achieved by defocusing the electron beam and scanning rapidly over the substrate, which allows a rapid and uniform preheating. This uniformity originates less residual stress and warpage [7, 45, 46].

4. Metallic powders

Today there are many metals suitable for AM, with several being proprietary of the brands that produce the machines. However, there are characteristics like powder size, shape, size distribution and composition, that are known to determine various aspects of the final part [7, 47].

Powder size for most commercially available metals is typically 10-50 μm , with a spherical shape which is the result of the gas atomization. This shape allows for higher apparent density that is around 50-60% for most metals. This shape also improves surface finishing and powder flowability. Finer powders will result in higher apparent density and produce parts with higher final density, better mechanical properties, higher accuracy, thinner layers and better surface finish, since they have a higher surface area, absorbing energy more efficiently than coarser particles. However, decreasing particle size may create some problems because surface energy increases, making the powder more reactive and for certain materials the presence of oxygen can make them burn or explode. They also have more tendency to become airborne settling in surrounding surfaces, leading to clouded optics and reduced sensor sensitivity. Another problem is that interparticle friction and electrostatic forces increase, resulting in a loss of flowability thus affecting powder delivery [7, 35, 39, 40, 44, 47]

Pre-alloyed powders are the most common composition of metallic AM powders, with various metals available, being the most used and researched metals titanium, nickel, iron and aluminum based alloys [5-7, 35, 44].

The titanium based alloys are mainly used in aeronautical and medical fields because of their chemical, mechanical and biocompatibility. Within these, the most studied alloy is Ti6Al4V because of the strong business case that can be developed around the low volume production of complex titanium parts [5, 35, 44].

Nickel based alloys are used due to the tensile properties, corrosion and oxidation resistance at high temperatures. Being normally developed for high performance components in jet engines and gas turbines. These alloys have high susceptibility to cracking during processing, with difficult elimination by just adjusting process parameters. Post-processing like HIP is required to regain and improve mechanical properties, with nearly fully dense parts being produced [35].

Iron based alloys are common in AM processes, being stainless, tool and high speed steels the most common alloys, although they have limited densification because iron and chromium have high reactivity to oxygen, which leads to the formation of oxides. Also the high carbon content tends to segregate to the melt surface, reducing wettability and causing the melt to spheroidize rather than flow. This high carbon content also tends to form complex interfacial carbides at grain boundaries which increases brittleness [35].

Aluminum based alloys are one of the most difficult to process, mainly because of high susceptibility of aluminum to oxidation. Although the upper oxide film evaporates, the oxide at the sides of the pool remain intact, reducing wettability and creating regions of weakness and porosity. Adding to this problem there is also the high reflectivity, high thermal conductivity, and poor flowability of the light aluminum powders [35].

Metal powders are expensive (>50 €/kg), making recycling of the unused powder an important factor for the cost efficiency of AM. Powders should be handled correctly, preferably under protective atmosphere. This way, they don't suffer from significant changes from build to build in, particle shape and size distribution, packing density and chemical composition. If so they can be reused, with new additions of virgin powder to compensate for the used powder between builds and screening of the powders through a 60 µm sieve to remove sintered particles [7, 46, 48, 49].

5. Quality Control in Additive Manufacturing

Qualification and certification of parts made by AM processes has been identified by various authors [5, 7, 27, 50, 51] as one of main challenges for the widespread adoption of AM in structurally critical components. Traditionally the qualification of parts is made by extensive non-destructive and destructive test in hundreds of copies of the final product. This kind of statistical evaluation is a slow and expensive process in any type of production, but in AM processes it also negates many of the identified advantages, namely, low-volume or one-off printings. With this problem, the qualification of AM parts demands a different approach from traditional methods [5, 50, 52].

5.1. Approaches for quality control of AM parts

Due to the unique capabilities of AM, two ways of qualification of AM parts arise. One of them through the control of the parameters, where these were thoroughly studied and standardized and the part is “certified-as-you-build”. The other through the control of the final proprieties by non-destructive methods [51, 53, 54].

Methods for qualification of AM parts through the build must accurately predict if the parts will meet the specifications and ensure repeatability, consistency and reliability across different AM machines. In order to achieve this, the pyramid plan on Figure 6 outlines the strategy to ensure quality on final parts [50].

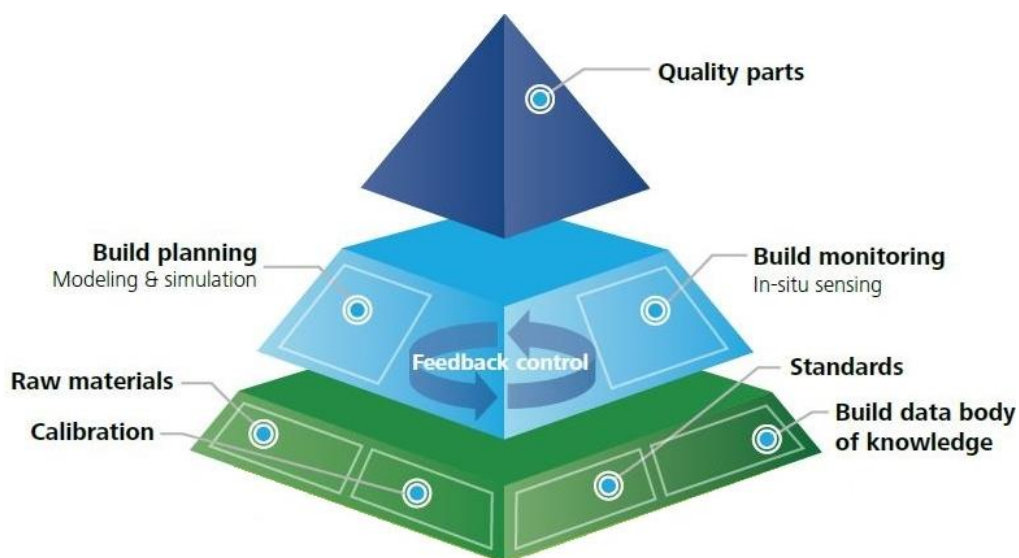


Figure 6 - AM quality pyramid, adapted from [50].

On top of the pyramid is *Quality parts*, where is defined in the beginning of the project the level of quality needed for the application [50, 55]. On second level there is *Build planning* and *Build monitoring*, which are linked by *feedback control* and in which most research work is being made [4, 7, 35, 56-61]. *Build planning* is focused on the pre-build stage and consists in advanced computational models that simulate the build. They take physical phenomena that occur during the build and associate them with the build parameters to predict the final properties of the part. This allows the development of building plans that adjust input parameters to avoid defects and improve proprieties. However, the physics involved in metal AM are quite complex, which creates a challenge in the creation of models that simulate multiple factors at the same time. This method of certification of parts is still requires more investigation because of the limited knowledge about some physical processes that occur during the build; the physical phenomena aren't properly mathematically described; and such complex simulations require high-performance computing facilities that can withstand such heavy computational loads [50, 51, 60].

Build monitoring is focused in control of the parameters during build, to predict final properties and microstructure based on real-time inspection, thermal history or melt pool monitoring [50, 62]. This can be achieved employing the equipment summarized on Table 1.

Table 1 - Various sensing equipment used in AM ,adapted from [50].

Sensing equipment	Objective
Accelerometers	Measure vibration of the print head during powder feed deposition and detect potential anomalies [63].
Ultrasound sensors	Ensure the final part is free of internal voids that create stress concentrations which lead to premature part failure [64].
High-resolution photography	Allows for near real-time inspection of parts in the build chamber [65].
Thermal imaging	Monitors size, shape, and relative temperature distribution of the melt pool [58].
Pyrometry (photodiode)	Measures light intensity at a single point and correlates to temperature [58].

The methods, though quite precise in prediction, originate large volumes of data. For example, video data that includes enough detail of the melt pool and a frame rate sufficiently fast to keep up with the motion of the laser can result in a file with size around 1500 TB for a six-hour build. The reduction of the area filmed can be achieved through a series of mirrors to provide the tracking view of the laser beam

to the melt pool, but even this solution results in a file of 12.7 TB for a six-hour build [50].

The effective application of such data is made through *feedback control*, where the data is used in real time and in closed-loop to correct and take action against detected anomalies. This capability to correct deviation from the *build planning* ensures consistent geometries, surface finishes and material properties. The machines that use this system show superior results, as shown in Figure 7.

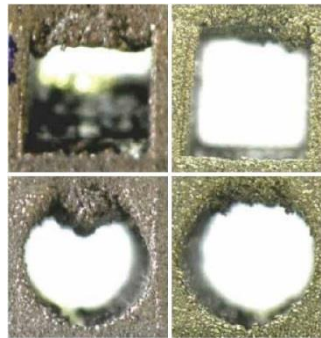


Figure 7 - Results of feedback control on LPBF of a closed overhand with 5mm length or diameter. Left - no feedback control, Right - With feedback control [50].

At pyramid base are general quality control procedures that are applied to any manufacturing process, where the raw material (powder) should be carefully controlled, periodic calibrations performed, standards followed, with the creation of a body of knowledge around the experience in the process [50]. International standards are essential to ensure uniformity and consistency across multiple machines and manufactures. However, these are quite recent and started being published in the year of 2013, with new appearing every year, in an effort of ASTM and ISO organizations to keep up with the fast pace of development of AM technologies [5, 50, 51, 66, 67].

This concept of a born certified is very promising for the qualification of AM parts; it is still in its infancy. This requires the control of final parts through non-destructive techniques (NDT) to be employed as complement, substitution or for correlation with build parameters. Although many of these provide vital information about part health, they are also limited on the general analysis of the part [54].

5.2. X-ray Computed Tomography (CT)

One of the most promising techniques in the quality control of AM parts is X-ray CT. This method allows scanning of all surfaces of an object, even if they are inside a

part (e.g., cooling channels), it enables volume and wall thickness measuring as well porosity (intended or accidental) and cracks analysis. The result of the CT is a fully digitalized combination of various qualitative and quantitative measurements from a single non-destructive experiment. This capacities of the CT systems are excellent tools to analyze and qualify parts made by AM, since the data obtained can be used for a direct comparison with the CAD file that served as building base. Those findings can also be used to understand the complex relations between design (size and shape) and building parameters (power source, orientation, build speed, etc.), and be employed on the building of algorithms for process modeling and simulation, to further improve build planning methodologies [7, 52, 68-70].

Despite all the possibilities and the large volume of research done [54, 68-73], there are still issues that need to be addressed. These focus mainly on quantification of error and accuracy, since in CT analysis there are many parameters that can be changed. The existing standards focus on dimensional measurements, like the popular VDI/VDE 2630. However, even in this standard is advised that measurement error can be smaller when measuring test specimens than in measuring real workpieces. This challenge is greater in porosity analysis since many factors affect the measurements, making the creation standards even more difficult [74, 75].

5.2.1. Working mechanism and parameters

There are many types of CT scans, with different X-ray sources, configurations and strategies, like the ones used in medicine. However, in this work it will be focused on industrial CT scan for materials inspection. CT scans use electrically generated high intensity X-rays to inspect parts. These X-rays pass through the object which suffer from attenuation due to absorption or scattering, which become associated with different gray values. Then are detected by the detector that register the image projection. The part is rotated 360° in front of the X-ray source and hundreds of projections are taken from different angles (Figure 8 - a), being the output thousands of cross-sectional images. These images are stacked together, and through mathematical algorithms are created 3D voxels (3D analog of the pixel with the associated gray value) which form the 3D reconstruction of the object, outlined on Figure 8 - b [7, 48, 75, 76].

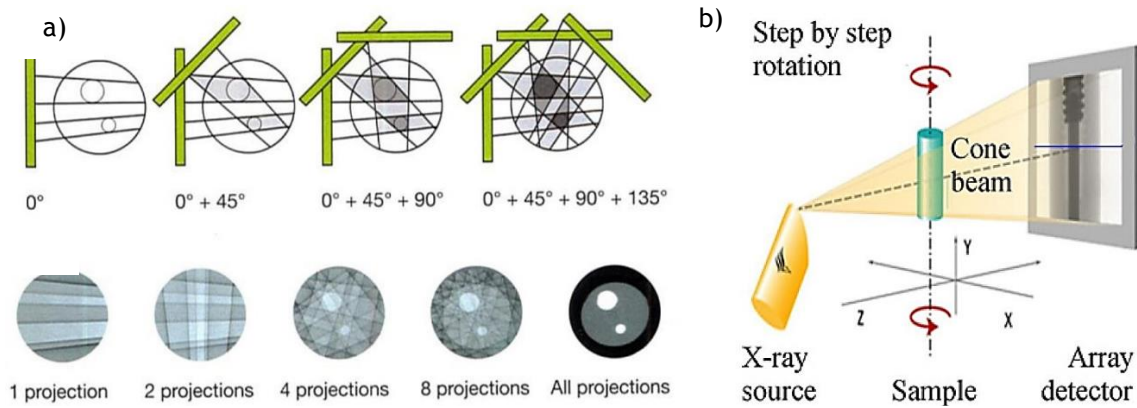


Figure 8 -a) Projection reconstruction principle [77]; b) Flat panel CT working principle [78].

The typical hardware on a CT machine are the X-ray tube, manipulator table and detector panel. There are various types of radiation sources but the most common are vacuum X-ray tubes that project X-rays in a cone-beam configuration. These consist in a cathode (tungsten filament) and an anode inside a vacuum tube, between which an electrical potential is applied, originating an electron beam. This electrons collide against a target, converting their kinetic energy into thermal (98%) and electromagnetic energy in the form of a continuous spectrum of X-rays (Figure 9) [78-81].

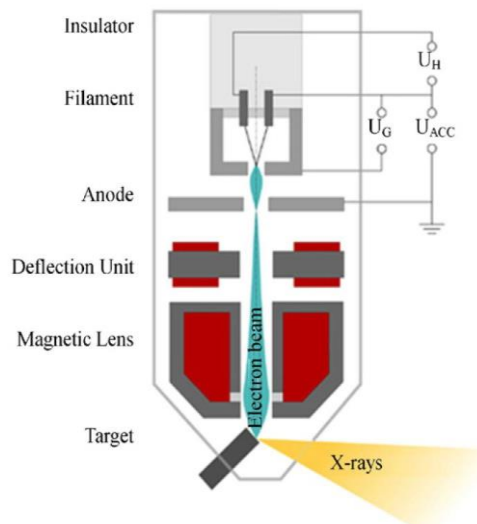


Figure 9 - Typical reflection X-ray tube [78].

Having a small focal spot is important for the spatial resolution of the CT. Being the X-rays tubes classified as macro, micro and nanofocus, in which, the smaller spot size the smaller feature resolution is possible. Although, with the reduction of the spot size, the energy will be focused on a smaller area, leading to an excessive heating of the target. Therefore many machines employ a water cooling system to reduce this problem. However, in the limit, it constrains the energy of the X-rays

that can be applied. The X-ray tube current and voltage are variables that can be chosen by the operator within a specific machine range, where the current affects the intensity (amount of radiation), without modifying the quality (penetration) of the emission spectrum, while voltage affects both [78, 79, 81].

The other important hardware component is the detector which converts incoming X-rays to electrical signals. The most common type are the scintillators, which exploit the fact that certain materials emit visible radiation when exposed to X-rays. The resulting visible light is then converted to an electrical signal that can be used by the computer to recreate the projection [78, 81].

The manipulator controls the position of the object and must be properly calibrated to avoid image errors. The relationship between X-ray source, detector and object is important, since it influences the size of the projection on the detector. The closer the object is to the source and the further the detector is, the larger the geometrical magnification will be. Larger geometrical magnification is good for resolution but will originate blurriness on the edges, reducing perceptibility of the boundaries (Figure 10) [78, 80, 81].

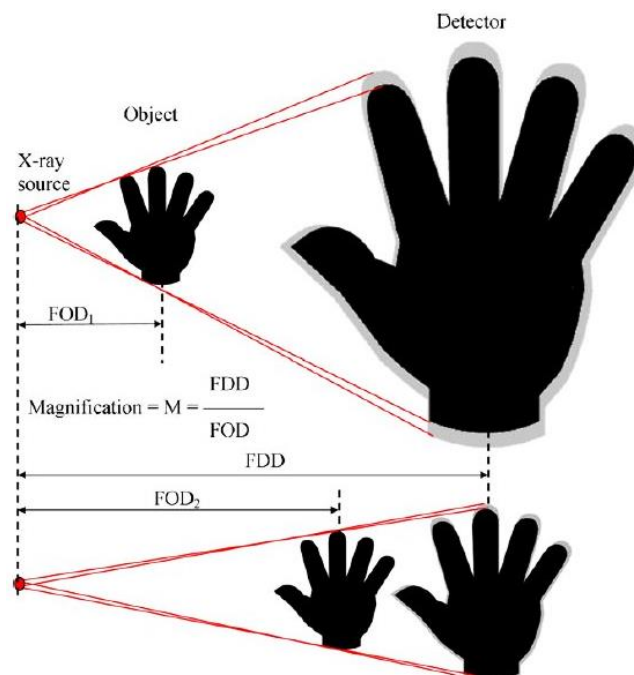


Figure 10 - Image magnification and blurring by moving the object towards the source having a finite X-ray spot. FOD- Focus object distance; FDD - Focus detector distance [78].

The software on CT plays a vital role and are used for reconstruction and analysis. The reconstruction software creates 3D volumes that are made of voxels, through the various 2D projections with the associated measured intensity of the X-rays

transmitted through the object cross section (gray values). To do this there are various algorithms like the Feldkamp, CERA, Radon, among others. The analysis software has the function of surface detection, visualization of the 3D object and dimensional analysis. The surface detection of the 3D object is done by various methods: assigning a threshold gray value to the “edge voxels” or interpolation between maximum gray values derivatives, among others [78, 79, 81-84].

The generated images by the CT can have discrepancies with the actual object. These manifest as artifacts which are artificial features that don't correspond to the physical object. Artifact content is one of the most difficult aspects of image quality to control or quantify, being almost impossible to have a reconstruction without them. Mitigating them is done by the careful setting of parameters or through the use of filters during reconstruction step. There are various type of artifacts like beam hardening artifacts, ring artifacts, edge artifacts, noise, among others.

Beam hardening is one of the more common when using polychromatic X-ray sources, because low energy photons (soft X-rays) are attenuated more quickly than high energy photons (hard X-rays). The consequence is that only the harder X-rays pass through the object, making the total attenuation no longer being a linear function, which will lead to an underestimation of the attenuation inside the sample. This will result in the reconstructed object appearing lighter on outside than in the core. This will affect surface determination since it affects the threshold value, leading to a loss of features when selecting the threshold gray value. The most practical approach to remedy this effect is to use a thin plate of aluminum, copper, brass or lead in front of the X-ray source to filter the softer X-rays (Figure 11 - a). The choice of material and thickness is dependent of on the attenuation of the material being analyzed and its thickness, with operator experience playing a major role. Although, there are software's (e.g. SpekCalc) that suggest the power, filter material and thickness for the specific material being analyzed. Another example is ring artifacts. They appear on the reconstructed image as concentric rings, with their center on the rotational axis of the CT. They appear because of non-linearity of signal, ageing of the detector or suboptimal calibration before the scan (Figure 11 - b) [68, 72, 78-81, 85, 86].

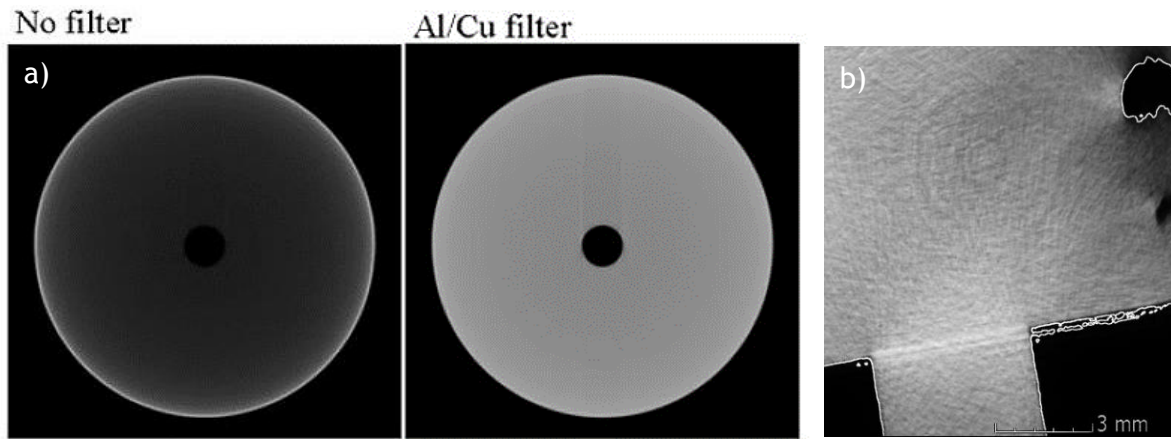


Figure 11 - CT artifacts examples. a) Effect of beam hardening without and with a physical filtering of the X-ray [78]. b) Ring artifact.

Other common artifact is noise. It is defined as an unwanted and randomly distributed disturbance of signal that tends to obscure the image, reducing resolution and contrast (Figure 12).

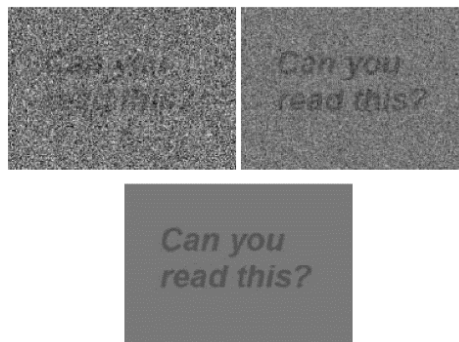


Figure 12 - Example of image noise [87].

It is impossible to have CT images without some degree of noise. It appears mainly for two reasons, statistical noise and interaction with matter. Statistical noise is governed by the number of X-ray photons absorbed by the detector. A good way to understand this effect is using an example of traditional radiography where is used X-ray sensitive film. Even after exposing uniformly the film to X-rays, it will reveal at close inspection that only a number of small grains have been exposed. This effect translates to the scintillator detectors used on CT, where they will originate a fine-grain image. Although unavoidable, it can be reduced by increasing the scan time, reducing the frame rate of the detector or by increasing the output of the X-ray source [79, 80, 87].

The other source of noise is the interaction of X-rays with matter. There are three types of interactions that can occur, coherent scattering, photoelectric absorption and Compton scattering. Compton scattering is the one that originates noise and occurs when high energy X-ray photons interact with the electron on the outer shell

of the atoms. This outer electron is bound with very little energy to the atom, so when the X-ray photon collides with it, the electron is ejected and the photon diverted from the initial direction [80, 81, 87].

There are many factors that can affect CT analysis ranging from the software to the hardware passing by the operator settings (Figure 13). All this possibilities make the measurement of uncertainty a difficult task, justifying the delay on the emission of new standards [74, 75, 78, 88].

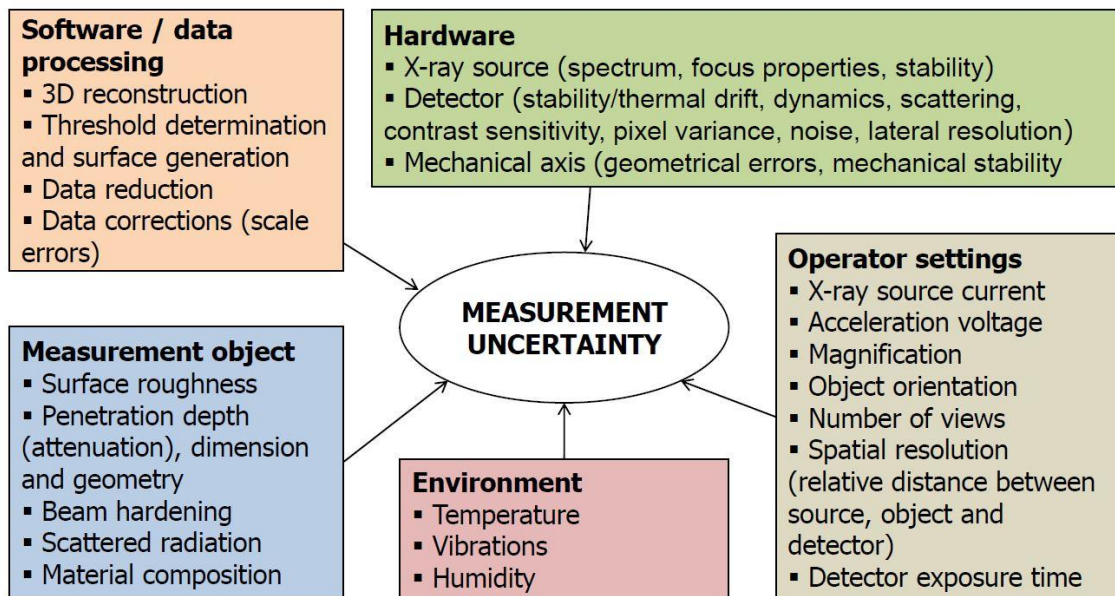


Figure 13 - Influence factors CT [81].

5.3. 3D Scanning

Scanning of an object using optical means is widely used to reverse engineer objects in AM. So the natural step was to use this technique to do the opposite, apply it for geometrical quality control of AM parts. There are various method to optically 3D scan an object, like photogrammetry, laser triangulation, structured light, among others. All these systems work through triangulation, in which light is projected into the object, then it reflects to the camera and by knowing the distance between camera and light source is possible to calculate de distance.

This work will be focused on structured light method of fringe projection. These scanners are used for reverse engineering and quality control of a wide array of part sizes on different industries like casting, forging, injection moulding, tool making, among others. The easy operation of this equipment allows a rapid inspection of

simple parts and the conversion to digital of physical models and prototypes with a good accuracy and resolution. They work by projecting a fringe pattern onto the object which will distort the lines depending on the object profile. Then the camera captures the distorted fringe images into the computer that analyzes the images and calculates millions of points of the object surface (Figure 14). All these points will form a point cloud that will originate a triangulated mesh representation of the object [89-96].

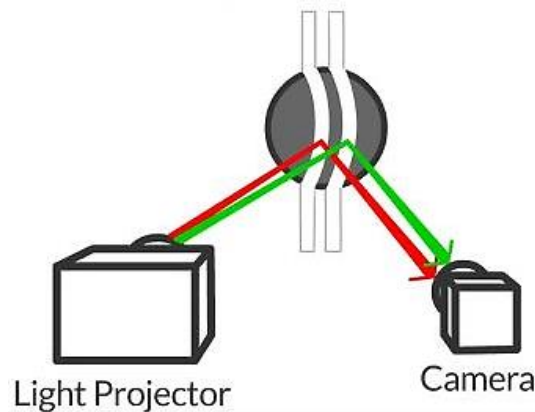


Figure 14 - Working mechanism of structured light 3D scanner devices [97].

Fringe projection systems can use one or more cameras to capture the images, which will increase the area registered in each capture. These systems are simple to set and operate giving resolutions up to 0.02 mm, although they struggle when scanning transparent or highly reflective surfaces. This issue can be overcome by spraying the surfaces with some kind of powder to allow surface recognition. Another problem is when scanning objects bigger than the field of view of the scanner, since the various frames need to be aligned accurately to reproduce the objects. There are three main strategies to overcome this. One of them is the alignment of frames through the software, where it aligns the frames using the unique geometry of the object through a sophisticated algorithm that tries to understand the surface. However, this kind of guess work doesn't always produce the best results since they tend to accumulate measurement error. The second method is to employ gyroscopes and accelerometers to locate the scanner in space in relation to the object. The third and most common method is the use of markers. These are high contrast objects that work as reference coordinates, allowing the software to locate in space the scan in relation to the object (Figure 15). These markers can be placed into the object or on the base; however, there must be always three markers on the field of view of the scanner [89, 91, 92, 95, 98].

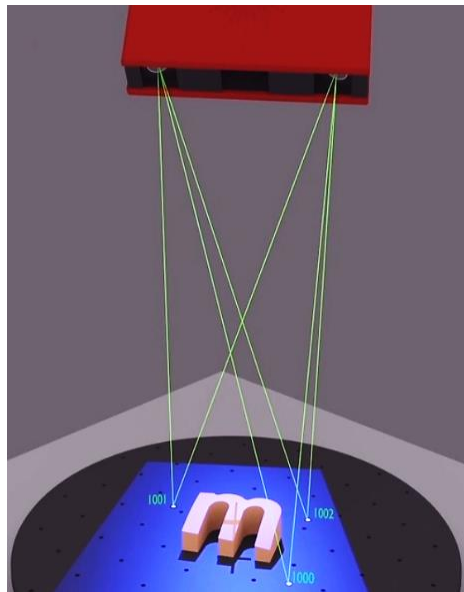


Figure 15 - Positioning system using markers [99].

5.4. Demonstrators

An important tool when testing any manufacturing method is the use of standardized test parts. AM is not different, being used demonstrators also known as artifacts. These have complex geometrical features known to the AM processes and are designed to test the limits of the process with features like overhangs, thin wall structures, among others (Table 2). Besides benchmarking the AM process, these also allow for optimization of the processes iteratively, by choosing more suitable parameters and materials [54, 73, 100, 101].

Table 2 - Geometric features and their intended purpose [101].

Feature	Purpose
Flat base	Flatness and straightness.
Cube	Squareness, parallelism, linear accuracy and repeatability.
Cylindrical hole	Roundness, cylindricity, accuracy and repeatability of radius (internal).
Sphere	Sphereness, relative accuracy and repeatability of continuously changing surface.
Solid cylinder	Roundness, cylindricity, accuracy and repeatability of radius (external).
Hollow cylinder	Roundness, cylindricity and coaxially of cylinders.
Cone	Concity, sloping and profile and taper.
Angled surfaces	Angularity, accuracy and repeatability of angled surfaces.

Over the years several authors have proposed different demonstrators [100-105], with varying purposes, features, sizes and complexity. One of the most known is the one suggested by the National Institute of Standards and Technology (NIST) (Figure 16).

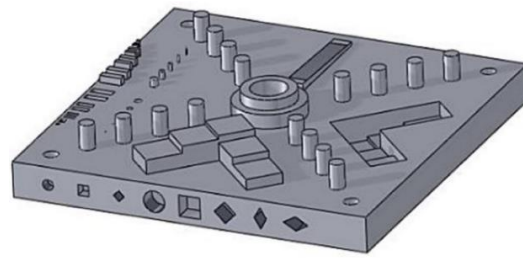


Figure 16 - Proposed demonstrator by the National Institute of Standards and Technology (NIST) [105].

However, the proposed demonstrators often lack some important features. For example, angled structures or internal channels. These omissions lead to the development of the Fraunhofer IWS demonstrator that was specifically designed to test metal AM processes. This demonstrator has all the features defined by the best practice design of demonstrators and was designed to be fully scalable like showed on Figure 17 and Figure 18.

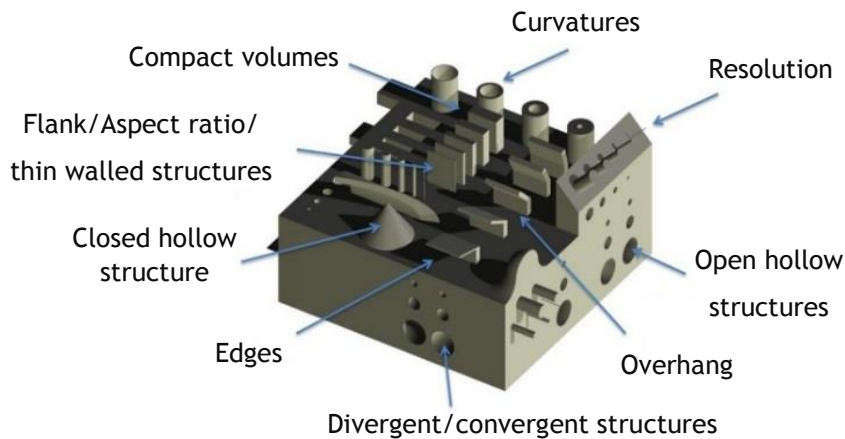


Figure 17 - Fraunhofer IWS demonstrator developed to evaluate different challenging geometrical features.

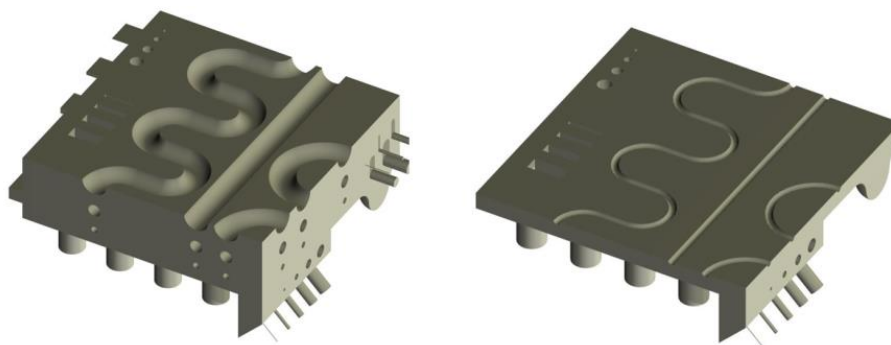


Figure 18 - Horizontal cut of the demonstrator highlighting the internal channels.

6. Experimental procedures

In this chapter it will be made a general explanation on the specific equipment and software used in order to better comprehend the reasons and challenges faced when using CT and 3D scanning for quality control. In this work were made various experiments as described in Table 3 in order to determine their advantages and limitations.

Table 3 - Performed experiments.

Measuring equipment	Part	Material	Process	Objective
CT	Demonstrators	Inconel 718 Ti6Al4V AlSi10Mg	LPBF EBM	Geometrical comparison against CAD
CT and 3D scanner	Nozzle Demonstrator	Ti6Al4V Inconel 718	EBM LPBF	Comparison of CT against 3D scanning in geometrical comparison against CAD
CT	Cubes	Inconel 718	DED	Porosity analysis
Reconstruction software	Cube	Inconel 718	DED	Assessment of reconstruction parameters on porosity analysis

6.1 Computer tomography

To perform a CT inspection specific steps were made using certain software. To better understand these steps they are outlined on Figure 19.

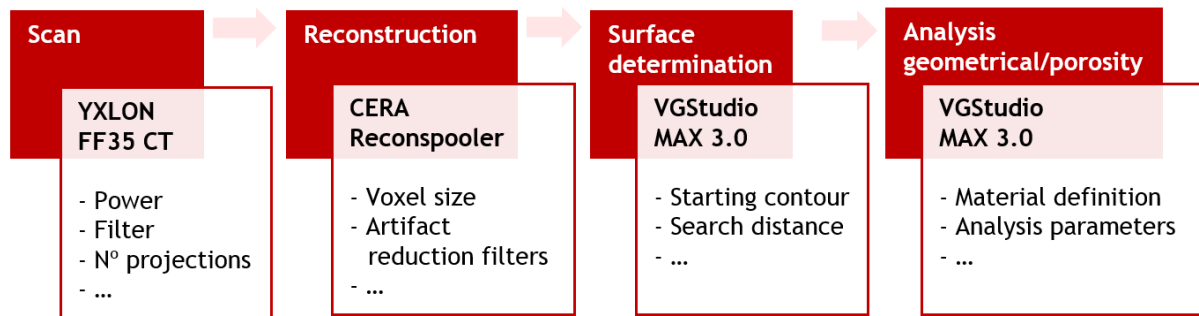


Figure 19 - Steps performed on the CT inspection with focus on the machine and software used and parameters needed to define in each stage.

6.1.1. Equipment

The computer tomograph used in this work was an YXLON FF35 CT made by YXLON (Figure 20). This equipment is ideally suited for inspection of small to medium sized items such as electronic devices, small metal parts, and small castings, among others [106]. The maximum part limit size is Ø 300 x 500 mm height and 30 kg.

Due to the necessity of high accuracy the atmosphere temperature inside the machine is controlled and all the moving parts are laid on a granite base which are controlled by high precision *Heidenhain* encoders.

The CT is equipped with a FXE-225.48 microfocus 225 kV reflection X-ray vacuum tube and an YXLON flat panel model 2530 with 1792x2176 pixel size. This setting allowed for minimum focal spot size of $<6 \mu\text{m}$ with a minimum detail recognizability of $<3 \mu\text{m}$ and a maximum permissible error (MPE) equal to $8 \mu\text{m} + L/75$ (where L is the length in mm) according to the VDI 2630-1.3 directive.



Figure 20 - Computer tomograph YXLON FF35 CT used.

In order to analyze the parts some steps were taken into consideration. First the parts were placed on the machine in a way that all the surface was projected on to the detector but with minimum travel path of the X-rays through the part. To keep the part in the correct position was used a support made of expanded polystyrene attached to a magnetic spiked support (Figure 21). It was chosen expanded polystyrene as a support material due to its low density comparing with the parts analyzed. The use of support material will prevent noise and post-processing work to eliminate the supports from the reconstructed 3D object.

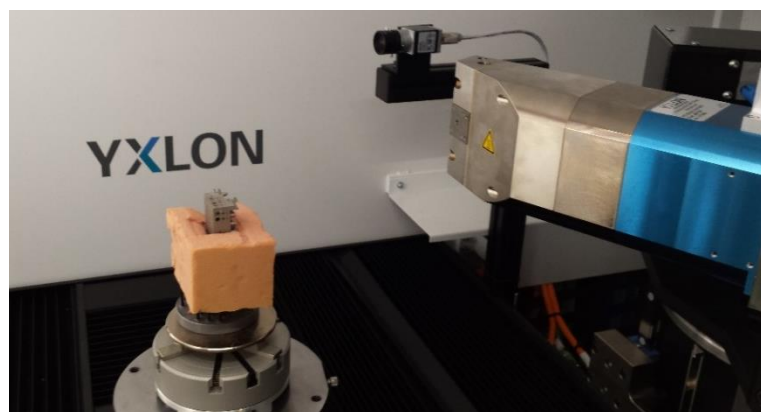


Figure 21 - Placement of the demonstrator inside the CT.

When the part was correctly placed on the machine it was defined the parameters for the X-ray tube, detector and positioning. This was attained with the help of the live image that shows the image that is being captured at that moment by the detector. X-ray tube and detector parameters were also defined with the assistance of the live histogram (Figure 22). The parameters were different for each part because of density and size difference between them, leading to different parameters and filters being used for different parts. The suggested values present on standard ISO 15708-2:2017 were used as a reference (Annex A).

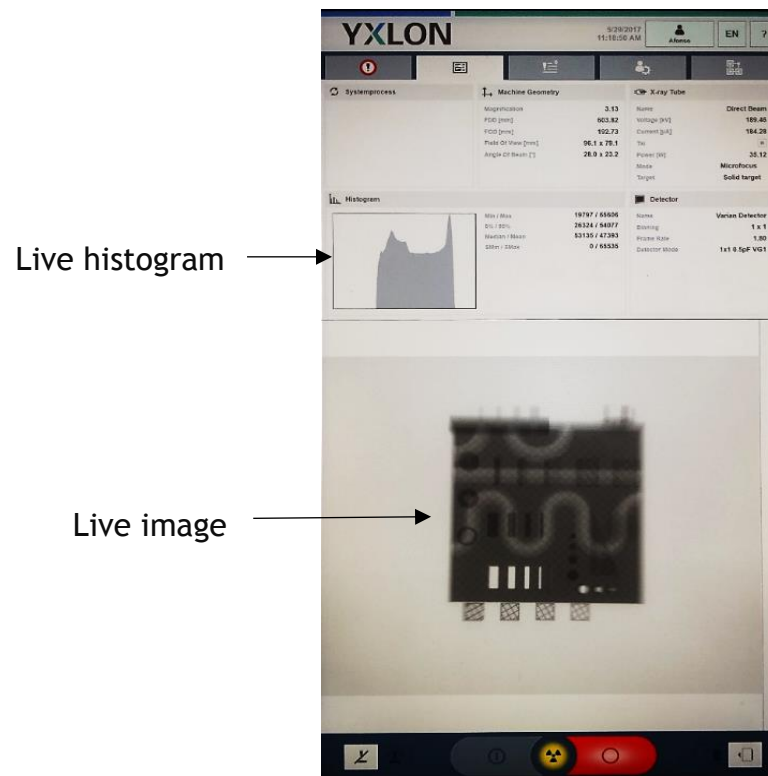


Figure 22 - YXLON FF35 CT live menu.

Once the X-ray tube, detector and position parameters were chosen it was made a detector calibration. This step was made every time that these parameters were changed to avoid artifacts and have a clear image. In this work was only performed the *Air calibration*, where the operator needs to move the tube/part so that no object is present in front of the detector. After this, the CT captures images with the X-ray tube OFF and ON, averaging the detector readings and correcting possible distortions or noise on the detector. Finally, was defined the type of scan and reconstruction parameters; in this work, it was only used the circular scan option.

6.1.2. Software

6.1.2.1. YXLON Reconspooler

This reconstruction software comes with the CT machines made by YXLON and uses the CERA algorithm created by Siemens. It allows adjustment of various parameters (Annex B) that makes it a very powerful software for the reduction of noise, artifacts as well image corrections. The parameters for this software were chosen on the last step of the scanning routine definition, but the reconstruction can be remade with the recorded data with a different set of parameters.

In this work the image correction parameters were kept the same for all of the samples, but the reconstruction volume size was changed in order to have a compromise between file size and voxel size; since a bigger reconstruction volume will originate a 3D object with smaller voxel size and better resolution but a much larger file size, making all kind of future analysis time consuming. So in order to have the smallest file size possible without being detrimental for the analysis, it was always chosen a voxel size smaller than the characteristic that was analyzed.

6.1.2.2. VGStudio MAX 3.0

The VGStudio software was developed by *Volume Graphics* for visualization and analysis of CT data and it is capable of perform various geometrical and material analysis. Geometrically it can do coordinate measurements, tolerance analysis, wall thickness analysis, comparison with the 3D CAD, among others. In material analysis it is capable of measure and quantify porosity, inclusions, cracks, analyze fiber composites, simulate mechanical resistance of the part with the detected defects and simulate transport phenomenons on porous/fibrous materials. In this work was used VGStudio MAX 3.0 for porosity analysis and comparison with the 3D CAD. This software was used following a specific procedure. First it was needed to register the part in space then was made the surface determination of the 3D object and finally the analysis (porosity or comparison).

6.1.2.2.1 Registration

Registration of the 3D object in space was needed because most of the times the scanned part is not perfectly centered on the axis or it was tilted on for better X-ray

path. This made the analysis on the 2D projection images more difficult, since they were not parallel with the axis of the CT, making the capture of images for reporting more challenging since the 2D image are locked once registered (Figure 23).

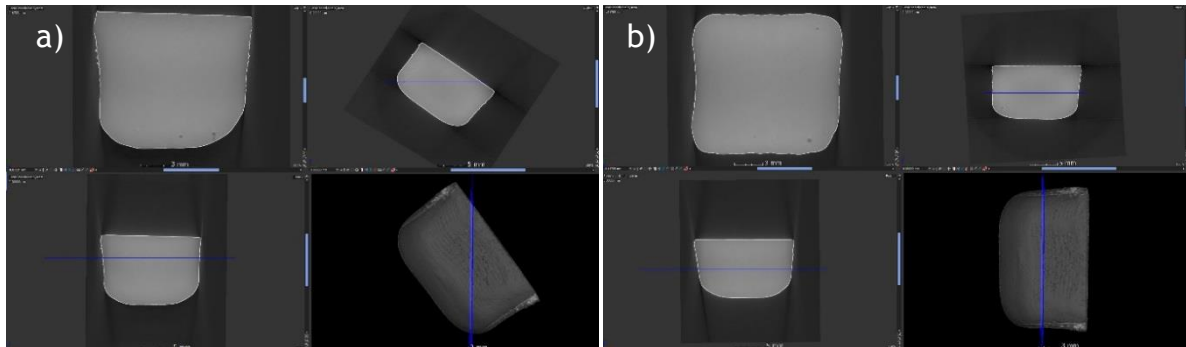


Figure 23 - 2D and 3D views of a part in VGStudio Max 3.0. a) Incorrectly registered; b) Correctly registered with the back plane of the sample through *Simple 3-2-1 Registration*.

Registration is also key when performing the *Nominal/actual comparison* since the CAD and the 3D object need to be aligned the best way possible in order to have a correct analysis. VGStudio MAX 3.0 provides various options to do this, but on this work it was only used the *Best Fit Registration* for the geometrical analysis and the *Simple 3-2-1 Registration* for the porosity analysis.

In *Best Fit Registration* there are references to which the 3D volume of the scanned part can be registered. It can be registered against a CAD model or a region of interest (ROI), that is a clipped region of a 3D object. The software uses a Gaussian best fit through the analysis of millions of points that define the objects, while the *3-2-1 Registration* works by defining a primary (e.g., a plane), a secondary (e.g., a line) and an optional tertiary datum reference (e.g., a point) for the object [107].

6.1.2.2.2. *Surface determination*

The surface determination is a very important step since it influences all further analysis. It works by determining the boundary between air and part through the gray values. The software allows various methods to determine this like, defining the gray value manually, through ROI's or intervals. However in this work it was used the automatic option to reduce operator influence. So the software automatically determines this through the calculation of the mean between the material and air mean on the histogram peaks (Figure 24), that results on a ISO value that will determine the surface with sub-voxel precision (it does not simply follow the voxel

grid) (see Figure 25). Although sometimes this process is not so straightforward due to noise, edge artifacts and beam hardening.

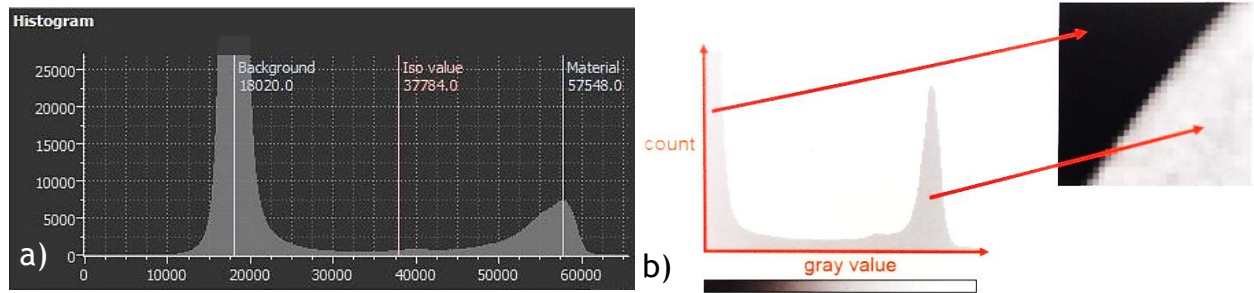


Figure 24 - Histogram. a) VGStudio MAX 3.0 histogram; b) Histogram illustration and correspondence.

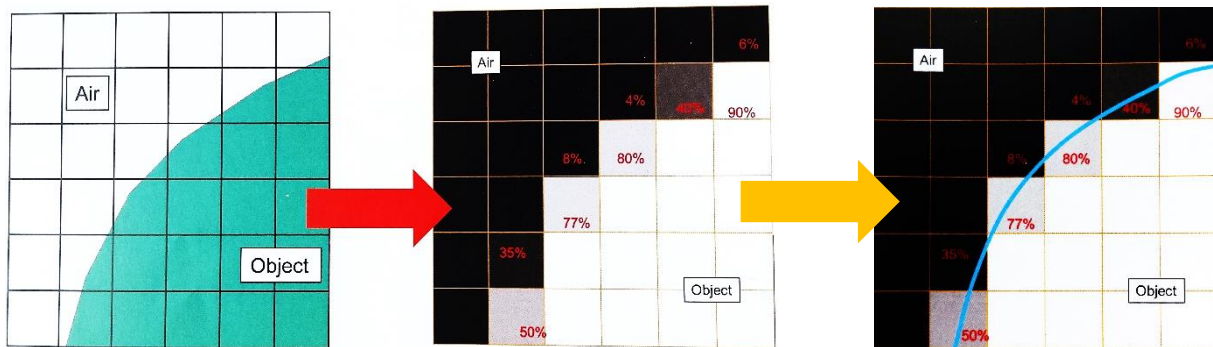


Figure 25 - Surface determination process through gray value means [108].

Another tool provided by the software is the *Advanced Surface Determination* that defines the material boundary by locally adapted gray values. The same gray value will be interpreted differently depending on the surrounding voxels within a determined search distance from the ISO value (Figure 26). This creates a more accurate determination of the part surface. Because it will compensate for local deviations originated from beam hardening or other artifacts. This tool also has the option of *Starting contour healing*, which removes noise particles outside the object and voids from inside. This is important for future porosity analysis, since the porosities won't be identified properly if they are considered to be part of the surface.

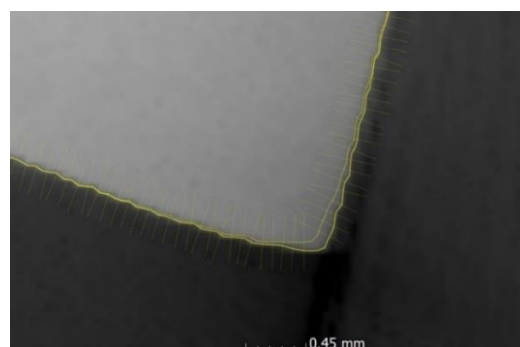


Figure 26 - Detail of the advance surface determination of an object corner with different gray values due to an edge artifact.

In this work were used the parameters of automatic ISO value determination with the *Advance surface determination* active, with a default search distance of 4 voxels and a starting contour healing for remove particles and all voids. These parameters were chosen to reduce the dependency on the operator and minimize uncertainty/errors related to the operator.

6.1.2.2.3. *Actual/Nominal comparison*

This tool was used to determine the deviation of the analyzed parts. It allows for comparison of volumes against CAD and mesh objects in order to detect deviations of the original build file at different tolerances. The result of the analysis is a report with deviation histogram (example in Annex C), cumulative histogram (Annex D) and deviation colored volume [107].

6.1.2.2.4. *Porosity/Inclusion analysis*

For porosity analysis the tool *Porosity/Inclusion Analysis* was used, that investigates voxel data for internal imperfections and provides detailed analysis results with information on each individual defect as well as overall statistical information. The generated report contains information like position, size, surface, and volume of each individual defect.

The defect analysis works through algorithms to check each voxel to determine if it might be a defect and then it checks if it matches with the specified gray value and filters set by the user (Figure 27). The algorithms provided are the *Only threshold* and *VGDefX*. In the *Only threshold* analysis each voxel gray value is examined and if it is below the specified value, then it is considered a defect. On the other hand, *VGDefX* is a more sophisticated algorithm since it allows for gray value variations, includes noise reduction for seed point location, and can detect defects which are connected to the surrounding air [107] (see Annex E). It also offers several probability criteria according to which the defects will be detected (see Annex F).

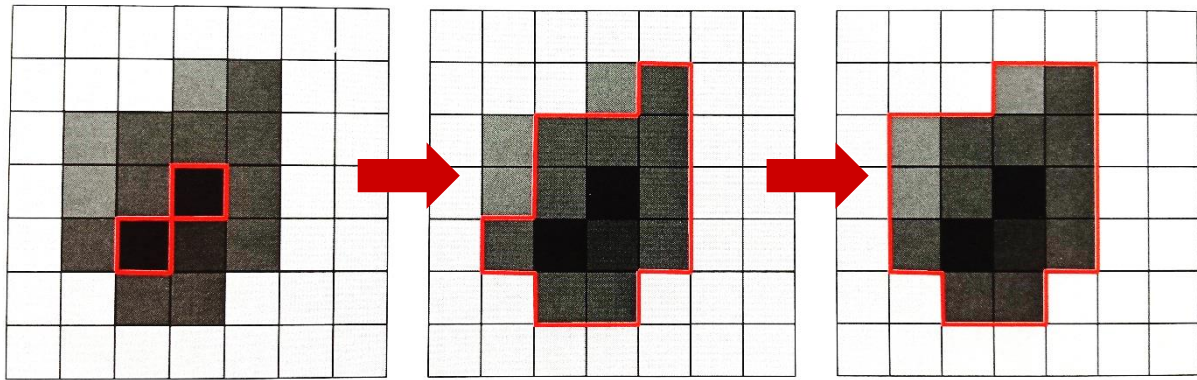


Figure 27 - Pore detection process, from seed to neighborhood analysis[109].

For the analysis it was necessary to define the void maximum gray value (*Void max.*) and filters. *Void max.* can be defined manually through example area or by *Auto threshold* mode. This last one, uses the histogram calculate the *Void max.*, whether by deviation or interpolation.

On deviation, this value is calculated through the material gray value of the surface determination; here it adds the standard deviation of the material plus the mean gray value of the material peak multiplied by a deviation factor (Equation 1). The deviation factor specifies a factor for the standard deviation of the material peak of the gray value distribution. This mode is more adequate for multi material analysis.

$$Void\ max. = mean_{material} + standard\ deviation_{material} \times Deviation\ factor$$

Equation 1 - Equation for Void max. through deviation [107].

Interpolation also uses the surface determination gray value but also the background peak value. This method works through Equation 2 to determine the *Void max.* On this it adds the mean background gray value to the difference between the material and background gray value, that is then multiplied by the defined interpolation factor. Interpolation is more suitable for mono material analysis because of the distinct peaks of material and background on the histogram.

$$Void\ max. = mean_{background} + (mean_{material} - mean_{background}) \times interpolation\ factor$$

Equation 2 - Equation for Void max. through interpolation [107].

Filters can also be defined before performing the analysis. These are based on probability, minimum/maximum defect size, compactness and sphericity range (see Annex G). However, they can be also filtered post-analysis, by selecting the defects identified with the filter parameters and eliminating them.

6.2. 3D scanning

To digitize parts to 3D objects, by using the 3D scanner the steps outlined on Figure 28 were followed.

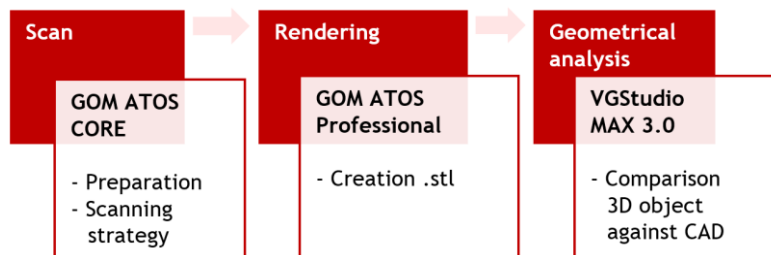


Figure 28 - Steps followed for 3D scanning.

6.2.1. Equipment

For the 3D scanner analysis the GOM ATOS Core fringe projector with stereo cameras was used. The 3D scanner has various scanner sizes for different applications, being that on this work the models 45 and 135 were used. The difference between them is pointed on Table 4. The larger measuring area allows shorter scanning times and fewer image captures because of the acquisition of a larger area in each acquisition. However, it has higher point spacing and consequently a lower resolution.

Table 4 - Different specification of the GOM ATOS CORE 45 and GOM ATOS CORE 135 [96].

	ATOS CORE 45	ATOS CORE 135
Measuring area	45 x 30 mm	135 x 100 mm
Working distance	170 mm	170 mm
Point spacing	0.02 mm	0.05 mm

In order to obtain a 3D rendering of the scanned part, some sample preparation was needed. First the markers were attached to the part; they were placed in a way that the scanner always detects three markers at any given point. Then the parts were lightly sprayed with penetration testing spray (Helling NORD-TEST - Developer U89), where the objective was not to test cracks or pores but to reduce the reflectivity of the scanned parts. After this the part was attached to the base plate using adhesive putty. Finally more markers to the base plate were attached, in order to further ensure the three point detection requisite.

Then the scan was made, making a capture and then rotating the part around 30°, repeating the process until all the part was scanned. After this the extra height added by the putty was trimmed of the 3D object. In the end the 3D object was transformed in a .stl file for further analysis.

6.2.2. Software

6.2.2.1. GOM ATOS Professional

It is a software created by GOM to control the GOM 3D scanners and generate the 3D object through the cloud points obtained through the scanner. It also self-monitors the calibration status, transformation accuracy and if the part has moved during scanning. This software allows polygon mesh generation, editing and sectioning, as well as quality control through various tools, for example, comparison against CAD, measurement of individual points and their deviation [110].

It works by controlling automatically the exposure time of the projector, tracking in real time the position of the identified markers, part and projector, that are displayed on the computer screen while the part is being scanned (Figure 29).

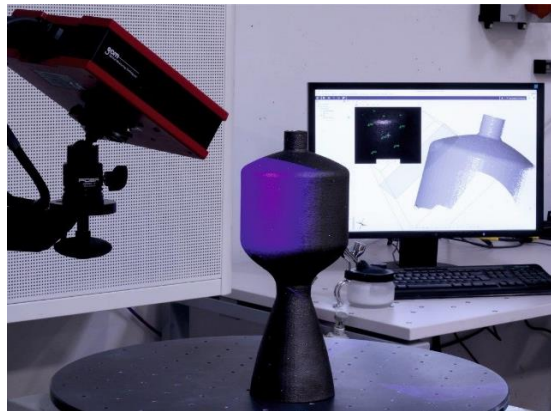


Figure 29- Scan of a part with GOM ATOS 135. Scanned area and live cam on the computer screen.

6.3. Measurements

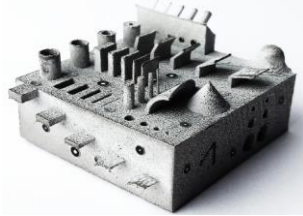


6.3.1. Geometric analysis

For the geometric analysis it was used as a standard part the demonstrator developed by Fraunhofer IWS which was built using the LPBF and EBM techniques. This demonstrator was developed to assess the process capacity of AM processes between different machines and manufacturers. It was also analyzed the capacity of this demonstrator to perform these functions. The technical drawing detailing some dimension can be found in Annex H.

6.3.1.1 LPBF demonstrators

The LPBF demonstrators were built to determine the capacity of the demonstrator to test machines with different materials. The three demonstrators were made on different institutes with different materials and machines, as seen on Table 5.

Table 5 - LPBF demonstrators used for the geometrical analysis.

Institute	Machine	Material	Demonstrator
Fraunhofer IWS	Renishaw AM 250	Inconel 718	
Fraunhofer IPK	SLM Solutions SLM250HL	Ti6Al4V	
Fraunhofer IWU	Concept laser M2 cusing	AlSi10Mg	

6.3.1.2. EBM demonstrators

The EBM demonstrators were all made on an Arcam A2X using Ti6Al4V and the same parameters of beam speed 700-4530 mm/s and beam power 5-17 mA. These demonstrators were built to study the effect of the support structures on the swelling defect. For this different support structures grid size were built, like those shown on Figure 30.

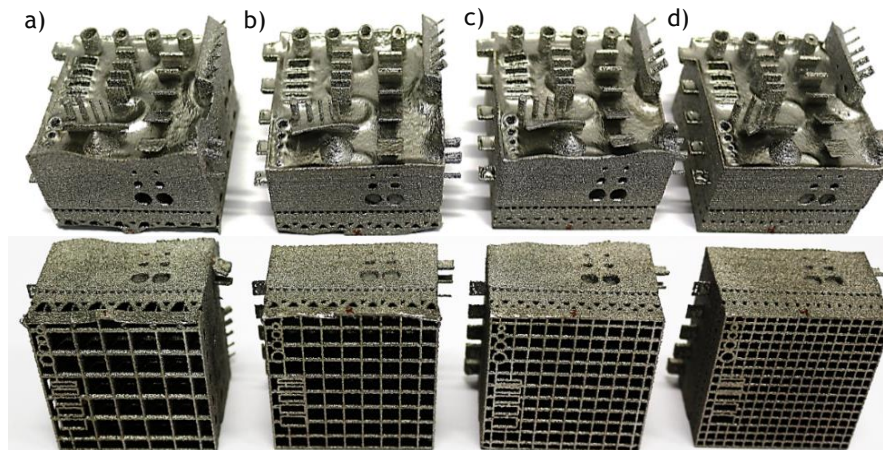


Figure 30 - EBM Ti6Al4V demonstrators made on Arcam A2X with different square base sizes: a) 6x6 mm square size; b) 5x5 mm square size; c) 4x4 mm square size; d) 3x3 mm square size.

6.3.1.3. CT analysis of the demonstrators

The demonstrators were scanned on the CT using different parameters (Annex I), because they were made of different materials, leading to different X-ray attenuations. The reconstruction parameters were the same for all demonstrators (Annex J) but the *Reconstruction Volume Size* was changed to have the minimum file size with the voxel size below 0.1 mm. On the *Surface determination* the parameters were the same for all demonstrators except the Inconel 718, where the *Surface determination* was made using the starting contour of the CAD file, because of the noise on the reconstructed volume (Annex K).

Then they were analyzed on VGStudio MAX 3.0 using the *Actual/Nominal comparison* tool with three tolerance distances, 0.1, 0.5 and 1 mm. They were registered using *Best Fit Registration* because there weren't clear points to align the parts, since AM parts can suffer warpage and shrinkage.

The EBM Ti6Al4V and LPBF AlSi10Mg demonstrator had supports that needed to be trimmed off in order to make the *Best Fit Registration*. For this it was used the VGStudio MAX 3.0 in which was used the *clipping box* tool to "cut off" the supports from the demonstrators. Then was created a ROI from the clipped object and used for the geometric comparison with the CAD.

6.3.2. Comparison of CT against 3D scanning

For the comparison of CT against 3D scanning it was chosen two different parts, the LPBF Inconel demonstrator and jet nozzle (Annex L). This choice was made because when using the 3D scanner it's impossible to scan the internal features. So it was also used a nozzle that had a more simple geometry, allowing for total scan by both methods and working as a direct comparison between them. While in the demonstrator it was used to scan of the top features and work as an indirect comparison.

In the indirect comparison it was used the Inconel 718 demonstrator made by LPBF. It had already been CT scanned on the previous geometrical comparison experiment. For the 3D scanning it was used the GOM ATOS 45 with 0.4 mm markers size and the

demonstrator wasn't turn over to ensure maximum accuracy during scanning of the features and the lack of a sturdy fastening point (like a screw base).

For the direct comparison it was used a Ti6Al4V nozzle produced by the EBM machine Arcam A2X where it was used a beam speed of 4000 mm/s and beam power 15 mA.

The CT parameters for scanning, reconstruction and surface determination of the parts are present on Annex I, Annex J and Annex K. For the 3D scanner it was used the GOM ATOS 135 with 0.8 mm marker size, where the part was scanned all around, starting of the top while inclining the rotating table (Figure 31). After both sides were scanned they were joined on the GOM ATOS Professional, using as reference points the markers that where attached to the nozzle.

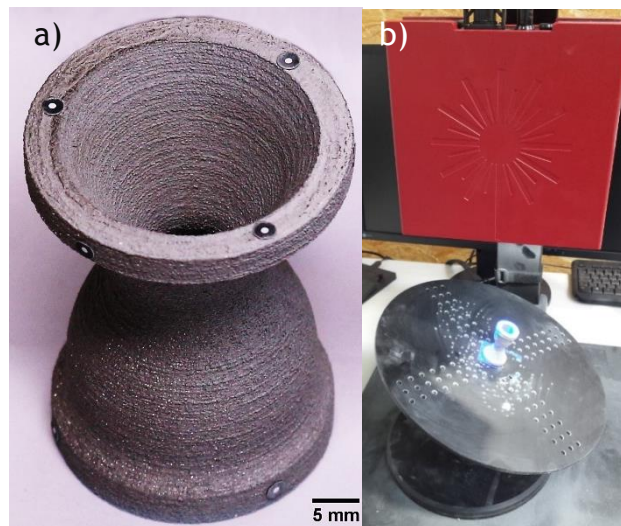


Figure 31 - a) Nozzle made by EBM with Ti6Al4V, b) Scanning of the nozzle using the GOM ATOS 135 and an inclinable turning table.

Then the 3D objects were compared against the CAD file on VGStudio MAX 3.0 using the *Nominal/Actual comparison* option. The objects were registered with the CAD using the *Best fit registration* and then performed the analysis with three maximum deviation values of 0.1 mm, 0.5 mm and 1 mm.

6.3.3. Porosity Analysis

For the porosity analysis were used seventeen samples made of Inconel 718 (Figure 32). These samples were made at Fraunhofer IPK using the DED machine TruLaser Cell 7020 with the build parameters in Annex N, resulting in cubes with the dimensions present on Annex O. These were generated according to the design of experiments using the statistical experimental planning software Visual-Xsel from

CRGRAPH. The goal was to study the effect of different build parameters on final density.



Figure 32 - Inconel 718 cubes made by DED process on TruLaser Cell 7020.

The density was determined through two methods: Archimedes method and porosity analysis by CT. For both methods was used the reference value of 8.19325 g/cm^3 for Inconel 718 [111]. The measurements were done on Fraunhofer IPK according to the standard DIN EN ISO 3369.

On the CT analysis the parameters used for the scan, reconstruction and surface determination were kept constant, which can be seen in greater detail on Annex I, Annex J and Annex K. On the reconstruction parameters the reconstruction volume of 512 hpc (horizontal pixel count) was chosen because it originated a voxel size below 0.1 mm and a small file size of $\pm 250 \text{ MB}$. This volume size allowed for a fast porosity analysis (around ten minutes) and permitted loading all 3D objects to a single project file. If other reconstruction volume size was used, for example ISO voxel, the file would have around 16 GB and the analysis time of more than eight hours per sample, which was not practical or realistic in any real world application.

The porosity analysis was made using the *VGDefX* algorithm with the parameters presented on Annex M; three analysis were made with different parameters to determine the difference in porosity detected. It was changed the *Void max.* value through the Interpolation factor and the filters applied but kept constant the Analysis parameters (see Annex E). On the first analysis the interpolation factor and filter were chosen by the operator for each sample in order to achieve the most correctly identified pores. For each sample the operator would choose the parameters and then travel through the horizontal 2D section of the sample to verify that the pores

have been correctly identified. For the second and third analysis the interpolation factor and filters were kept constant for all samples that were chosen through various analysis in order to find the best parameters that identified all the pores with minimum noise. The parameters chosen were: interpolation factor 1.4 and probability threshold 0.3 for the second and interpolation factor 1 and probability threshold 1 for the third one. Interpolation was used to guarantee uniformity through all samples on the second and third analysis. This option allowed the *Void max.* gray value to be always the same middle point between peak values, despite slight differences between histograms.

Analysis parameters were chosen based on the type of defect to be identified (pores). It was chosen *Noise reduction - High*, because it was verified that it reduced the misidentified pores without affecting the correctly identified ones.

6.3.4. Reconstruction settings assessment

In this work it was investigated the influence of the reconstruction settings on the detected volume and porosity. For this it was performed nine reconstructions of the same Inconel 718 cube with different reconstruction parameters. These parameters were changed one at a time between reconstructions while the others were kept constant, like represented in Annex P. The values on parameters are the ones that appear by default when they are activated.

Afterwards the surface determination and porosity analysis were made using the same parameters as for previous experiments (Annex K) and porosity analysis with interpolation factor 1 and probability 1 (Annex Q).

7. Results and Discussion

7.1 Geometric analysis

7.1.1. LPBF demonstrators

CT was fully capable of digitize the metal LPBF parts, like shown on Figure 33. This allowed the comparison with the original build CAD file, holistic analysis of all the part including the small features.

For the Inconel 718 demonstrator it was necessary the use of the CAD as a contour for surface determination, since nickel has a high X-ray attenuation. In order to achieve full penetration it was required also higher energy X-ray and a denser filter (1 mm lead). However, on the center of the demonstrator the contrast was not enough for correct reconstruction through advanced mode surface determination, although on the 2D projection the inner geometries were clearly visible. The use of the CAD file as a starting contour allowed the software to locally adapt on the correct place the best gray value depending of the surrounding voxels.

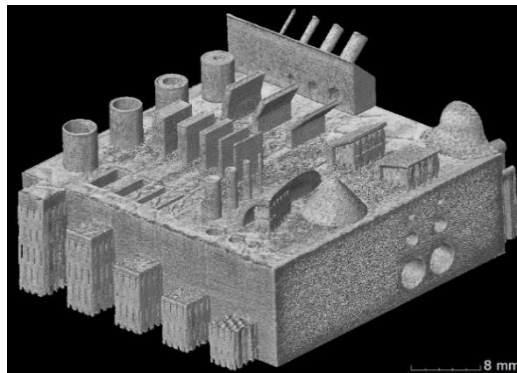


Figure 33 - Digitized Ti6Al4V LPBF demonstrator.

The visual comparison analysis of the demonstrators shows that LPBF was capable of reproduce almost all features with minimum warpage and shrinkage, see Figure 34. The demonstrator made of Ti6Al4V wasn't capable of reproducing the solid cylindrical features with sizes inferior to 0.1 mm and overbuild the thin walled structures (Figure 34 - a).

The Inconel 718 demonstrator was the only that could reproduce all the features despite the 0.1 mm solid cylindrical features showing a high deviation value. However, this high deviation value is due to warping during handling of the part. It also appears to have more shrinkage on the corners of the features (Figure 34 - b).

The AlSi10Mg demonstrator wasn't capable of reproduce the features with sizes inferior to 0.1 mm, while also suffering warpage on a corner (Figure 34 - c). The lack of the thin features might be due to the difficulty in processing aluminum through LPBF. The high reflectivity of these powders decrease the energy absorption and because the features are very small they require that the laser stays very short time on those spots, which may have been insufficient time for effective melting.

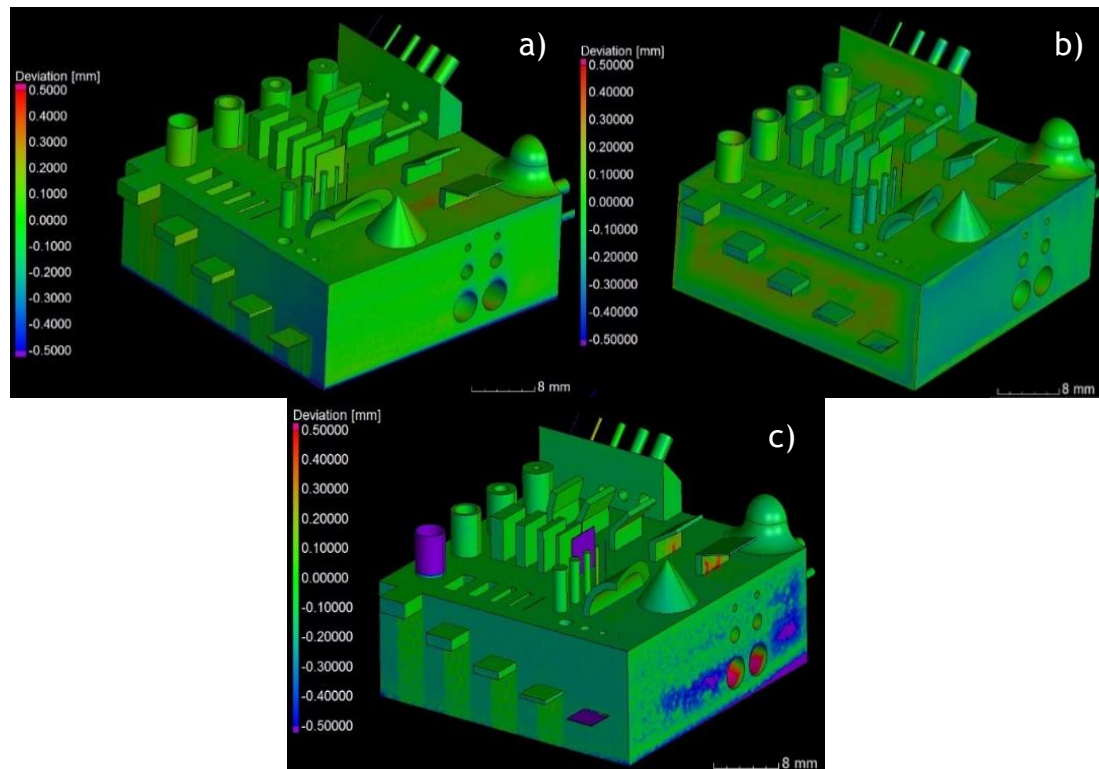


Figure 34 - Demonstrator comparison at ± 0.5 mm tolerance with CAD file. a) Ti6Al4V LPBF demonstrator; b) Inconel 718 LPBF demonstrator; c) AlSi10Mg LPBF demonstrator.

One of main advantage of CT is the capability to analyze internal features like the ones present in the demonstrators. With this internal visualization it can be concluded that the LPBF processes were capable of reproducing the internal channels present in the CAD file (Figure 35).

However, some internal defects and deviations were detected in CT analysis; the Ti6Al4V demonstrator showed the typical drop shaped defect of closed overhang structures, that contributed for the deviation of this demonstrator (Figure 35-a)). The Inconel 718 demonstrator was the one that better reproduced the internal channels with minimum deviation, as seen visually in Figure 35 - b), while the analysis of AlSi10Mg demonstrator showed an obstruction on the 1 mm diameter channel, (purple color in Figure 35 - c).

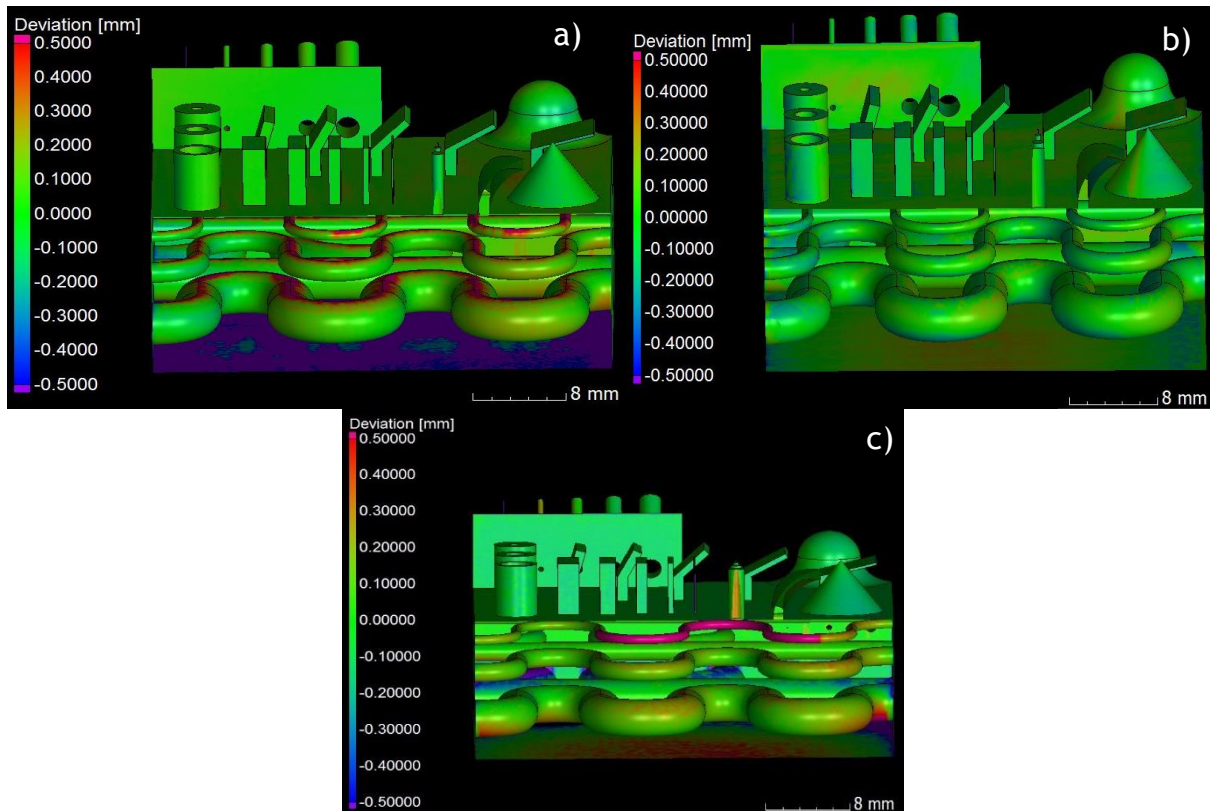


Figure 35 - Internal channels deviation at ± 0.5 mm. a) Ti6Al4V LPBF demonstrator; b) Inconel 718 LPBF demonstrator; c) AlSi10Mg LPBF demonstrator.

The *Nominal/Actual comparison* analysis on VGStudio MAX 3.0 was also capable of generating quantifiable percentage value for the deviation, like shown on Figure 36. The analysis also provided the deviation from the determined values that are represented on top of the bars on Figure 36. However, the values are very small because of the large number of measurements that the software performs.

The analysis of the deviation values reiterate that Inconel 718 demonstrator has low deviation values. This might be to two reasons: first, due to the use of the CAD to make the surface determination, since the software will try to determine the surface closer to the CAD file; the second, due to the higher melting temperature of Inconel (± 1250 °C), which allows for a smaller melt pool size and better control, resulting on less deviation and capability to reproduce finer features.

Through the analysis of Figure 36 it can be inferred that the LPBF processes weren't capable of making parts within tolerances below 0.5 mm, despite the values in the bibliography for the accuracy of LPBF machines is around ± 0.04 mm [35]. There are many factors that might affect the dimensional accuracy of the parts, like the laser power, layer thickness, scanning strategy and direction, among others. These

parameters require a careful setting of parameters and an experienced user. However, it's known that the particle size of the powders used will affect the dimensional accuracy. Being the average particle size of the powders of 20-50 μm, one particle will lead to a precision difference of 0.05 mm. In addition to this, the laser spot diameter is usually 50-100 μm, which originates a molten pool with sizes varying from 120 to 150 μm. With this dimensions in mind, the precision difference results in a half width of the molten pool, originating a theoretical maximum dimensional accuracy of 0.1 mm [112]. This inferences demonstrate one common problem, that is the exaggeration of machine capacities by the machines makers.

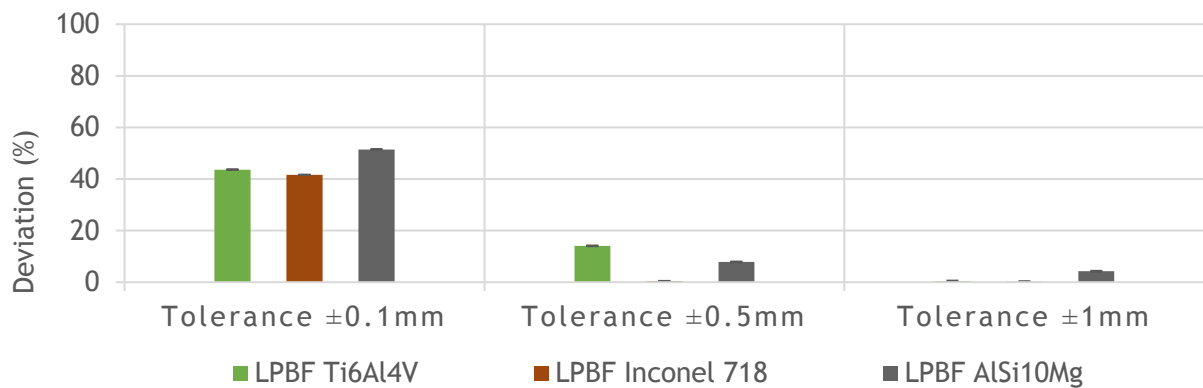


Figure 36 - Deviation values at different tolerances of the LPBF demonstrators.

7.1.2. EBM demonstrators

The CT analysis was also capable of analyzing the EBM demonstrators. Even though, the placement inside the CT was different from the ones made through LPBF. This was because of the supports on the demonstrators increased the travel path of the X-rays. This required that the EBM demonstrators were placed on the horizontal instead of the parallel position like the LPBF ones.

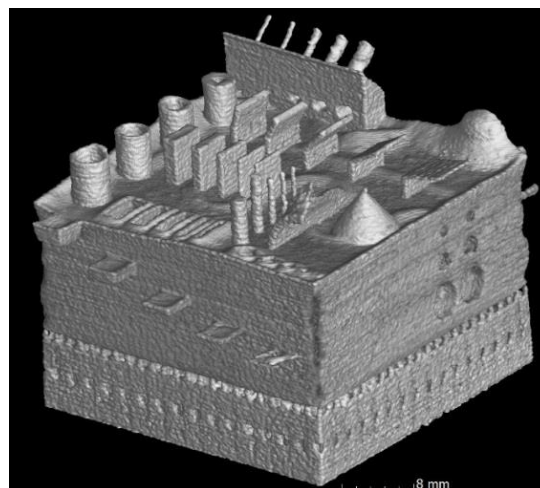


Figure 37 - EBM demonstrator with 3x3 mm base square size.

The EBM demonstrators didn't reproduce accurately the features on the CAD file, since they suffered from swelling on the Z direction that distorted the overall part and also shrinkage around the part. The swelling defect has been studied by various authors [113-117] and indicates that high beam energies of 300 J/m or above were used (Annex R). The exact mechanism that originates swelling is still unclear, but seems to be linked with excessive temperature and surface tension effects on the weld pool, being more predominant on sharp corners of the parts.

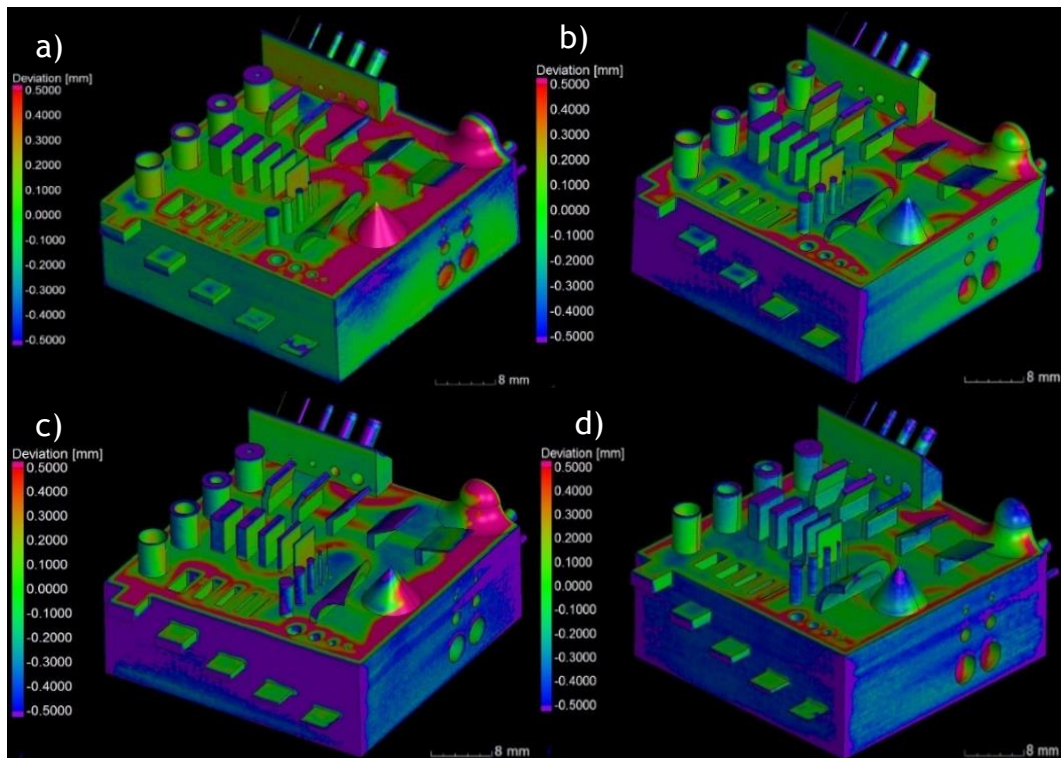


Figure 38 - Comparison of the EBM demonstrators against the CAD file at ± 0.5 mm tolerance. A) 6x6 mm; b) 5x5 mm; c) 4x4 mm; d) 3x3 mm square size.

CT analysis of the internal channels shows that the excessive temperature used during the EBM process led to the sintering of powder inside the internal channels of all demonstrators (Figure 39). This sintered powder obstructed totally the channels and was impossible to remove by finishing processes.

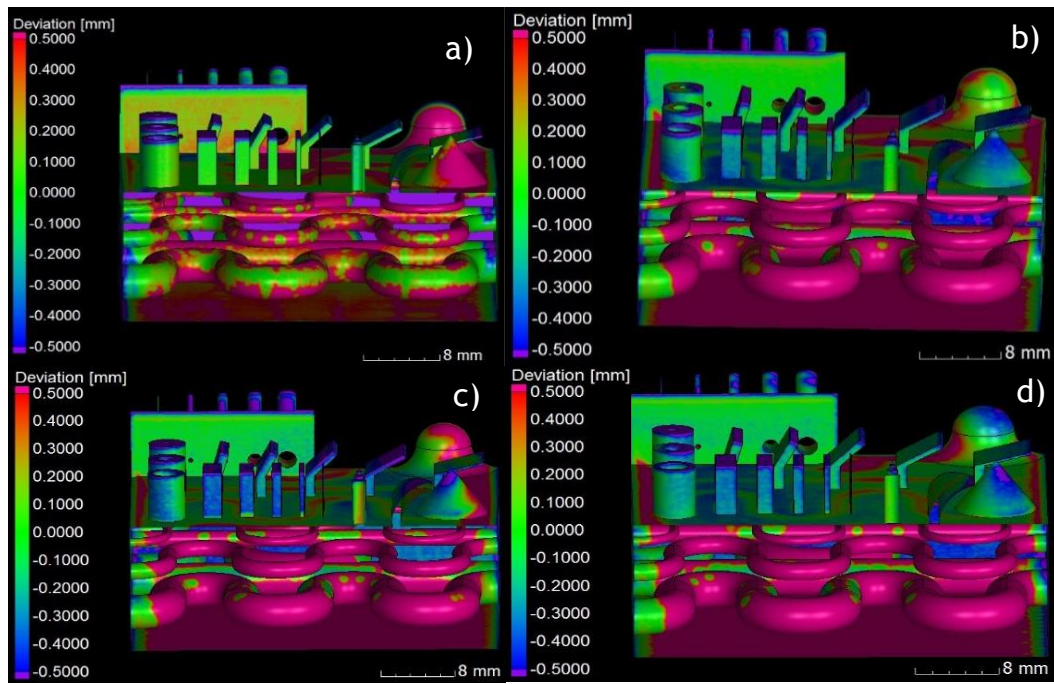


Figure 39 - Comparison between the CAD at ± 0.5 mm tolerance with a perpendicular cut of the EBM demonstrators. a) 6x6 mm; b) 5x5 mm; c) 4x4 mm; d) 3x3 mm square size.

Comparison of deviation percentage of EBM demonstrators at different tolerance distances (Figure 40) revealed a positive effect of smaller square grid size that promotes higher heat transfer from the part to the base, which results in less swelling and distortion. But even at ± 1 mm tolerance the demonstrators didn't reach a minimum threshold of 10% deviation to be considered good parts. The 6x6 mm demonstrator displayed visually the highest distortion, though displaying slightly best results at ± 0.1 mm and ± 1 mm tolerance (85.8 and 32.8 % respectively). This improvement might be due to the *Best fit registration* of the part made on VGstudio MAX. This kind of registration will tend to match the part to the CAD file by minimizing the deviation and because the demonstrator was so deformed it could fit them in such a way that masked the deviation.

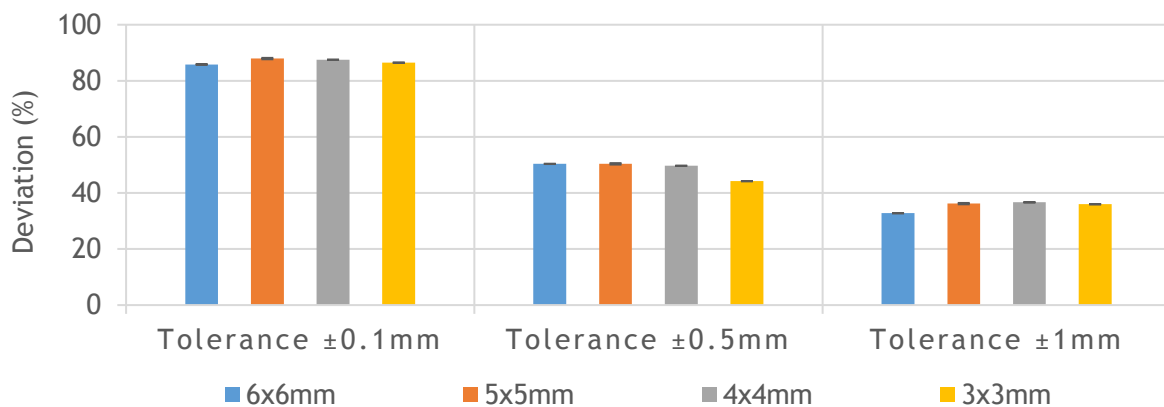


Figure 40 - Deviation of the EBM demonstrators at different tolerances.

7.1.3. Overview of LPBF and EBM

For an overview of the LPBF and EBM processes it was compared the EBM demonstrator that displayed lower deviation values (3x3 mm grid) against the ones produced through LPBF. Figure 41 shows that EBM had a much higher deviation values than the LPBF, reported on chapter 3.2.1. It was also noted that the higher precision of LPBF remains even when different materials are used.

However, this variation of the results also highlights the necessity of careful parameter selection and the high user experience when producing parts through AM processes. This precautions undermine the common notion of AM as a direct CAD to part technology that only needs a push of a button to produce a part.

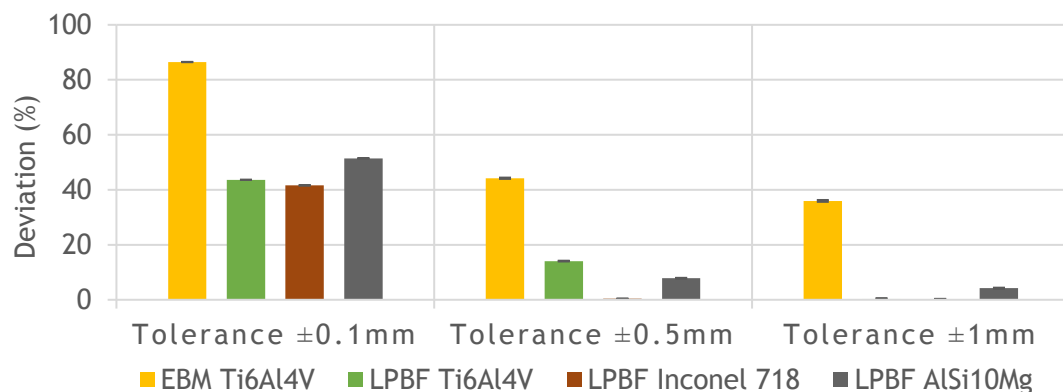


Figure 41 - Comparison of deviation of the EBM demonstrator 3x3 mm and the LPBF demonstrators at different tolerances.

7.2. Comparison of CT against 3D scanning

Both techniques could digitize the simple geometry of the nozzle made by EBM, but in the 3D scanner it is noticeable a loss of surface texture (Figure 42 - b). Since the access to interior of the nozzle is difficult for the 3D scan, this resulted in a missing spot on the interior of the nozzle digitalization, marked green on Figure 42 - d). On the other hand, the CT didn't have any difficulties to perform the scan.

The loss of surface texture on the 3D scanner might be due to two factors: the spray used to reduce the reflection of the metal part, or the minimum feature resolution of the 3D scan GOM ATOS 135. The loss of surface texture could be reduced by using a finer spray powder, as well a 3D scanner with higher resolution like the GOM ATOS 45. Nevertheless, when using this 3D scanner with a smaller scanning area the

scanning time will be much longer and the need of more image captures will increase, leading to the risk of increasing the error measurement.

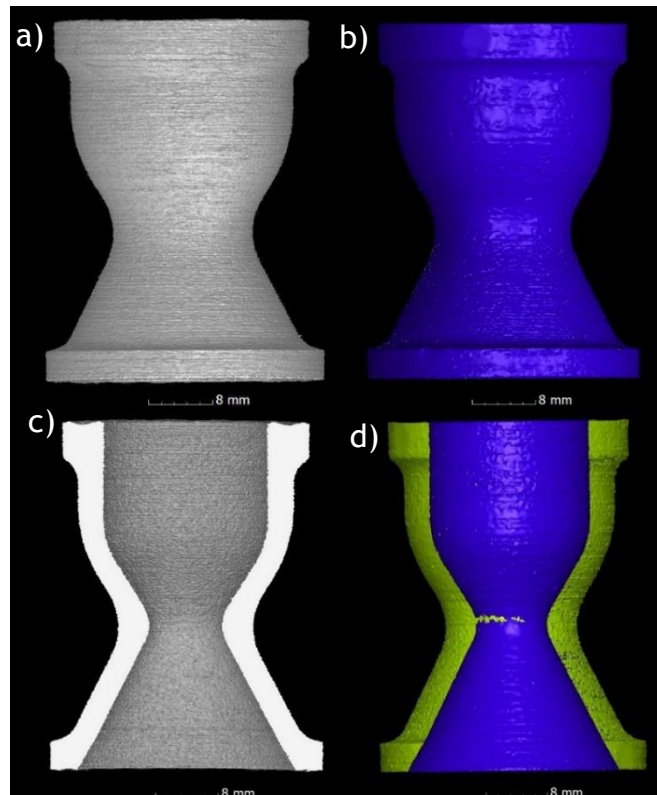


Figure 42 - EBM nozzle scanned by CT and 3D scanner. a) CT reconstruction front view; b) 3D scanner, front view; c) CT half cut; d) 3D scanner half cut.

Both CT and 3D scan made 3D objects that during the comparison with CAD showed the shrinkage that occurred on the Z direction on the base of the nozzle (Figure 43).

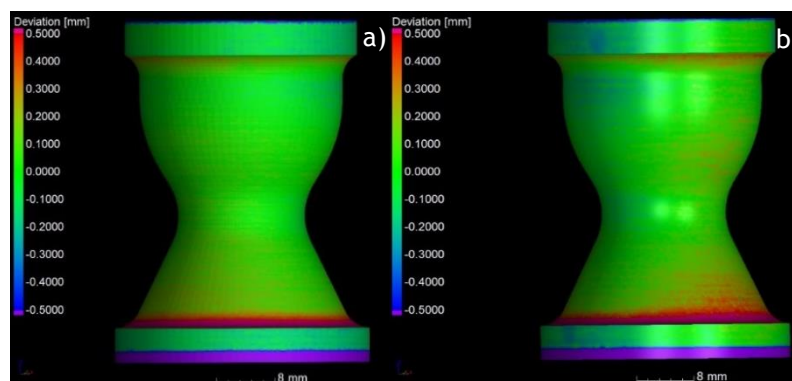


Figure 43 - Nominal/actual comparison of the nozzle at ± 0.5 mm tolerance. a) Comparison against the CT object; b) Comparison against the 3D scanned object.

The *nominal/actual comparison* of both scans against the CAD file reveals similar results, but a highest divergence is more noticeable at ± 0.1 mm tolerance (Figure 44). Ideally both measurements should give the same deviation values. The present results might be explained by the fact that the markers used appear on the surface

of the nozzle after the scan, although the GOM ATOS Professional trims them flat with the part, leaving a flat spot (Figure 45 - a).

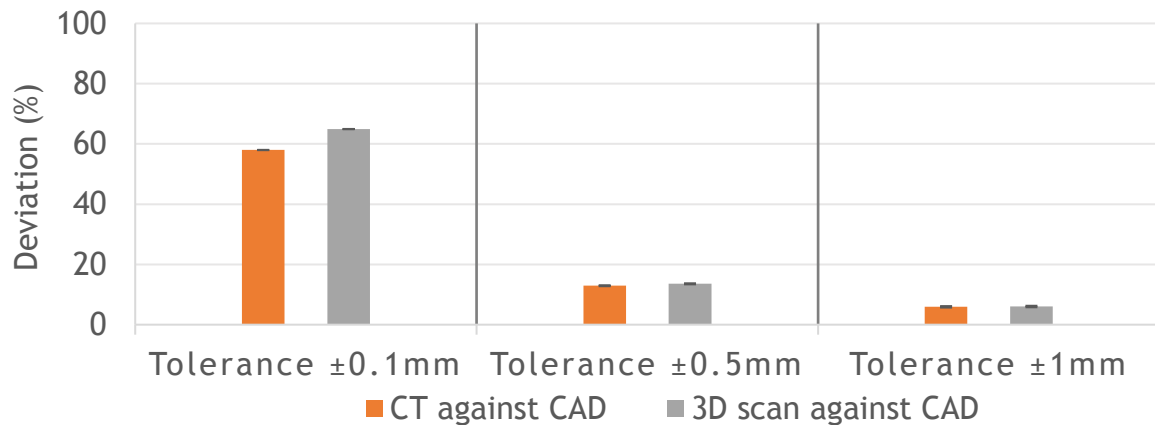


Figure 44 - Comparison of the CT and 3D scanning against the same CAD file at different tolerances.

Another reason is the apparent periodic deviation that appears around the nozzle that is especially visible on the comparison at ±0.1 mm tolerance (Figure 45 - b)). These strips of deviation indicate that measurement error is being introduced during the rotation and tilting of the part during scan.

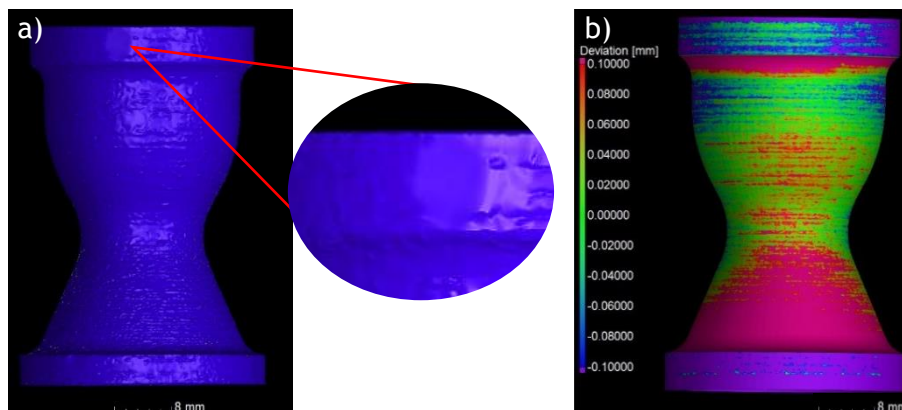


Figure 45 - 3D scanned nozzle. a) Detail of the marker used on the nozzle; b) Comparison of the 3D scanned nozzle with the CAD file at ±0.1 mm tolerance.

Concerning to 3D scan of the LPBF Inconel 718 demonstrator the part wasn't tilted to ensure maximum accuracy of the features on the top of the demonstrator, which originated large gaps of the scan (Figure 46 - a). Nevertheless the resulting 3D digitalization of the demonstrator was enough to make a deviation analysis of the individual features present on top of the demonstrator (Figure 46 - b).

The deviation of the three set of features measured are presented on the Table 6. These results show that deviation tends to increase for smaller features and that

sizes below 0.5 mm are largely over built, which is consistent with previous experiments done in this work, described on the Geometric analysis chapter 7.1.1.

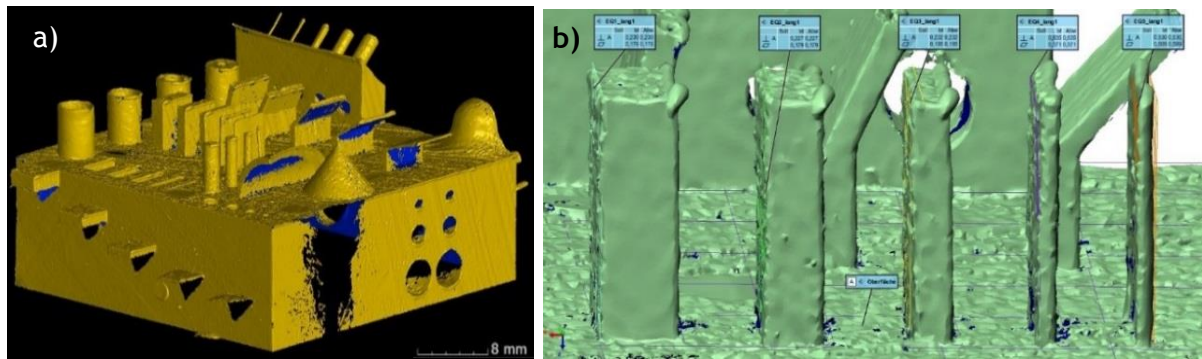


Figure 46 - a) 3D scan of the LPBF demonstrator made of Inconel 718; b) Detail of the compact volumes.

Table 6 - Deviation of the measured features through 3D scan on the LPBF demonstrator made of Inconel 718.

Feature	Objective	Dimension (mm)	Deviation (%)
Cylinders	Cylindricity	0.5	-24
		1	-12
		1.5	-9
		2	-6
Overhangs	Angle	15	2
		30	-4
		45	0
		60	-1
		75	-4
Compact volumes	Thickness	0.1	193
		0.5	-34
		1	-9
		1.5	-8
		2	-7

Comparing 3D with the CT analysis, CT scan can also make similar feature measurements but presents the advantage of inspection of the internal geometries, as can be seen in Figure 47. This renders 3D scanning more adequate for simple geometries with swallow holes where it is possible to make some accuracy measurements and deductions of part quality, being an economic approach for part inspection, since an industrial 3D scanner can cost around 30000 € and a CT scan more than 500000 €. In terms of time taken to scan a part, both methods present almost the same time of around two hours. The 3D scan is more labor intensive, requiring more sample preparation, needing the placement of markers, powder spraying and manual rotation of the part. The 3D scan can be automatized through a robotic arm or other method, which performs always the same routine. However, this is not viable for AM industry where the objective is a total flexibility on the parts

produced. On the other hand, after the parameters are set on the CT the scan is made automatically, but the result of the two hours scan it's only known at the end. If the results have a lot of artifacts/noise, the scan must be repeated with different parameters, taking an additional two hours. In the 3D scan this problem doesn't appear since the capture of the object is displayed on the computer screen while the scan is being made.

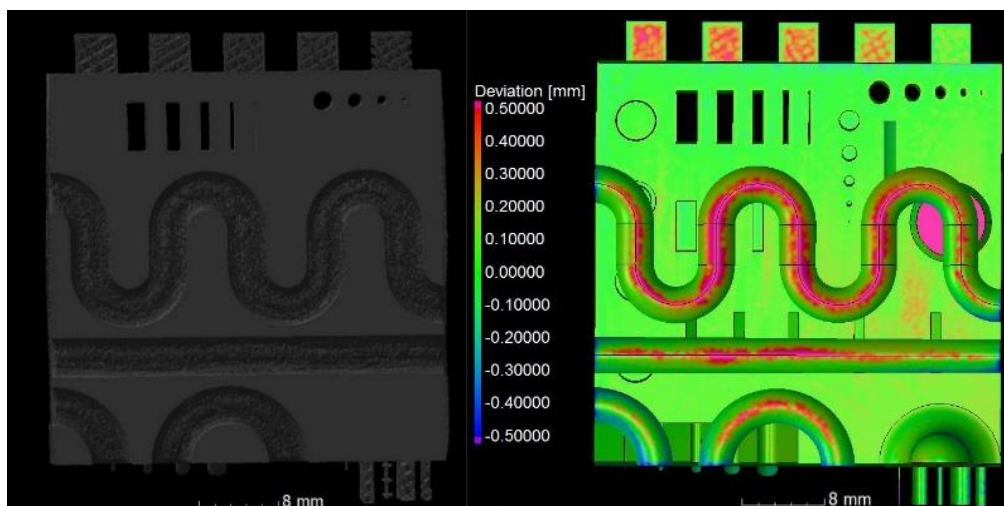


Figure 47 - Horizontal cut of the Ti6Al4V LPBF demonstrator and comparison with CAD.

7.3. Porosity Analysis

One of the main advantages of CT scanning is the possibility to analyze porosity, inclusions and cracks in a non-destructive way. In this work the porosity present on the Inconel 718 cubes was identified (Figure 48) and was clearly visible on the 2D projections (Figure 48 - d)). The porosity present in the cubes was uniformly distributed, with the exception of cube n° 14 where it displayed an elongated form. However, during the course of this work the parameters chosen for the porosity analysis revealed as a major factor, since they influence heavily the amount of porosity detected.

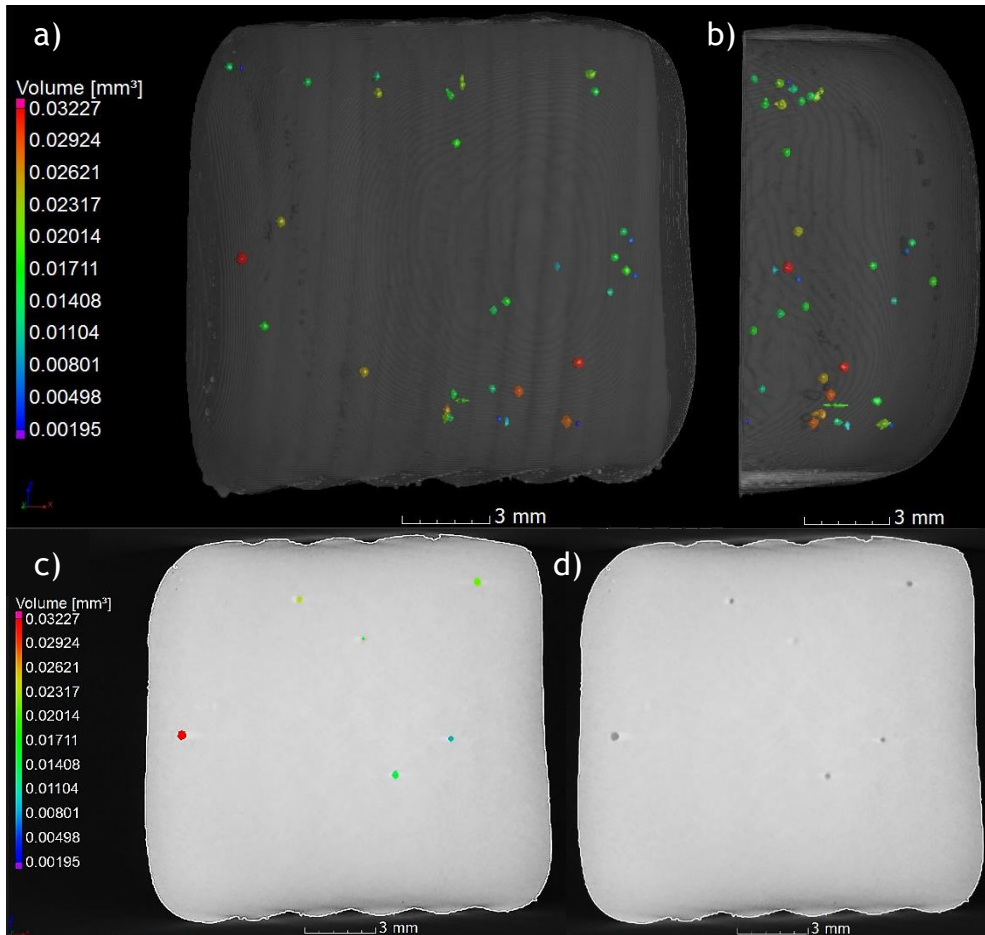


Figure 48 - Porosity analysis of cube n°2 with interpolation factor 1 and probability filter 1. a) 3D front view with 70% transparency; b) 3D side view with 70% transparency; c) 2D front view; d) 2D front view without analysis.

The parameters influenced so much the detection that it could make pores pass completely undetected (Figure 49 - a). This is due to the fact that increasing the interpolation factor makes possible the detection of lighter gray values. This allows the detection of pores with low contrast (Figure 49 - b). However, it will also increase the amount of noise detected because of the different gray shades along the part.

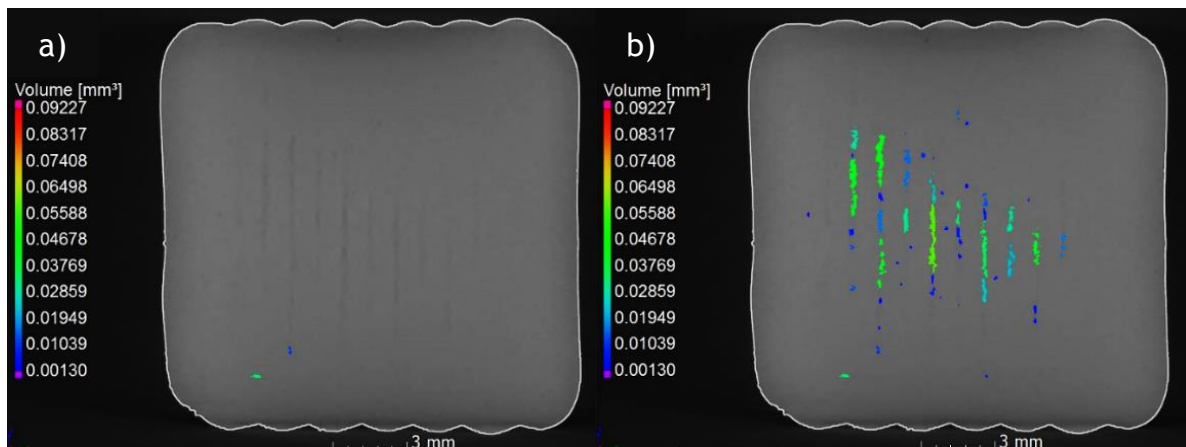


Figure 49 - Porosity analysis of cube n°14. a) Interpolation factor 1 and probability 1; b) Interpolation factor 1.4 and probability 0.3.

The detection of lighter gray values will also influence the shape and volume of the detected porosity, since it will detect more voxels on the surrounding pore (Figure 50 - a)). In addition the sharpness of the pore image leads to some uncertainty to the exact limits of the pore (Figure 50 - b)).

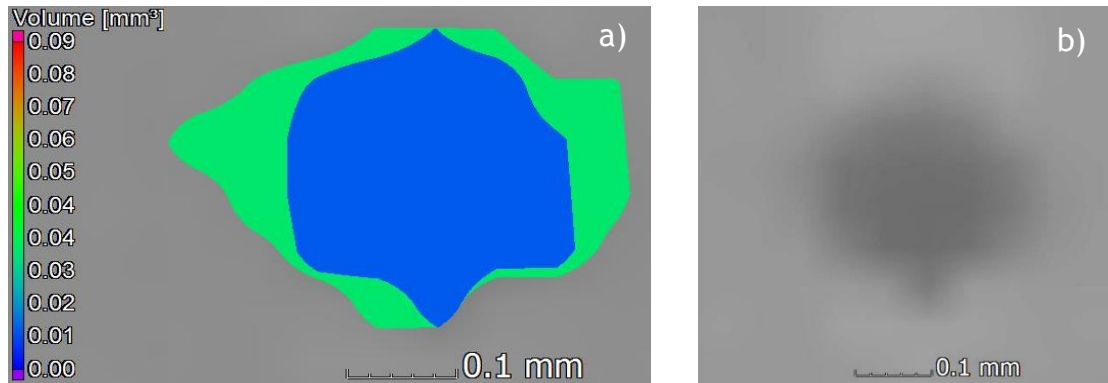


Figure 50 - Front view of a pore on cube n°3. a) Analysis of the pore with different parameters. Green - interpolation factor 1.4 and probability 0.3; blue- interpolation factor 1, probability 1; b) Pore without analysis.

It was also noted that the detection of lighter gray values made the porosity shape change to a more elongated form (Figure 51). That might be due to two different reasons: one of them being the true nature of the pore being detected, that has a tendency to grow in the build direction; the other reason might be due to streak artifacts, since the cubes were mounted parallel to the X-ray source and the narrower part of the cube is on the Z direction.

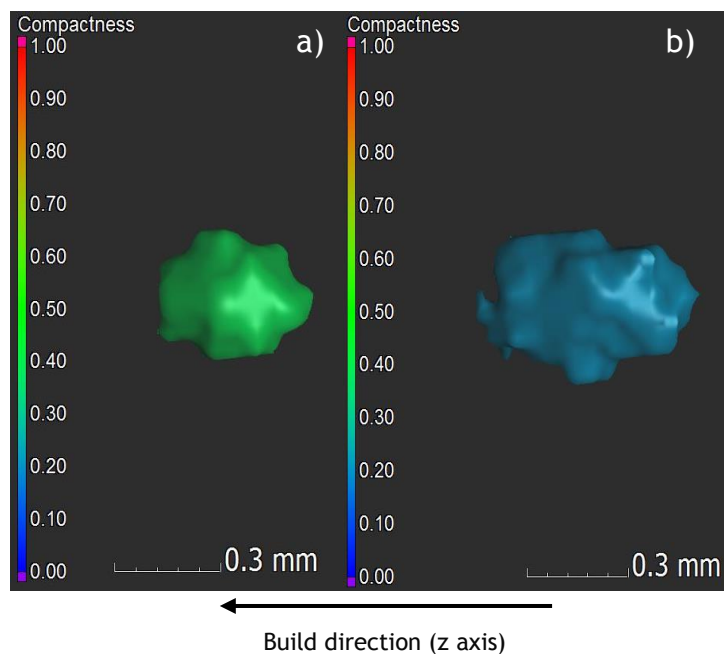


Figure 51 - Side view of a pore on cube n°3 with different parameters. a) Interpolation factor 1 and probability 1; b) Interpolation factor 1.4 and probability 0.3.

By analyzing the average between the characteristics of the porosity detected through different parameters, it can be noticed the decrease on sphericity and compactness values when analyzing lighter gray shades. It also increases the detection of noise (small dimension pores falsely identified) that reduce the average size of the detected porosity (Table 7).

Table 7 - Average of different characteristics detected through different parameters.

Conditions	Average sphericity	Average compactness	Diameter average (mm)	Average nº of pores identified
Interpolation 1 Probability 1	0.59	0.31	0.50	36
Interpolation 1.4 Probability 0.3	0.57	0.28	0.47	118

Comparing the results of relative density through CT analysis and Archimedes method (Figure 52), it can be seen that the analysis through VGStudio MAX 3.0 was capable of identifying the porosity but it didn't quantify precisely the amount of porosity on the samples. Setting different sets of parameters for the porosity analysis didn't make the quantity of porosity detected greatly diverge. Even with the operator choosing the best parameters for each sample in order to ensure that the pores had been identified, wasn't enough to provide results below 99% relative density. The difficulty to measure porosity accurately was also noted by other authors [68, 71].

The difficulty might be due to the inability of the CT analysis in detecting pores with a diameter inferior to 0.1 mm, which might be present on the samples. They might not appear on the analysis because this pore size is below the resolution capacity of the CT for this kind of material, or during the reconstruction the selected options suppressed those pores through the averaging of gray values and bad pixel reduction.

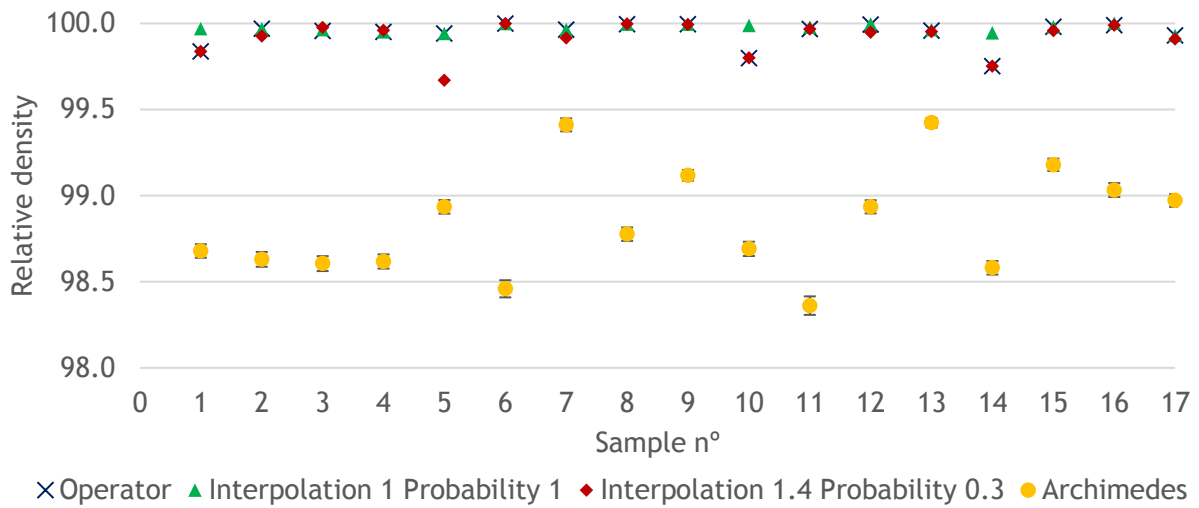


Figure 52 - Relative density obtained by CT with different analysis parameters and Archimedes method.

Archimedes method measures all pores indiscriminately disregarding size, sphericity and compactness of the pores. The morphology of the pores could be measured by CT and correlated with the building parameters (

Annex N). However, in this work it wasn't detected any relationship between build parameter's and porosity shape. The results on the morphology of the porosity was dependent of the parameters chosen for the porosity analysis, which also hindered the conclusions taken.

The relative density value is also dependent on the total volume. Figure 53 shows the total volume determined for each Inconel cube through CT and Archimedes method. The volume determined through CT registered a deviation mean of $-1.2 \pm 0.6\%$ from the one registered through Archimedes method. Although the Archimedes method had an average measurement error of 0.5% it is not enough to justify the difference of relative density between the two methods, but highlights the tendency of CT to slightly under detect volumes, mainly due to image sharpness and artifacts. However, it shows the high accuracy capacity of CT in these kind of measurements.

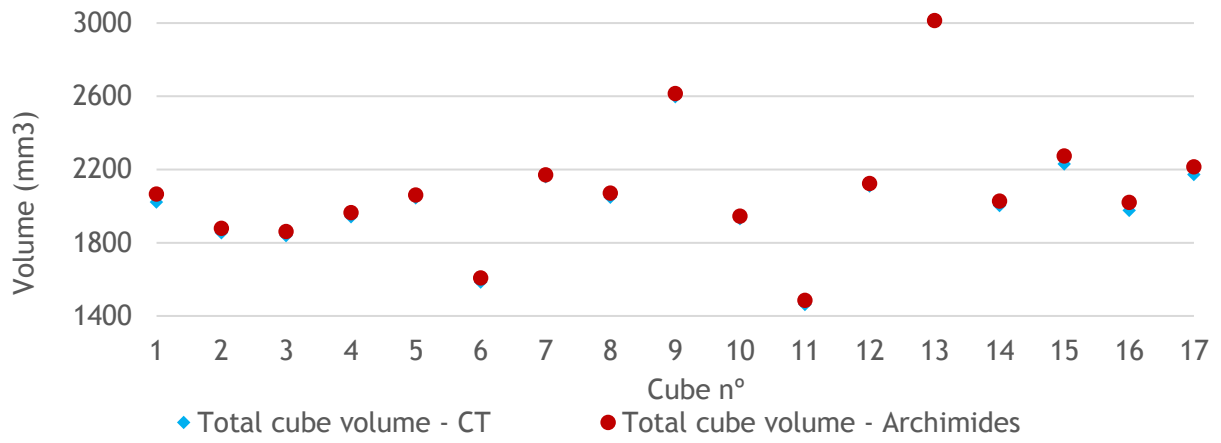


Figure 53 - Total volume for each Inconel cube done by CT and Archimedes method.

The current standards for CT mainly focus on dimensional accuracy measurements and there are lacking standards for porosity analysis. The only way to improve the porosity results through CT would be to calibrate the CT parameters to match the porosity measured through microscopy. For this it would be necessary to analyze a sample through CT, identify the porosity present on the sample and then make a metallographic analysis of the sample where a specific pore would be measured through microscopy. Afterwards, the parameters used on the porosity analysis on VGStudio MAX 3.0 would be selected to match with the measurements made through microscopy. The scan and reconstruction parameters would also need adjustment in order to match the overall porosity identified on the microscopy and the volume measured by Archimedes method.

This kind of destructive method process might be adequate for measuring large series but it is not a very practical process to measure one of a kind of AM parts. One solution would be the suggestion by P.Hermanak and S. Carmignato [118], by using a reference object with demountable pins that have micro milled defects on the surface, which are used for calibration. This method has also various short comings like:

- The need to make pins of the same material as the one analyzed;
- It doesn't account for sample thickness, that influences X-ray penetration and gray value distribution along the sample;
- The geometry of the samples influence the appearance of artifacts that hinder the surface determination, which will affect the volume of the sample detected.

7.4. Reconstruction settings assessment

During the CT analysis one of the steps is to define the reconstruction parameters for the reconstruction on the YXLON ReconsPOOLer. To evaluate the effect of the parameters on the properties of the reconstructed object these parameters were changed one at a time while keeping the others constant.

In Figure 54 it is represented the total volume of cube n°3 measured by Archimedes method and CT with different reconstruction parameters. The variation of the reconstruction parameters resulted on a mean total volume of $1838 \pm 1 \text{ mm}^3$ with the

highest value of 1841 mm³ for all filters inactive. The values are all lower than the 1860 ±10 mm³ measured by the Archimedes method. These results show that CT analysis has certain difficulty with high precision measurements comparing with well-established physical methods. Although, the reconstruction parameters didn't affect greatly the volume detected, they highlight the variation that can be achieved through the parameters selected during reconstruction.

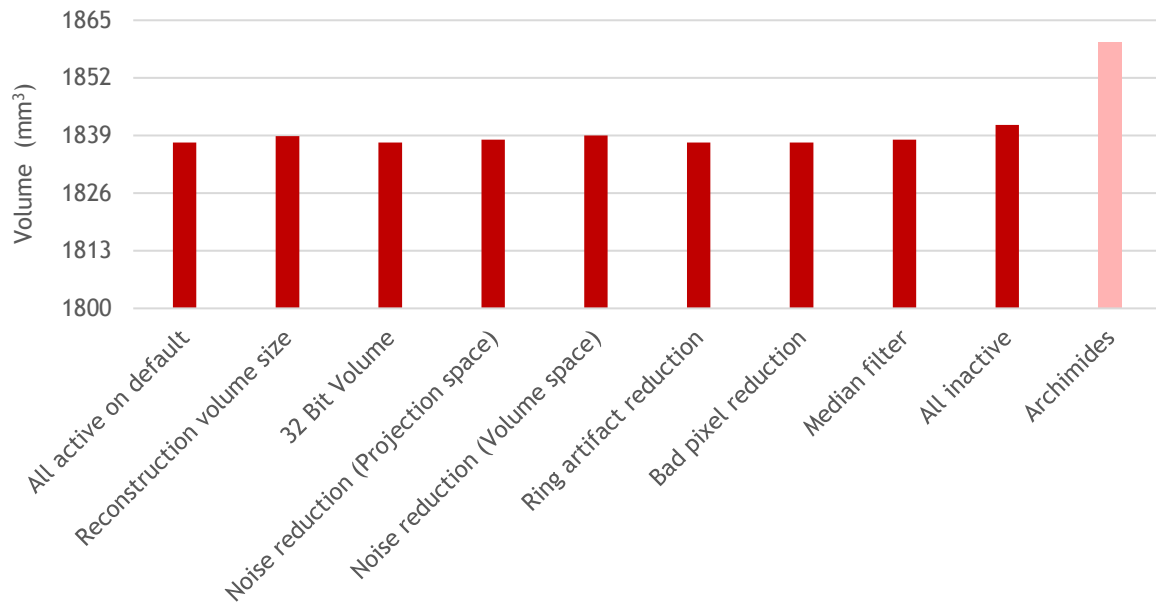


Figure 54 - Total volume of cube n°3 measured through CT with different deactivated reconstruction parameters and Archimedes method.

This difference from the volume measured through Archimedes method might be due mainly to two factors: magnification and artifacts.

Magnification is done by approaching the sample to the X-ray source: this enlarges the image on the detector and allows the observation of smaller defects but also increases edge blurriness, which in turn affects the volume detected during surface determination. This effect increases for smaller samples since they need higher magnification to avoid the use of a very large reconstruction volume size, which would increase exponentially the file size. It might also be expected an increase of the effect of the reconstruction parameters on the volume detection, since they will reduce noise and average out the blurriness.

The main type of artifacts that might affect the volume detected are beam hardening artifacts; this kind of image defect affected the reconstruction mainly on sharp edges, which have thinner section and therefore lower attenuation of X-rays. This originated darker gray values that affected surface determination.

The porosity detected on cube n°3 was also different for the different parameters as shown on Figure 55. The mean porosity volume detected during the variation of the filters was $0.7 \pm 0.3 \text{ mm}^3$ (reconstruction volume is not a filter); this value is lower than the one obtained through Archimedes ($25.9 \pm 0.2 \text{ mm}^3$). Previous studies by other authors [68] also state the inferior detection of porosity in comparison with Archimedes method.

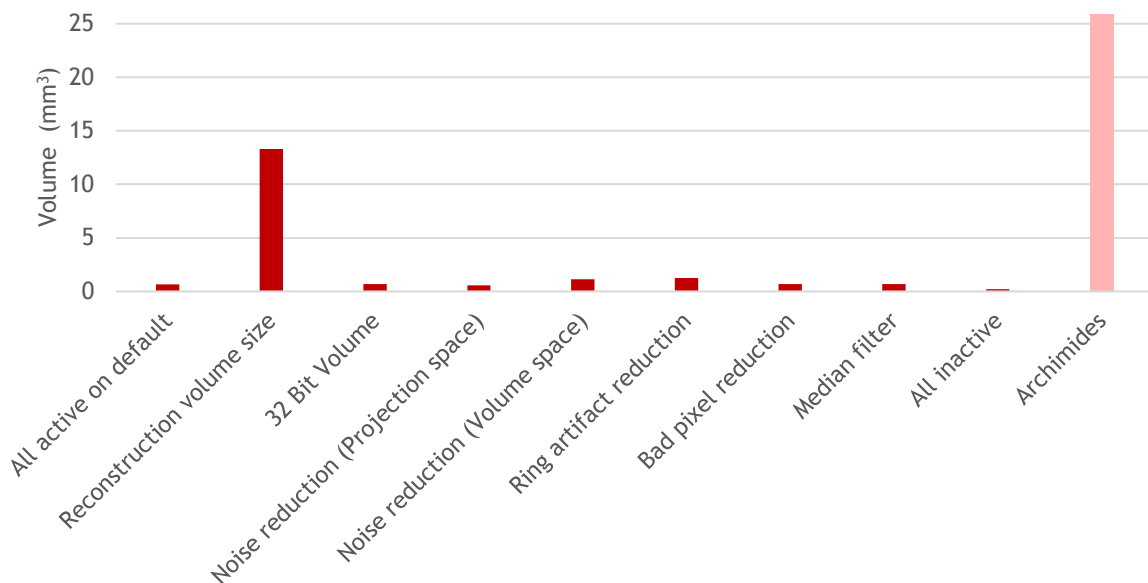


Figure 55 - Total porosity volume detected through CT with different reconstruction parameters and Archimedes method.

The lowest value detected was for all inactive filters (0.2 mm^3). This setting was the one that registered a higher total volume but it generated image projections with a lot of noise (Figure 56). This leads to a difficulty on the detection of the pores since the parameters chosen for the porosity analysis (*Noise reduction - High*) eliminated many of the pores.

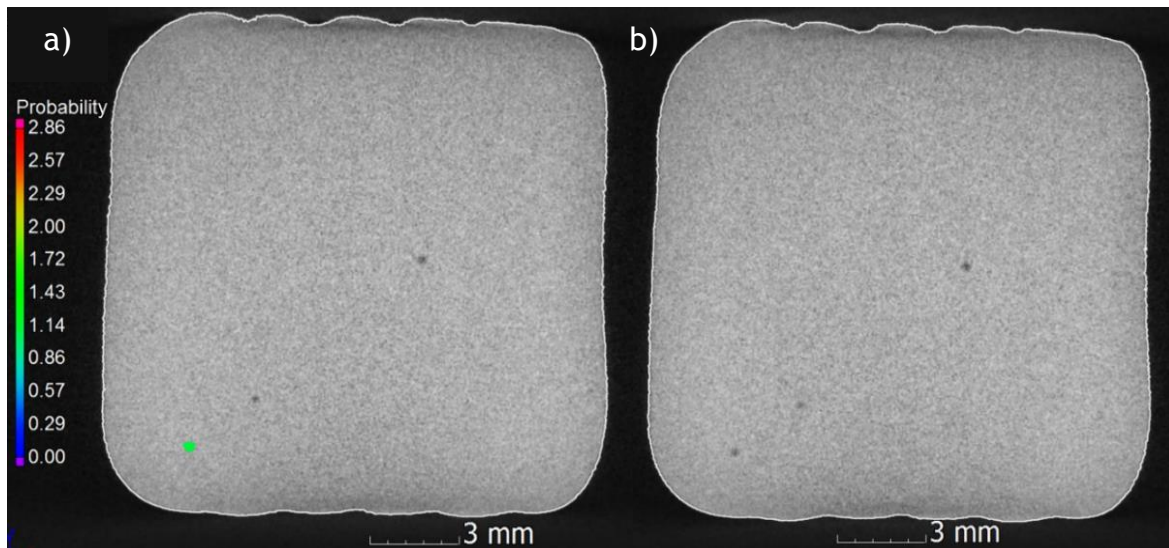


Figure 56 - Front view 2D projection of cube n°3 with all filters disable.

On the other hand the parameter that registered more porosity was the Reconstruction volume. This parameter was set to ISO voxel that automatically sets the horizontal pixel count according to the current detector settings that curiously is always 2166. This originated a voxel size of 0.013 mm and a file size of 16 GB, while the reconstruction volume of 512 originated a voxel size of 0.054 mm and a file size of 236 MB. This lower voxel size allowed the detection of more noise but with smaller dimensions (Figure 57).

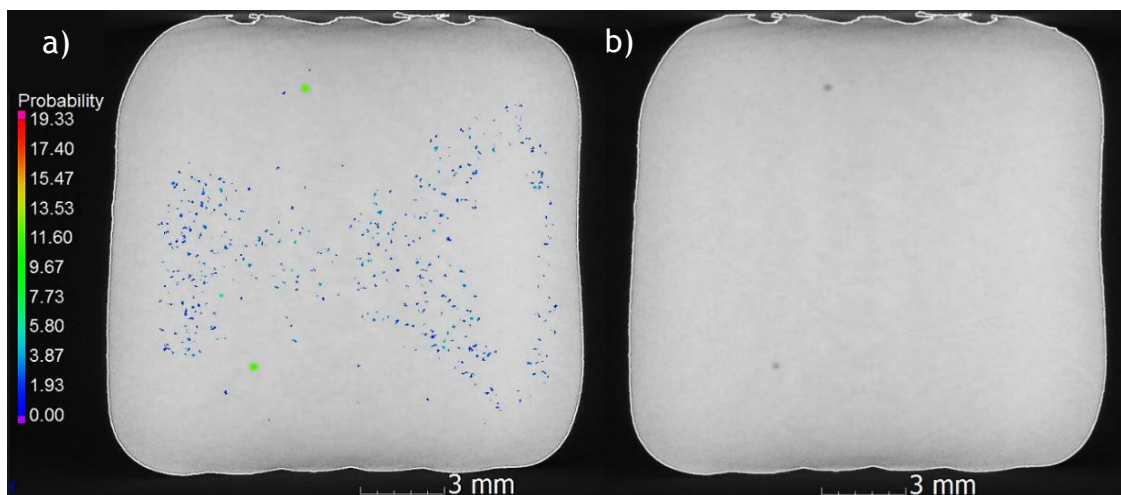


Figure 57 - Front view 2D projection of cube n°3 with reconstruction volume size set to ISO voxel - 2166 hpc.

8. Conclusions and Outlook

AM is truly a digital era production method as it opens new doors and has true potentialities in making complex geometries and difficult processing metals while reducing time between concept to final part, allowing an economic production of one-of-a-kind parts. However, AM is to a certain extent, a victim of media attention, that so many times happens in science due to excessive optimism on a newly discovered process. The internship developed at Fraunhofer Institute IWS allowed the sight of the state of the art of development in AM and the challenges that need to be overcome until AM becomes a more widely applied production method and turn out as an alternative to conventional production methods. One of the main challenges in AM is the qualification and certification of parts, being identified as a critical issue when AM is adopted for the production of structurally critical components. The qualification of parts through optimization of build parameters and in build monitoring still needs more development and research; quality control on the final part is for the time being the only method to control the quality of AM parts. For this CT is the method that allows a more complete non-destructive inspection, allowing dimensional measurement of inner features and verification of porosities/cracks.

In this work there were compared CT and 3D scanner in quality control through several experiments. On the geometric comparison with the CAD file of the demonstrators the CT was capable of analyze them internally and provide a value for total deviation. In the analysis of the demonstrators made through LPBF they registered different deviation values, with the best result being the one made of Inconel 718 by Fraunhofer IWS in a Renishaw AM250. During the geometric analysis of the Inconel demonstrator, the high X-ray attenuation caused a possible reduction of the deviation values made by VGStudio MAX 3.0 during the *Best fit registration*. The analysis of the deviation of all demonstrators at different tolerances revealed that the machines couldn't reproduce accurately features with sizes below 0.5 mm. The analysis of the EBM demonstrators showed a reduction swelling effect when using supports with smaller square grid sizes. However, the high energy/temperatures used still caused some swelling and sintering of the powders inside the internal channels which caused higher deviation in comparison with the ones made through LPBF. The demonstrator developed by Fraunhofer IWS proved to be a good standard

to test different institutes, machine limits and materials. Nevertheless, it is recommended that the demonstrator should be thinner, to allow a better X-ray penetration for high attenuation materials.

The comparison of CT against 3D scan highlighted some challenges when measuring parts with 3D scan. It demonstrated the difficulty of analyzing highly reflective objects, requiring the use of powder to mask the brightness, which hindered the surface resolution and accuracy. Also it was showed that the rotation of the nozzle during scan introduced a periodic deviation around the part and that the markers used appear on the scanned 3D object; so 3D scanned nozzle displayed a higher deviation value when comparing with the results through CT.

The scan of the top features on the Inconel 718 demonstrator using the 3D scan revealed that the features with size of 0.1 mm were largely overbuild. This result matches the previous conclusion made in the geometric comparison of the demonstrators, where it is stated that the LPBF machine couldn't reproduce accurately features with sizes inferior to 0.5 mm. This results render 3D scanner as a good and more economic approach for quality control of the geometrical accuracy on external features in parts made by AM.

In the analysis of seventeen samples made of Inconel 718 through DED, the CT was able to determine the volume of the sample with minimum deviation of $-1.2 \pm 0.6\%$, besides identifying the porosity and its distribution on the samples. However, it was unable to quantify correctly the total volume of the porosity, which resulted in a higher relative density in comparison to the result through Archimedes method. The main reason for this difference stems from the resolution limits of the CT, since it was unable to detect porosity with a diameter size inferior to 0.1 mm. Further study into the porosity analysis parameters in VGStudio MAX 3.0 also revealed that the quantity and morphology of the identified pores changed with the different parameters. Being that the detection of lighter gray values allowed the detection of pores with lower contrast, but increased detection of noise. It also reduced the sphericity/compactness of the pores, which became more elongated.

Finally, the study of the reconstruction parameters revealed that they don't vary significantly the determined volume ($1838 \pm 1 \text{ mm}^3$) for the analyzed sample, although, it was lower than the volume measured through the Archimedes method

($1860 \pm 10 \text{ mm}^3$). This difference is mainly due to magnification and beam hardening artifacts. On the porosity analysis the variation of parameters registered an average porosity of $0.7 \pm 0.3 \text{ mm}^3$ that was significantly lower than the determined through Archimedes method ($25.9 \pm 0.2 \text{ mm}^3$). The higher porosity registered was 13.3 mm^3 for the ISO voxel, but the 2D projections reveal that much of identified porosity was noise.

The results on this work confirm that CT is a technique that fills many of the needs for non-destructive quality control of AM parts, with 3D scan as an economic alternative. Although it was also shown that it is very reliant on of the parameters set with a three level dependency between the three main stages of scanning, reconstruction and analysis. In each stage, there are even more parameters that can be changed that might modify the final measurements. All this variation makes it very difficult to quantify the accuracy of the CT and its traceability, revealing the necessity for more standards that uniform the measurements through different machines and operators. CT is also a time-consuming procedure that requires several hours to set, run, analyze and generate a report for each new part. In the present time, CT machines are more optimized for industrial measurement of large series of parts. But with the expected growth of the AM market, future CT machines should be more focused on the necessities of the AM industry to shorten time scanning and analyzing. This specialization might come with the possibility to import CAD/.stl part file and also the definition of the material to be analyzed which would allow the machine to suggest and pre-set the best strategy and parameters, as for example, part placement, power to use, filter material and thickness. Such possibilities would also decrease the variation of the results between different CT machines.

In this work the challenges faced in practice when using non-touching methods for quality control of AM parts were thoroughly explored. With CT being the most complete approach for part inspection of AM parts, providing a very good picture of the health of the part. Nonetheless there are still some issues that need to be better understood before CT is used as a final approval method. However, with the resolution of these issues, the towering problem of quality control in AM could be finally solved, making the great promises of AM be a little closer to the present.

References

- [1] "A third industrial revolution | The Economist." [Online]. Available: <http://www.economist.com/node/21552901>. [Accessed: 10-Oct-2016].
- [2] S. H. Huang, P. Liu, A. Mokasdar, and L. Hou, "Additive manufacturing and its societal impact: A literature review," *Int. J. Adv. Manuf. Technol.*, vol. 67, no. 5-8, pp. 1191-1203, 2013.
- [3] E. Atzeni and A. Salmi, "Economics of additive manufacturing for end-usable metal parts," *Int. J. Adv. Manuf. Technol.*, vol. 62, no. 9-12, pp. 1147-1155, 2012.
- [4] G. Tapia and A. Elwany, "A Review on Process Monitoring and Control in Metal-Based Additive Manufacturing," *J. Manuf. Sci. Eng.*, vol. 136, no. 6, p. 60801, 2014.
- [5] W. E. Frazier, "Metal additive manufacturing: A review," *J. Mater. Eng. Perform.*, vol. 23, no. 6, pp. 1917-1928, 2014.
- [6] N. Guo and M. C. Leu, "Additive manufacturing: Technology, applications and research needs," *Front. Mech. Eng.*, vol. 8, no. 3, pp. 215-243, 2013.
- [7] I. Gibson, D. Rosen, and B. Stucker, *Additive Manufacturing Technologies*. New York, NY: Springer New York, 2015.
- [8] T. Wohlers and T. Gornet, "History of Additive Manufacturing," *Wohlers Rep. 2014 - 3D Print. Addit. Manuf. State Ind.*, pp. 1-34, 2014.
- [9] ".STL File Format In 3D Printing: Explained in Simple Terms | All3DP." [Online]. Available: <https://all3dp.com/what-is-stl-file-format-extension-3d-printing/>. [Accessed: 25-Oct-2016].
- [10] Jon Cobb VP of Global Marketing Stratasys Inc., "Additive Manufacturing 101: How the Future of Product Development and Manufacturing is Changing - YouTube." [Online]. Available: <https://www.youtube.com/watch?v=001b4Ha4hOA>. [Accessed: 20-Oct-2016].
- [11] I. Campbell, D. Bourell, and I. Gibson, "Additive manufacturing: rapid prototyping comes of age," *Rapid Prototyp. J.*, vol. 18, no. 4, pp. 255-258, 2012.
- [12] K. V. Wong and A. Hernandez, "A Review of Additive Manufacturing," *ISRN Mech. Eng.*, vol. 2012, pp. 1-10, 2012.
- [13] W. Y. Y. Chee Kai Chua, "Bioprinting - Principles and Applications," *World Sci.*, 2010.
- [14] J. I. Lipton, M. Cutler, F. Nigl, D. Cohen, and H. Lipson, "Additive Manufacturing for the Food Industry - A review," *Trends Food Sci. Technol.*, vol. 43, no. 1, pp. 114-123, 2015.
- [15] F. P. W. Melchels, M. A. N. Domingos, T. J. Klein, J. Malda, P. J. Bartolo, and D. W. Hutmacher, "Additive manufacturing of tissues and organs," *Prog. Polym. Sci.*, vol. 37, no. 8, pp. 1079-1104, 2012.
- [16] ISO/ASTM, "Standard terminology for additive manufacturing," vol. 2013, 2013.
- [17] B. B. Karl Rundman, *Metal Casting - Quickest least expensive route to near net shape product*. Michigan: Dept. of Materials Science and Engineering Michigan Tech. University, 2005.
- [18] F. Cooper, "Sintering and additive manufacturing: 'additive manufacturing and the new paradigm for the jewellery manufacturer,'" *Prog. Addit. Manuf.*, no. 3, pp. 233-242, 2016.
- [19] S. Mellor, L. Hao, and D. Zhang, "Additive manufacturing: A framework for implementation," *Econ. Ind. Prod.*, vol. 149, pp. 194-201, 2014.
- [20] Stratasys, "Converting cad files to stl." [Online]. Available:

- https://www.google.pt/url?sa=t&rct=j&q=&esrc=s&source=web&cd=12&cad=rja&uact=8&ved=0ahUKEwjYzvGKpZnVAhUJXBQKHxKjDKMQFghbMAs&url=http%3A%2F%2Fglobal72.stratasys.com%2F-%2Fmedia%2FMain%2FFiles%2FBest-Practices_BP%2FBP_DU_CADtoSTL_EN_1115.ashx&usg=AFQjCNGfTGW4q35U__BAoYpvSw9Qk2CvQQ. [Accessed: 11-Nov-2016].
- [21] ISO/ASTM, "ISO/ASTM 52915:2016 - Specification for Additive Manufacturing File Format (AMF) Version 1.2," 2016.
- [22] J. Parthasarathy, "15 - Medical Applications of Additive Manufacturing," in *Additive Manufacturing: Innovations, Advances, and Applications*, T. S. S. T.S. Srivatsan, Ed. Boca Raton: Taylor & Francis Group, LCC, 2015, pp. 389-402.
- [23] C. Weller, R. Kleer, and F. T. Piller, "Economic implications of 3D printing: Market structure models in light of additive manufacturing revisited," *Int. J. Prod. Econ.*, vol. 164, pp. 43-56, 2015.
- [24] "Industry - Laser sintering applications for Additive Manufacturing - EOS." [Online]. Available: <https://www.eos.info/industry>. [Accessed: 11-Nov-2016].
- [25] E. O. Olakanmi, R. F. Cochrane, and K. W. Dalgarno, "A review on selective laser sintering/melting (SLS/SLM) of aluminium alloy powders: Processing, microstructure, and properties," *Prog. Mater. Sci.*, vol. 74, pp. 401-477, 2015.
- [26] "Wohlers Associates Publishes 20th Anniversary Edition of Its 3D Printing and Additive Manufacturing Industry Report | Wohlers Associates." [Online]. Available: <https://wohlersassociates.com/press71.html>. [Accessed: 15-Nov-2016].
- [27] S. L. N. Ford, "Additive Manufacturing Technology: Potential Implications for U . S . Manufacturing Competitiveness," *J. Int. Commer. Econ.*, vol. 6, no. September, pp. 1-35, 2014.
- [28] Wohlers Associates, "Wohlers Report 2016 - 3D Printing and Additive Manufacturing State of the Industry - Annual Worldwide Progress Report," Fort Collins, Colorado, 2016.
- [29] DG Research and Innovation - European Commission, "Additive Manufacturing in FP7 and Horizon 2020," no. June, p. 69, 2014.
- [30] G. Esteban Muñiz, "Additive Manufacturing and 3D-Printing Technologies in the EC," *CNRS Work. AM*, 2016.
- [31] "Additive manufacturing innovation: apply for funding." [Online]. Available: <https://www.gov.uk/government/news/additive-manufacturing-innovation-apply-for-funding>. [Accessed: 15-Nov-2016].
- [32] "\$8M Awarded From America Makes For 3D Printing Problem Solving." [Online]. Available: <http://www.forbes.com/sites/tjmccue/2015/08/25/8m-awarded-from-america-makes-for-3d-printing-problem-solving/#731181fa8fcb>. [Accessed: 15-Nov-2016].
- [33] "Metal Powders | MetalYSIS." [Online]. Available: <http://www.metalYSIS.com/metal-powders>. [Accessed: 31-Dec-2016].
- [34] J. Hammell, M. Langerman, J. Tomich, and B. Trotter, "Application of Radiometry in Laser Powder Deposition Additive Manufacturing," *Addit. Manuf.*, pp. 155-178, 2015.
- [35] D. D. Gu, W. Meiners, K. Wissenbach, and R. Poprawe, "Laser additive manufacturing of metallic components: materials, processes and mechanisms," *Int. Mater. Rev.*, vol. 57, no. 3, pp. 133-164, May 2012.
- [36] B. Baufeld, E. Brandl, and O. Van Der Biest, "Wire based additive layer manufacturing: Comparison of microstructure and mechanical properties of Ti-6Al-4V components fabricated

- by laser-beam deposition and shaped metal deposition,” *J. Mater. Process. Technol.*, vol. 211, no. 6, pp. 1146-1158, 2011.
- [37] S. H. Mok, G. Bi, J. Folkes, and I. Pashby, “Deposition of Ti-6Al-4V using a high power diode laser and wire, Part I: Investigation on the process characteristics,” *Surf. Coatings Technol.*, vol. 202, no. 16, pp. 3933-3939, 2008.
- [38] A. Gasser, G. Backes, I. Kelbassa, A. Weisheit, and K. Wissenbach, “Laser additive manufacturing: laser metal deposition (LMD) and selective laser melting (SLM) in turbo-engine applications,” *Laser Mater. Process.*, no. 2, pp. 58-63, 2010.
- [39] B. V. J.-P. K. Sasan Dadbakhsh and J. V. H. K. K. Jef Vleugels, “Additive Manufacturing of Metals via Selective Laser Melting: Process Aspects and Material Developments,” in *Additive Manufacturing*, CRC Press, 2015, pp. 69-99.
- [40] J. Kruth, G. Levy, F. Klocke, and T. H. C. Childs, “Consolidation phenomena in laser and powder-bed based layered manufacturing,” vol. 56, no. 1, pp. 730-759, 2007.
- [41] L. E. Murr *et al.*, “Metal Fabrication by Additive Manufacturing Using Laser and Electron Beam Melting Technologies,” *J. Mater. Sci. Technol.*, vol. 28, no. 1, pp. 1-14, 2012.
- [42] V. Bhavar, P. Kattire, V. Patil, S. Khot, K. Gujar, and R. Singh, “A Review on Powder Bed Fusion Technology of Metal Additive Manufacturing,” *Mater. Sci. Technol.* 2014, 2014.
- [43] “Laser Melting - Additively.” [Online]. Available: <https://www.additively.com/en/learn-about/laser-melting#read-advantages>. [Accessed: 30-Dec-2016].
- [44] X. Gong, T. Anderson, and K. Chou, “Review on powder - based electron beam additive manufacturing technology,” *Manuf. Rev.*, vol. 1, no. 2, 2014.
- [45] D. Cormier, O. Harrysson, and H. West, “Characterization of H13 steel produced via electron beam melting,” *Rapid Prototyp. J.*, vol. 10, no. 1, pp. 35-41, 2004.
- [46] S. Biamino *et al.*, “Electron beam melting of Ti-48Al-2Cr-2Nb alloy: Microstructure and mechanical properties investigation,” *Intermetallics*, vol. 19, no. 6, pp. 776-781, 2011.
- [47] “Metal powders - the raw materials.” [Online]. Available: <http://www.metal-am.com/introduction-to-metal-additive-manufacturing-and-3d-printing/metal-powders-the-raw-materials/>. [Accessed: 31-Dec-2016].
- [48] J. A. Slotwinski, E. J. Garboczi, P. E. Stutzman, C. F. Ferraris, S. S. Watson, and M. A. Peltz, “Characterization of Metal Powders Used for Additive Manufacturing,” vol. 119, pp. 460-493, 2014.
- [49] L. Grainger, “Blog post: How much can you recycle metal additive manufacturing powder?” [Online]. Available: <http://www.renishaw.com/en/blog-post-how-much-can-you-recycle-metal-additive-manufacturing-powder--38882>. [Accessed: 23-Jan-2017].
- [50] I. Wing, R. Groham, and B. Sniderman, “3D opportunity for quality assurance and parts qualification: Additive Manufacturing clears the bar,” *Deloitte Univ. Press*, 2015.
- [51] Y. Huang, M. C. Leu, J. Mazumder, and A. Donmez, “Additive Manufacturing: Current State, Future Potential, Gaps and Needs, and Recommendations,” *J. Manuf. Sci. Eng.*, vol. 137, no. 1, p. 14001, 2015.
- [52] Christian Lohmüller, “Quality Control in Additive Manufacturing,” *tctmagazine*. [Online]. Available: https://www.google.pt/url?sa=t&rct=j&q=&esrc=s&source=web&cd=1&cad=rja&uact=8&ved=0ahUKEwi_7GpZnVAhUF1hQKHZmZB4cQFggnMAA&url=https%3A%2F%2Fwww.volumegraphics.com%2F_Resources%2FPersistent%2F6b5a2181b9562ff76d13398cb699c7487cafec14%2FTCT2016_24-

- 5.pdf&usg=AFQjCNFEudM3HLYDFQXFH9M3tmsZ9DNzPQ. [Accessed: 15-Nov-2016].
- [53] ManSYS, "Quality assurance and Quality control in metal AM: Applications, regulations and requirements." [Online]. Available: http://www.mansys.info/publish/pages/8380/applications_v2.pdf. [Accessed: 20-Nov-2016].
- [54] B. M. Sharratt, "Non-Destructive Techniques and Technologies for Qualification of Additive Manufactured Parts and Processes: A Literature Review," no. March, 2015.
- [55] J. Coykendall, M. Cotteleer, L. Holdowsky, and M. Mahto, "3D opportunity in Aerospace and Defense," *Deloitte Univ. Press*, pp. 1-28, 2014.
- [56] D. Hu and R. Kovacevic, "Sensing, modeling and control for laser-based additive manufacturing," *Int. J. Mach. Tools Manuf.*, vol. 43, no. 1, pp. 51-60, 2003.
- [57] A. Simchi, "Direct laser sintering of metal powders: Mechanism, kinetics and microstructural features," *Mater. Sci. Eng. A*, vol. 428, no. 1-2, pp. 148-158, 2006.
- [58] S. Berumen, F. Bechmann, S. Lindner, J.-P. Kruth, and T. Craeghs, "Quality control of laser- and powder bed-based Additive Manufacturing (AM) technologies," *Phys. Procedia*, vol. 5, pp. 617-622, 2010.
- [59] R. Ponche, O. Kerbrat, P. Mognol, and J. Y. Hascoet, "A novel methodology of design for Additive Manufacturing applied to Additive Laser Manufacturing process," *Robot. Comput. Integr. Manuf.*, vol. 30, no. 4, pp. 389-398, 2014.
- [60] "The challenges of quality control in additive manufacturing - Innovation in Manufacturing." [Online]. Available: <https://innovation-in-manufacturing.deloitte.com/2016/06/13/the-challenges-of-quality-control-in-additive-manufacturing/>. [Accessed: 19-Jan-2017].
- [61] Z. Y. Chua, I. H. Ahn, and S. K. Moon, "Process monitoring and inspection systems in metal additive manufacturing: Status and applications," *Int. J. Precis. Eng. Manuf. - Green Technol.*, vol. 4, no. 2, pp. 235-245, 2017.
- [62] T. Srivatsan, K. Manigandan, and T. Sudarshan, "Additive Manufacturing of Materials: Viable Techniques, Metals, Advances, Advantages, and Applications," in *Additive Manufacturing*, CRC Press, 2015, pp. 1-48.
- [63] P. K. Rao, J. (Peter) Liu, D. Roberson, Z. (James) Kong, and C. Williams, "Online Real-Time Quality Monitoring in Additive Manufacturing Processes Using Heterogeneous Sensors," *J. Manuf. Sci. Eng.*, vol. 137, no. 6, p. 61007, 2015.
- [64] H. Rieder, A. Dillhöfer, M. Spies, J. Bamberg, and T. Hess, "Online Monitoring of Additive Manufacturing Processes Using Ultrasound 2. Additive Manufacturing and Quality Assurance Considerations 3. Ultrasonic Process Monitoring," *Proc. 11th Eur. Conf. Non-Destructive Test.*, vol. 1, no. Ecnndt, pp. 2194-2201, 2014.
- [65] S. Kleszczynski, J. Zur Jacobsmühlen, J. T. Sehr, and G. Witt, "Error detection in laser beam melting systems by high resolution imaging," *23rd Annu. Int. Solid Free. Fabr. Symp.*, pp. 975-987, 2012.
- [66] "Additive Manufacturing Technology Standards." [Online]. Available: <https://www.astm.org/Standards/additive-manufacturing-technology-standards.html>. [Accessed: 17-Jan-2017].
- [67] "ISO - ISO Standards - ISO/TC 261 - Additive manufacturing." [Online]. Available: http://www.iso.org/iso/iso_catalogue/catalogue_tc/catalogue_tc_browse.htm?commid=629086. [Accessed: 17-Jan-2017].
- [68] A. Thompson, I. Maskery, and R. K. Leach, "X-ray computed tomography for additive manufacturing: a review," *Meas. Sci. Technol.*, vol. 27, no. 7, p. 72001, 2016.

- [69] N. V. Y. Scarlett, P. Tyson, D. Fraser, S. Mayo, and A. Maksimenko, "Synchrotron X-ray CT characterization of titanium parts fabricated by additive manufacturing. Part I. Morphology," *J. Synchrotron Radiat.*, vol. 23, no. 4, pp. 1006-1014, 2016.
- [70] S. Van Bael, G. Kerckhofs, M. Moesen, G. Pyka, J. Schrooten, and J. P. Kruth, "Micro-CT-based improvement of geometrical and mechanical controllability of selective laser melted Ti6Al4V porous structures," *Mater. Sci. Eng. A*, vol. 528, no. 24, pp. 7423-7431, 2011.
- [71] J. A. Slotwinski, E. J. Garboczi, and K. M. Hebenstreit, "Porosity Measurements and Analysis for Metal Additive Manufacturing Process Control," *J. Res. Natl. Inst. Stand. Technol.*, vol. 119, p. 494, 2014.
- [72] N. V. Y. Scarlett, P. Tyson, D. Fraser, S. Mayo, and A. Maksimenko, "Synchrotron X-ray CT characterization of titanium parts fabricated by additive manufacturing. Part II. Defects," *J. Synchrotron Radiat.*, vol. 23, no. 4, pp. 1015-1023, 2016.
- [73] P. Shah, R. Racasan, and P. Bills, "Comparison of Different Additive Manufacturing Methods Using Optimized Computed Tomography," *6th Conf. Ind. Comput. Tomogr.*, vol. 1, pp. 1-10, 2016.
- [74] "ISO/ASTM NP 52905 - Additive manufacturing -- General principles -- Non-destructive testing of additive manufactured products." [Online]. Available: http://www.iso.org/iso/home/store/catalogue_tc/catalogue_detail.htm?csnumber=71988. [Accessed: 18-Jan-2017].
- [75] L. De Chiffre, S. Carmignato, J. P. Kruth, R. Schmitt, and A. Weckenmann, "Industrial applications of computed tomography," *CIRP Ann. - Manuf. Technol.*, vol. 63, no. 2, pp. 655-677, 2014.
- [76] S. R. Stock, *MicroComputed Tomography: Methodology and Applications*, 1st ed. Boca Raton: CRC Press, 2009.
- [77] B. Gapinski, M. Wieczorowski, L. Marciniak-Podsadna, B. Dybala, and G. Ziolkowski, "Comparison of different method of measurement geometry using CMM, optical scanner and computed tomography 3D," *Procedia Eng.*, vol. 69, pp. 255-262, 2014.
- [78] J. P. Kruth, M. Bartscher, S. Carmignato, R. Schmitt, L. De Chiffre, and A. Weckenmann, "Computed tomography for dimensional metrology," *CIRP Ann. - Manuf. Technol.*, vol. 60, no. 2, pp. 821-842, 2011.
- [79] International Organization for Standardization, *ISO 15708: Non-destructive testing – Radiation methods for computed tomography*. Geneva, Switzerland, 2017.
- [80] ASTM, *ASTM E1441-11: Standard Guide for Computed Tomography (CT) Imaging*. 2011.
- [81] A. Cantatore and P. Muller, *Introduction to Computed Tomography Technology*. DTU Mechanical Engineering, 2011.
- [82] ASTM, *ASTM E1672-12 Standard Guide for Computed Tomography (CT) System Selection*. 2011.
- [83] ASTM, *ASTM E1570-11 - Standard Practice for Computed Tomographic (CT) Examination*. 2011.
- [84] P. Klein, F. Herold, and Y. I. Gmbh, "Automatic Object Position Recognition : Increasing the Position-Accuracy in Robot CT," no. iCT, pp. 1-7, 2016.
- [85] J. Hiller and P. Hornberger, "Measurement accuracy in X-ray computed tomography metrology: Toward a systematic analysis of interference effects in tomographic imaging," *Precis. Eng.*, vol. 45, pp. 18-32, 2016.
- [86] Y. Tan *et al.*, "Simulation-aided investigation of beam hardening induced errors in CT dimensional metrology," *Meas. Sci. Technol.*, vol. 25, no. 6, p. 64014, 2014.

- [87] R. D. Lee, "Common Image Artifacts in Cone Beam CT," *AADMRT Newsl.*, pp. 1-7, 2008.
- [88] J. F. Barrett and N. Keat, "Artifacts in CT: recognition and avoidance," *Radiographics*, vol. 24, no. 6, pp. 1679-1691, 2004.
- [89] C. Xiaobo, X. Jun, J. Tao, and J. Ye, "Research and development of an accurate 3D shape measurement system based on fringe projection : Model analysis and performance evaluation," vol. 32, pp. 215-221, 2008.
- [90] G. J. Lora and J. Garcia-sucerquia, "Evaluation of Fringe Projection and Laser Scanning for 3D Reconstruction of Dental Pieces Evaluación De Proyección De Franjas Y Escaneo Láser Para La Reconstrucción 3D De Piezas Dentales," pp. 65-73, 2012.
- [91] S. Z. Ā, "Recent progresses on real-time 3D shape measurement using digital fringe projection techniques," *Opt. Lasers Eng.*, vol. 48, no. 2, pp. 149-158, 2010.
- [92] P. Kühmstedt, C. Munckelt, M. Heinze, and C. Bräuer-burchardt, "3D shape measurement with phase correlation based fringe projection," *Opt. Meas. Syst. Ind. Insp.*, vol. 6616, pp. 1-9, 2007.
- [93] A. Kumar, P. K. Jain, and P. M. Pathak, "Reverse Engineering in Product Manufacturing: An Overview," 2013, pp. 665-678.
- [94] V. Raja and K. J. Fernandes, *Reverse engineering- An Industrial Perspective*. London: Springer Verlag, 2008.
- [95] G. Sansoni, M. Trebeschi, and F. Docchio, "State-of-the-art and applications of 3D imaging sensors in industry, cultural heritage, medicine, and criminal investigation," *Sensors*, vol. 9, no. 1, pp. 568-601, 2009.
- [96] GOM Optical Measuring Techniques, "Atos Core Optical 3D Scanner For Small and Medium-size Components - Brochure," 2013.
- [97] "Structured Light 3D Scanning with Machine Vision Cameras - YouTube." [Online]. Available: <https://www.youtube.com/watch?v=U0Q9QnYRsoU>. [Accessed: 25-Jun-2017].
- [98] "Everything about markers and how they help 3D scanning," *Thor3D*, 2016.
- [99] ATOS CORE, "Dynamic Referencing & Self Monitoring." [Online]. Available: <http://www.atos-core.com/pt/features.php>. [Accessed: 26-Jun-2017].
- [100] S. Moylan, J. Slotwinski, A. Cooke, K. Jurrens, M. A. Donmez, and A. Donmez, "Proposal for a Standardized Test Artifact for Additive Manufacturing Machines and Processes," *Solid Free. Fabr. Symp. Proc.*, pp. 902-920, 2012.
- [101] M. Fahad and N. Hopkinson, "A new benchmarking part for evaluating the accuracy and repeatability of Additive Manufacturing (AM) processes," *2nd Int. Conf. Mech. Prod. Automob. Eng.*, pp. 234-238, 2012.
- [102] M. Mahesh, Y. S. Wong, J. Y. H. Fuh, and H. T. Loh, "Benchmarking for comparative evaluation of RP systems and processes," *Rapid Prototyp. J.*, vol. 10, no. 2, pp. 123-135, 2004.
- [103] J. Kruth, B. Vandenbroucke, J. Vaerenbergh, and P. Mercelis, "Benchmarking of different SLS/SLM processes as rapid manufacturing techniques," *Int. Conf. Polym. Mould. Innov. (PMI), Gent, Belgium, April 20-23, 2005*, pp. 1-7, 2005.
- [104] W. M. Johnson, M. Rowell, B. Deason, and M. Eubanks, "Benchmarking evaluation of an Open Source Fused Deposition Modeling Additive Manufacturing System," *Proc 22nd Annu. Int. Solid Free. Fabr. Symp.*, pp. 197-211, 2011.
- [105] S. Moylan, J. Slotwinski, A. Cooke, K. Jurrens, and M. A. Donmez, "An Additive Manufacturing

- Test Artifact,” vol. 119, pp. 429-459, 2014.
- [106] YXLON International, “YXLON FF35 CT.” [Online]. Available: <http://www.yxlon.com/products/x-ray-and-ct-inspection-systems/yxlon-ff35-ct>. [Accessed: 25-May-2017].
- [107] Volume Graphics, *VGStudio MAX 3.0 - Reference Manual*. Heidelberg, Germany, 2016.
- [108] Volume Graphics GmbH, *Basic Training VGStudio MAX 3.0 - Geometry*. Heidelberg, Germany: VG Academy, 2016.
- [109] Volume Graphics GmbH, *Basic Training VGStudio MAX 3.0 - Material*. Heidelberg, Germany: VG Academy, 2017.
- [110] “ATOS Professional,” 2017. [Online]. Available: <http://www.gom.com/3d-software/gom-system-software/atos-professional.html>. [Accessed: 25-May-2017].
- [111] “Inconel 718 density.” [Online]. Available: <http://www.matweb.com/search/datasheet.aspx?matguid=94950a2d209040a09b89952d45086134&ckck=1>. [Accessed: 19-Jul-2017].
- [112] B. Song *et al.*, “Differences in microstructure and properties between selective laser melting and traditional manufacturing for fabrication of metal parts: A review,” *Front. Mech. Eng.*, vol. 10, no. 2, pp. 111-125, 2015.
- [113] R. Ammer, U. Rude, M. Markl, V. Juchter, and C. Körner, “Validation experiments for LBM simulations of electron beam melting,” *Int. J. Mod. Phys. C*, vol. 25, no. 12, p. 1441009, Dec. 2014.
- [114] X. Tan, Y. Kok, S. B. Tor, and C. K. Chua, “Application of Electron Beam Melting (EBM) in Additive Manufacturing of an Impeller,” in *Proceedings of the 1st International Conference on Progress in Additive Manufacturing*, 2014, pp. 327-332.
- [115] D. Cornu, A. Lenain, and R. Salapete, “Direct Manufacturing Processes for Structural Parts and Engines Design in Aeronautics,” in *Proceedings of the 13th World Conference on Titanium*, Hoboken, NJ, USA: John Wiley & Sons, Inc., 2016, pp. 1527-1535.
- [116] W. J. Sames, F. Medina, W. H. Peter, S. S. Babu, and R. R. Dehoff, “Effect of Process Control and Powder Quality on Inconel 718 Produced Using Electron Beam Melting,” in *8th International Symposium on Superalloy 718 and Derivatives*, Hoboken, NJ, USA: John Wiley & Sons, Inc., 2014, pp. 409-423.
- [117] A. Kirchner, B. Kloden, J. Luft, T. Weisgarber, and B. Kieback, “Process Window for Electron Beam Melting of Ti-6Al-4V,” *Euro PM2014 - AMTechnologies*, pp. 6-11, 2014.
- [118] P. Hermanek and S. Carmignato, “Reference object for evaluating the accuracy of porosity measurements by X-ray computed tomography,” *Case Stud. Nondestruct. Test. Eval.*, vol. 6, pp. 122-127, 2016.
- [119] International Organization for Standardization, *ISO 15708-2: Non-destructive testing – Radiation methods for computed tomography – Part 2: Principles, equipment and samples*, vol. 2017. Geneva, Switzerland, 2017.

Annexes

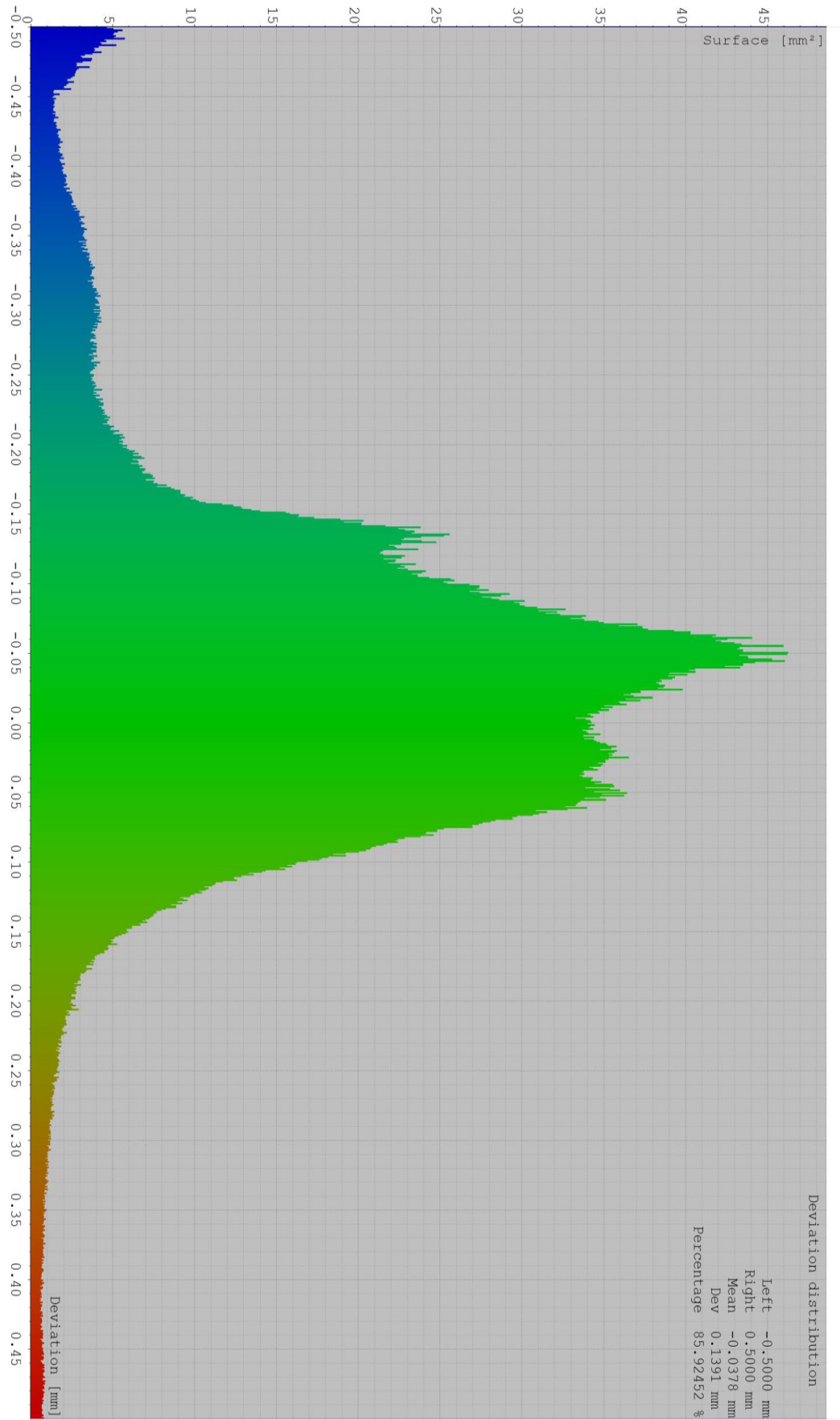
Annex A - 10% transmission thicknesses for various materials and energies [119]

Materials	10 % transmission thicknesses mm				
	Accelerating voltage				
	90 kV	160 kV	225 kV	300 kV	450 kV
	Scintillation screen				
100 µm CsI	150 µm CsI	200 µm CsI	300 µm Gadolinium Oxysulphide	500 µm Gadolinium Oxysulphide	
Filtration					
0,25 mm Cu	0,5 mm Cu	2 mm Cu	1 mm Pb	3 mm Pb	
Al	25	35	50	60	80
Fe	2	4	9	16	26
Ti	5	10	20	30	50
Pb	0,3	0,5	0,7	2	5
W	0,2	0,3	0,4	1,3	3,5
Ni	1,4	3	7	13	20
Zirconia	1,1	2,4	6	15	30
PMMA	95	105	120	140	170
Water	100	115	130	150	200

Annex B - Parameters for the YXLON CERA ReconsPOOLer [93] adapted.

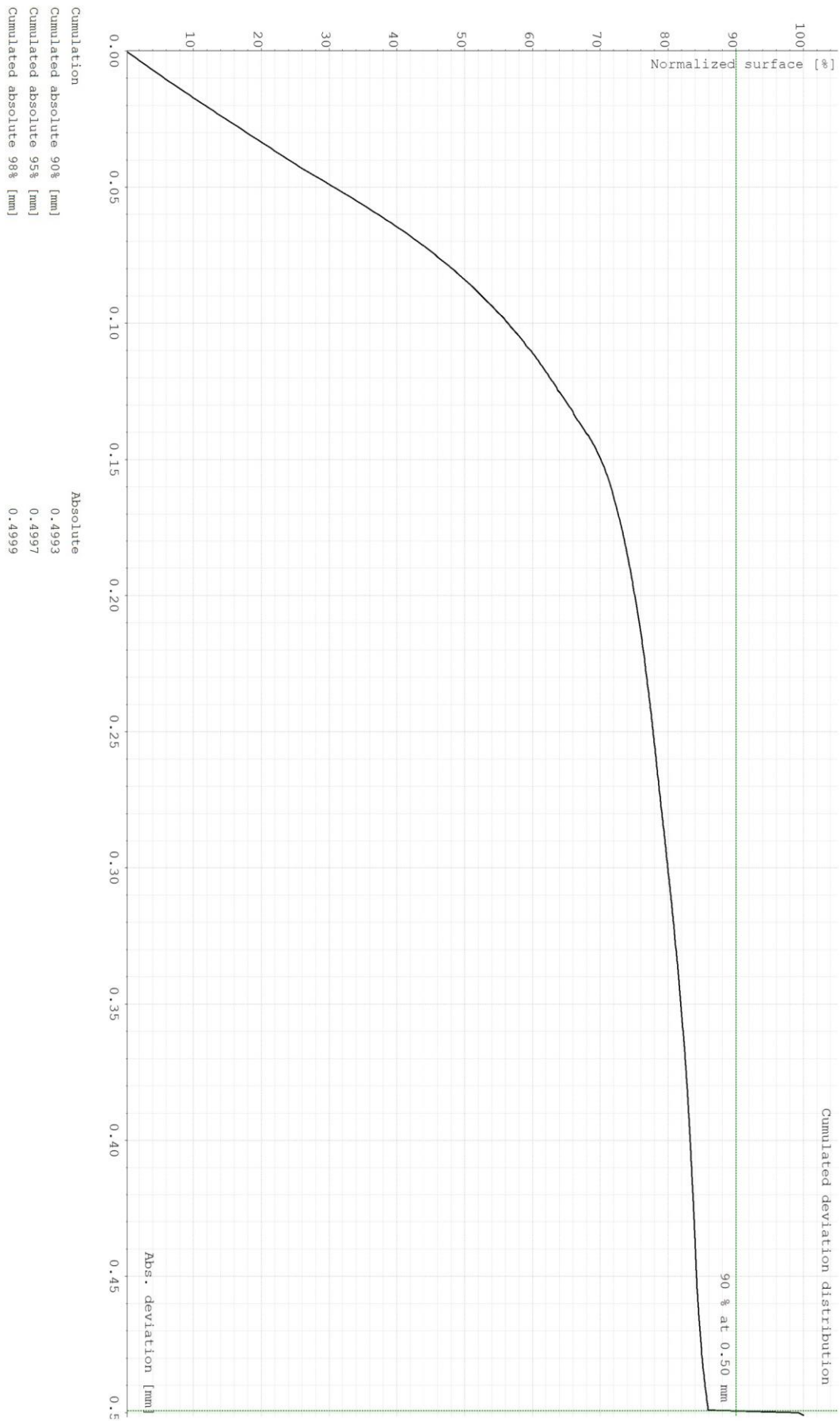
Parameter	Description
Iso Voxel	The “reconstruction volume size” parameter is automatically set to the horizontal pixel count according to the current detector settings.
Reconstruction Volume Size	Size of the reconstruction volume. Depending on the set size, there is a shorter runtime for a lower level of detail or a longer runtime for a higher level of detail. The resulting voxel size is displayed under the slide control. It results from the geometric enlargement, the detector size and the set volume size.
Beam Hardening Correction	Reducing beam hardening artefacts. After this function has been activated, a filter - as well as an object material - can be selected. In addition, the thickness of the filter material can be set.
32 Bit float Volume	The reconstructed volume is represented by 32-bit floating-point values. When the option is active, the reconstructed volume requires twice as much memory. The option should be used when there are bright objects in the reconstructed volume.
Truncation Correction	With the option enabled, an attempt is made to reduce barreling effects by extrapolation. The option should be enabled when the inspection object partially moves out of the image during rotation or, due to sub-optimum illumination, barreling effects can be seen in the reconstructed volume.
Noise Reduction (Projection Space)	Enable noise reduction on the projections. Noise reduction can be adjusted with the following two parameters, Range Sigma and Spatial Sigma.
Range Sigma	Strength of the edges that should be retained despite smoothing. Higher values produce a stronger smoothing effect.
Spatial Sigma	Strength of the edge retaining smoothing effect.
Noise Reduction (Volume Space)	Enable noise reduction on the reconstructed volume. Noise reduction can be adjusted with the following three parameters, Iteration, P1 and P2.
Iterations	Number of filtering iterations. Higher values produce a stronger smoothing effect.
P1	Width at half the maximum of the influence curve used for edge retaining. Higher values produce a stronger smoothing effect.
P2	Offset of the influence curve used for edge retaining. Higher values produce a stronger smoothing effect.
Ring Artifact Reduction	Enable “retrospective” ring object correction. In contrast to the option in the scans, this correction does not change the projections permanently. As a result, an initial “strong” correction can be reversed even with repeated reconstruction. The stronger the objects expected, the higher the parameter must be set. A higher value, however, is at the cost of resolution in the reconstructed volume.

	<p>For the ring object correction values between 0 and 3 can be set:</p> <ul style="list-style-type: none"> - 0: Correction switched off. - 1: Rings with a width up to 2 pixels can be reduced. - 2: Rings with a width up to 4 pixels can be reduced. - 3: Rings with a width up to 8 pixels can be reduced. <p>Large values can cause even non-annular structures to be smeared.</p>
Bad Pixel Reduction	Enable correction of individual defective pixels in the projections. The correction can be adjusted with the following four parameters, Filter size, Global Threshold, Low Domain Deviation and High Domain Deviation.
Filter Size	Edge length in pixels of the region used for bad pixel reduction.
Global Threshold	Grey value for the division in the “lower domain” (dark areas) and the “upper domain” (bright areas).
Low Domain Deviation	If a pixel of the lower domain deviates by this percentage from the mean value of the region defined in the “Filter size” parameter, its value is replaced by the median of the neighboring pixels.
High Domain Deviation	If a pixel of the upper domain deviates by the set percentage from the mean value of the region defined in the “Filter size” parameter, its value is replaced by the median of the neighboring pixels.
Median Filter	Size of the median filter mask in pixels. Larger values provide a stronger filter effect.

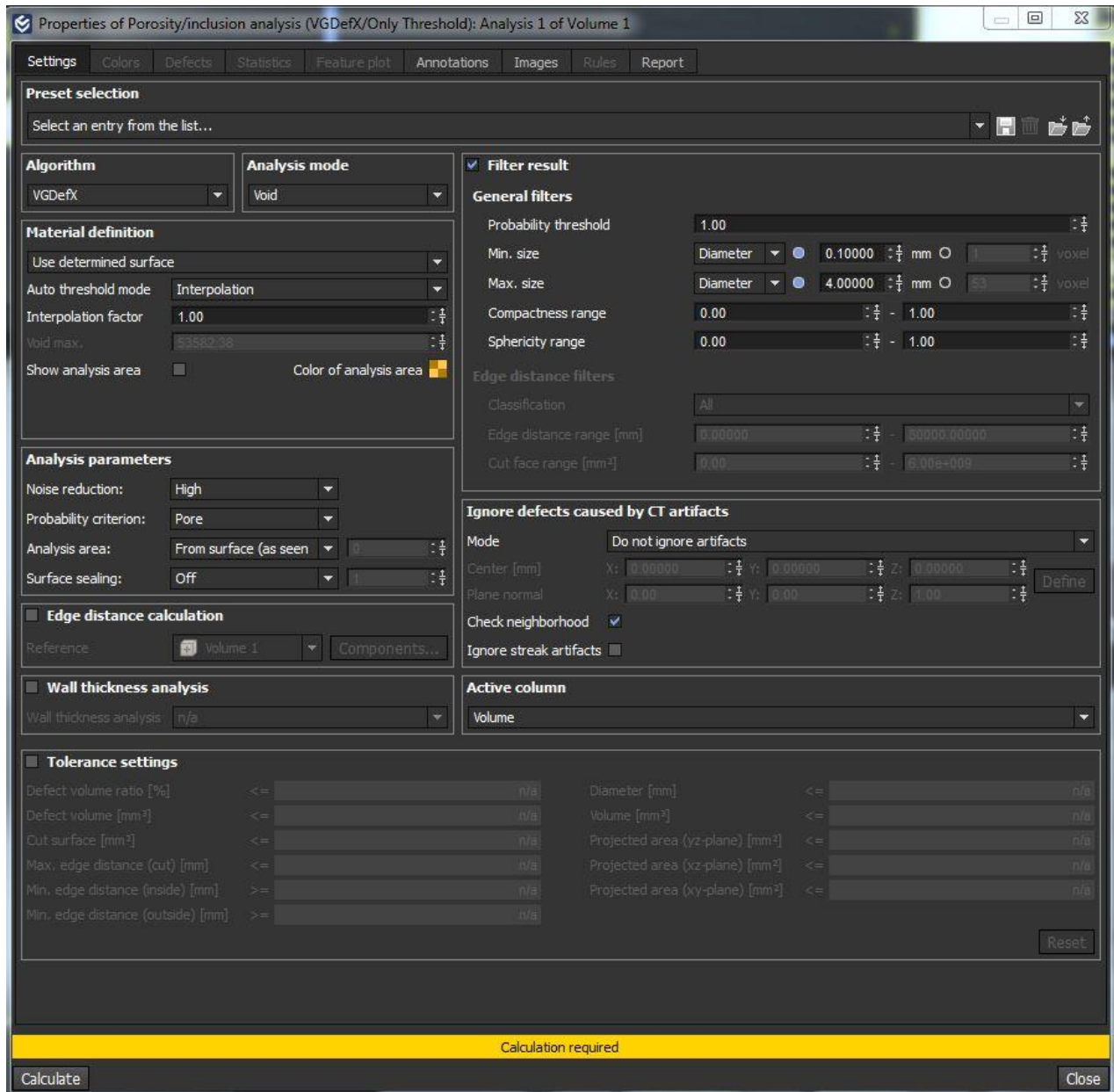


Annex C - Deviation histogram of the LPBF Ti6Al4V at 0.5 mm max. deviation

Annex D - Cumulative histogram of the LPBF Ti6Al4V at 0.5 mm max. deviation.



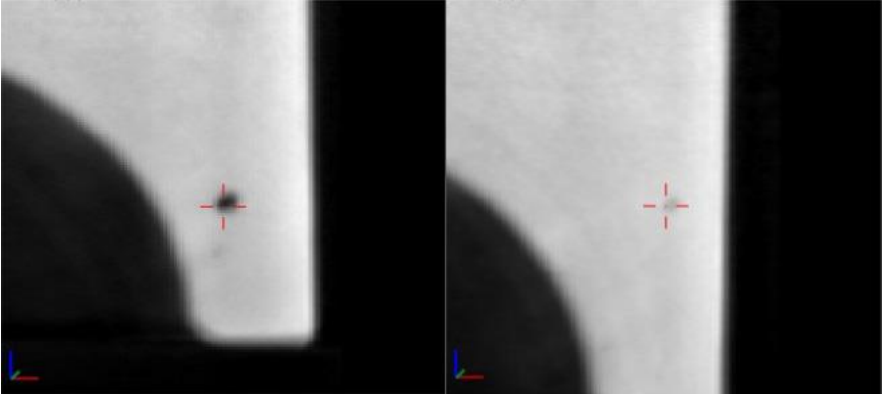
Annex E - VGDefX Porosity/ Inclusion analysis menu.

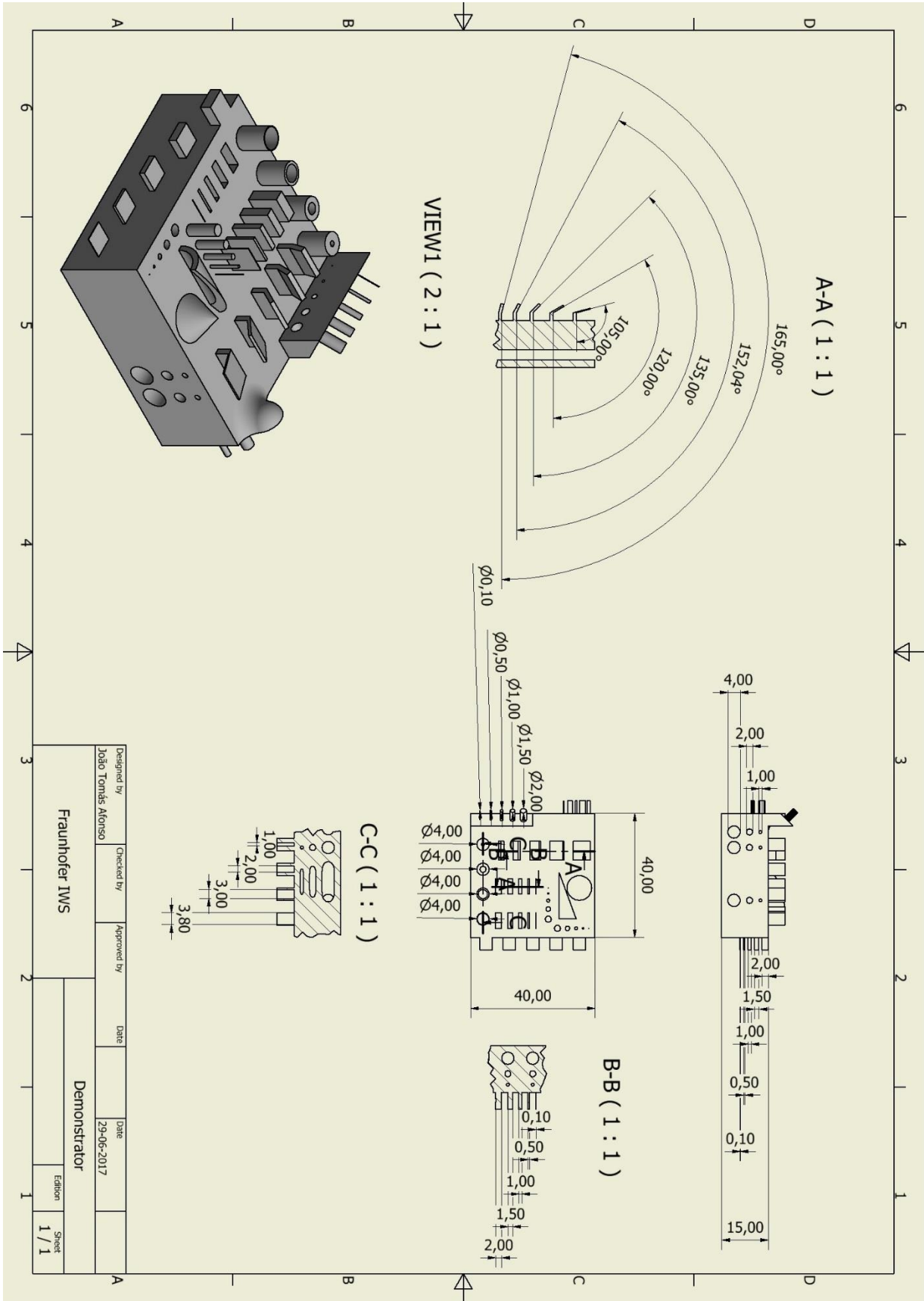


Annex F - Controls in the Analysis parameters section for the VGDefX algorithm. Adapted from [107].

Control	Description
Noise reduction	Specifies a noise reduction mode to filter the data when looking for seed points. Several (adaptive) Gauss filters (Low, Low adaptive, Medium, Medium adaptive, High, High adaptive). The raw data is not modified.
Probability criterion	Specifies the criterion according to which the defects will be grown and their probability calculated, being size, pore or contrast.
Analysis area	<p>Specifies the area of the selected volume/ROI on which the VGDefX algorithm will be performed. The analysis area is based on the surface determination of the volume. This option does not change the actual surface determination. This is an internal representation used for defect analysis only.</p> <ul style="list-style-type: none"> • From surface (as seen): uses the area within the original surface determination. • Internal cleaning, small: also includes small defects that are separated by the determined surface from the material. • Internal cleaning, all: also includes larger defects that are separated by the determined surface from the material. This will use the outermost parts of the determined surface only for defect analysis. • Overall closing: also includes defects that are separated by the determined surface from the material. This is achieved by performing a closing with the specified number of voxels.
Surface sealing	<p>Off: restrains the defect growing according to the Material definition parameters and Probability criterion.</p> <ul style="list-style-type: none"> • On: restrains the defect growing to the analysis area. To avoid detecting 'false' defects along the surface, due to the partial volume effect, you can reduce the area by the selected number of voxels.

Annex G - Controls in the general filters section. Adapted [107].

Control	Description
<p>Probability threshold</p>	<p>All potential defect areas passing the size check will be further processed by several analysis stages. These stages try to differentiate between real defects and artifacts by utilizing sophisticated image processing algorithms. Each detected defect is tagged with a value indicating the probability that it is a real defect. Specify the Probability threshold in a way that only defects with a probability above the threshold will be included in the list. Start with a Probability threshold of zero if you run the defect detection on a new data set for the first time to make sure you do not filter real defects from the list. There is no absolute value for the threshold applicable to all data sets.</p> <p>The following figure shows two defects with different probabilities, where the defect on the left-hand side has a ten times higher probability than the defect on the right-hand side:</p> 
<p>Min. size</p>	<p>Specifies the minimum defect size. Depending on the selection in the drop-down field, this parameter refers to the volume, radius, or diameter of a defect.</p>
<p>Max. size</p>	<p>Specifies the maximum defect size. Depending on the selection in the drop-down field, this parameter refers to the volume, radius, or diameter of a defect. When specifying the Max. size of the defect, consider that longish cracks have a rather large volume and that an accumulation of nearby very small defects might be interpreted as one large defect. Specify the Max. size rather generously.</p>
<p>Compactness range</p>	<p>Specifies the range for the compactness of the defect, i.e., the ratio between the volume of the defect and the volume of the circumscribed sphere.</p> $Compactness = \frac{V_{defect}}{V_{sphere}}$
<p>Sphericity range</p>	<p>Specifies the range for the sphericity of the defect, i.e., the ratio between the surface of a sphere with the same volume as the defect and the surface of the defect.</p> $Sphericity = \frac{A_{sphere}}{A_{defect}}$



Annex H - Technical drawing of the Fraunhofer IWS demonstrator.

Annex I - Scanning parameters used for the analyzed samples.

Sample	Part position	Tube				Detector	Manipulator					Circular Scan					
		Voltage (kV)	Amperage (µA)	Filter material	Thickness (mm)		Frame rate (Hz)	X	Y	FOD	FDD	Velocity factor	Rotation	Number of projections	Frames per projection	Skip Frames	Ring Artifact Reduction
Demonstrators	EBM 1	Horizontal	185	275	Copper	2.5	1	0	107.039	200.73	700	0.5	360	360	5	2	Active
	EBM 2	Horizontal	185	275	Copper	2.5	1	0	107.039	200.73	700	0.5	360	360	5	2	Active
	EBM 3	Horizontal	185	275	Copper	2.5	1	0	107.039	200.73	700	0.5	360	360	5	2	Active
	EBM 4	Horizontal	185	275	Copper	2.5	1	0	107.039	200.73	700	0.5	360	360	5	2	Active
	Titanium aluminate	Paralel	200	330	Copper	2	2	-0.283	81.967	157.773	700	0.5	360	720	7	3	Active
	Inconel 718	Paralel	225	360	Lead	1	0.9	-0.352	92.981	166.73	607.822	0.5	360	720	11	3	Active
	Aluminum	Paralel	185	200	Lead	0.5	1.2	-0.352	93	166.73	650	0.5	360	720	11	3	Active
	Nozzle	Vertical	200	115	Copper	2	1.5	0	105.259	149.259	611.589	0.5	360	360	5	1	Active
	Cubes	Paralel	220	310	Copper	2.5	1.5	0	-50	60	647	0.5	360	360	11	5	Active

Legend

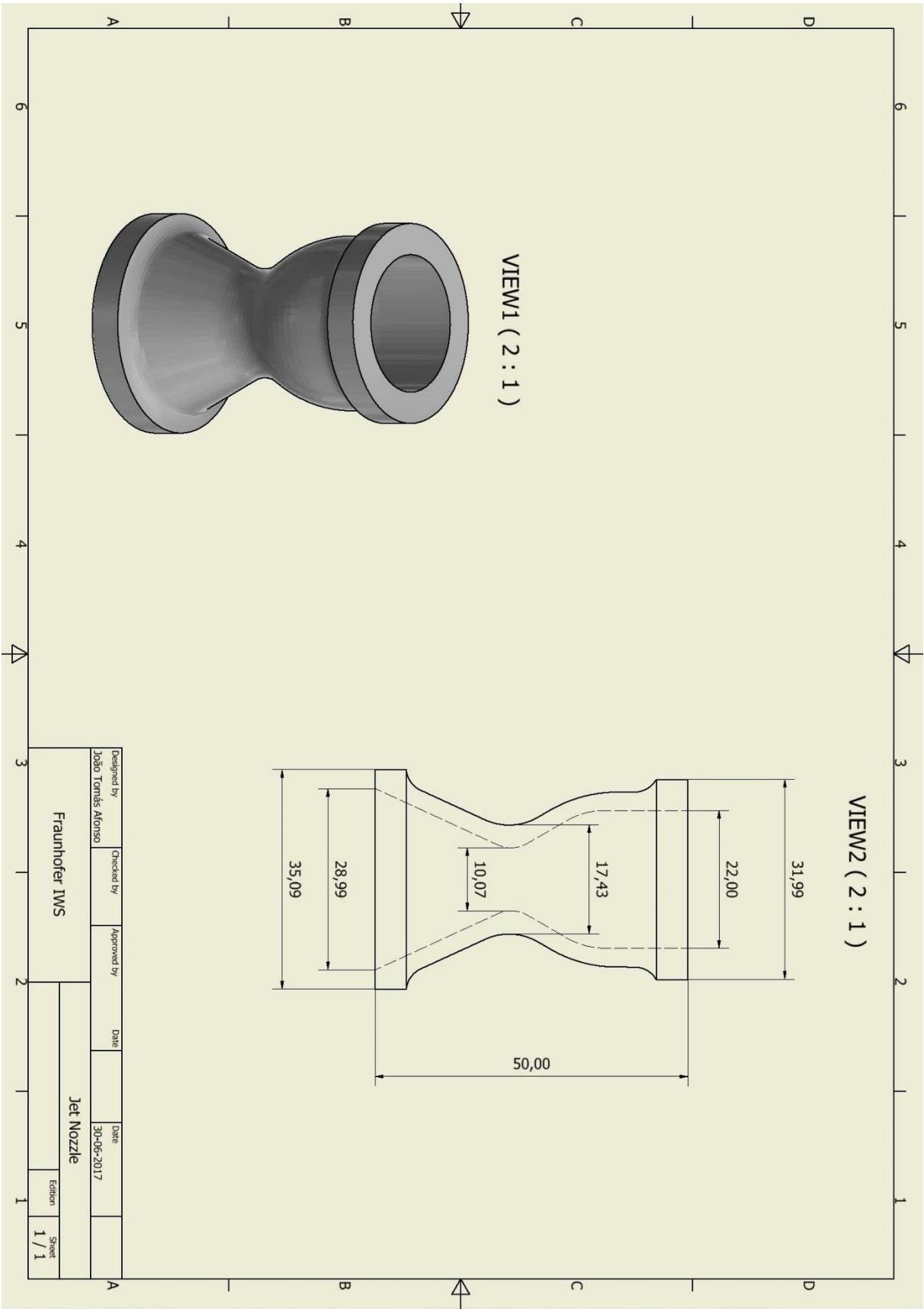
- X and Y - Movement in X and Y.
- FOD - Focus-Object-Distance: Distance between X-ray tube and inspection object.
- FDD - Focus-Detector-Distance: Distance between X-ray tube and detector.

Annex J - Reconstruction parameters on ReconsPOOLer for the different samples.

Sample	Reconstruction volume size (hps)	Voxel size (mm)	Integration time (µs)	Beam hardening		32 Bit Volume	Noise reduction (projection)		Noise reduction (Volume space)			Ring artifact reduction	Bad pixel reduction			Median filter	
				Filter	Material analysed		Range sigma	Spatial sigma	Iterations	P1	P2		Filter size	Global threshold	Low domain deviation		High domain deviation
Demonstrators																	
EBM 1	768	0.092	10000000	2.5 mm Cooper	Titanium	Deactivate	1.5	3	4	0.7	0.3	3	3	32768	100	100	3
EBM 2	768	0.092	10000000	2.5 mm Cooper	Titanium	Deactivate	1.5	3	4	0.7	0.3	3	3	32768	100	100	3
EBM 3	768	0.092	10000000	2.5 mm Cooper	Titanium	Deactivate	1.5	3	4	0.7	0.3	3	3	32768	100	100	3
EBM 4	768	0.092	10000000	2.5 mm Cooper	Titanium	Deactivate	1.5	3	4	0.7	0.3	3	3	32768	100	100	3
Titanium aluminate	2166	0.088	500000	2.5 mm Cooper	Titanium	Deactivate	1.5	3	4	0.7	0.3	3	3	32768	100	100	3
Inconel 718	1024	0.081	11111111	1 mm Lead	Nickel	Deactivate	1.5	3	4	0.7	0.3	3	3	32768	100	100	3
Aluminium	1024	0.075	8333333	0.5 mm Lead	Aluminium	Deactivate	1.5	3	4	0.7	0.3	3	3	32768	100	100	3
Nozzle	1280	0.056	1000000	2 Copper	Titanium	Deactivate	1.5	3	4	0.7	0.3	3	3	32768	100	100	3
Cubes	512	0.055	666667	2.5 Cooper	Nickel	Deactivate	1.5	3	4	0.7	0.3	3	3	32768	100	100	3

Annex K - Surface determination parameters for the analyzed samples.

Sample		Material definition	Advanced mode		
			Starting contour	Starting contour healing	Search distance (mm)
Demonstrators	EBM 1	Automatic	As defined in histogram	Remove particles and all voids	0.43935
	EBM 2	Automatic	As defined in histogram	Remove particles and all voids	0.43935
	EBM 3	Automatic	As defined in histogram	Remove particles and all voids	0.43935
	EBM 4	Automatic	As defined in histogram	Remove particles and all voids	0.43935
	Titanium aluminide	Automatic	As defined in histogram	Remove particles and all voids	0.35334
	Inconel 718	Automatic	CAD	Remove particles and all voids	0.5
	Aluminum	Automatic	As defined in histogram	Remove particles and all voids	0.30167
Nozzle		Automatic	As defined in histogram	Remove particles and all voids	0.22401
Cubes		Automatic	As defined in histogram	Remove particles and all voids	0.21813



Annex L - Technical drawing of the jet nozzle.

Annex M - Porosity analysis parameters of the Inconel 718 cubes.

Cube	Algorithm	Analysis mode	Material definition		Analysis parameters					Filter result			
			Use determined surface Auto threshold mode	Interpolation factor	Noise reduction	Probability criterion	Analysis area	Surface sealing	Probability threshold	Min. Size		Compactness range	Sphericity range
										Diameter (mm)	Diameter (mm)		
Cube 1	VGDefX	Void	Interpolation	1.4	High	Pore	From suraface (as seen)	Off	0.3	0	20	0 to 1	0 to 1
Cube 2	VGDefX	Void	Interpolation	1	High	Pore	From suraface (as seen)	Off	1	0	20	0 to 1	0 to 1
Cube 3	VGDefX	Void	Interpolation	1.2	High	Pore	From suraface (as seen)	Off	1	0	20	0 to 1	0 to 1
Cube 4	VGDefX	Void	Interpolation	1	High	Pore	From suraface (as seen)	Off	1	0	20	0 to 1	0 to 1
Cube 5	VGDefX	Void	Interpolation	1	High	Pore	From suraface (as seen)	Off	1	0	20	0 to 1	0 to 1
Cube 6	VGDefX	Void	Interpolation	1	High	Pore	From suraface (as seen)	Off	1	0	20	0 to 1	0 to 1
Cube 7	VGDefX	Void	Interpolation	1	High	Pore	From suraface (as seen)	Off	1	0	20	0 to 1	0 to 1
Cube 8	VGDefX	Void	Interpolation	1	High	Pore	From suraface (as seen)	Off	1	0	20	0 to 1	0 to 1
Cube 9	VGDefX	Void	Interpolation	1	High	Pore	From suraface (as seen)	Off	1	0	20	0 to 1	0 to 1
Cube 10	VGDefX	Void	Interpolation	1.3	High	Pore	From suraface (as seen)	Off	0.3	0	20	0 to 1	0 to 1
Cube 11	VGDefX	Void	Interpolation	1.4	High	Pore	From suraface (as seen)	Off	0.3	0	20	0 to 1	0 to 1
Cube 12	VGDefX	Void	Interpolation	1.05	High	Pore	From suraface (as seen)	Off	1	0	20	0 to 1	0 to 1
Cube 13	VGDefX	Void	Interpolation	1.05	High	Pore	From suraface (as seen)	Off	1	0	20	0 to 1	0 to 1
Cube 14	VGDefX	Void	Interpolation	1.4	High	Pore	From suraface (as seen)	Off	0.3	0	20	0 to 1	0 to 1
Cube 15	VGDefX	Void	Interpolation	1	High	Pore	From suraface (as seen)	Off	1	0	20	0 to 1	0 to 1
Cube 16	VGDefX	Void	Interpolation	1.4	High	Pore	From suraface (as seen)	Off	1	0	20	0 to 1	0 to 1
Cube 17	VGDefX	Void	Interpolation	1	High	Pore	From suraface (as seen)	Off	1	0	20	0 to 1	0 to 1
Cubes	VGDefX	Void	Interpolation	1.4	High	Pore	From suraface (as seen)	Off	0.3	0	20	0 to 1	0 to 1
Cubes	VGDefX	Void	Interpolation	1	High	Pore	From suraface (as seen)	Off	1	0	20	0 to 1	0 to 1

Annex N - Build parameters of the Inconel 718 cubes. Parameters generated by the statistical experimental planning software Visual-Xsel.

Cube n°	Laser Power (W)	Laser velocity (mm/s)	Powder mass flow (rpm)
1	800	850	3.75
2	1250	725	2.75
3	1250	725	2.75
4	1250	725	2.75
5	1250	918.3375	2.75
6	1700	850	1.75
7	800	600	1.75
8	1250	725	1.2033
9	1700	600	3.75
10	553.985	725	2.75
11	1946.015	725	2.75
12	1700	850	3.75
13	1250	725	4.2967
14	800	600	3.75
15	1250	531.6625	2.75
16	1700	600	1.75
17	800	850	1.75

Annex O - Dimension of the DED cubes made of Inconel 718.

Cube nº	Height (mm)	Width (mm)	Length (mm)
1	9.3	15	15
2	8.5	15	15
3	8.5	15	15
4	9	15	15
5	9.7	15	15
6	8.1	15	15
7	9.9	15	15
8	9.9	15	15
9	10.1	15	15
10	9.2	15	15
11	6.5	15	15
12	9.7	15	15
13	12.6	15	15
14	9.2	15	15
15	10	15	15
16	9.1	15	15
17	16	15	15

Annex P - Parameters changed during the reconstruction assessment. Active parameters are on default values.

Parameter changed	Reconstruction volume size	Beam hardening		32 Bit Volume	Noise reduction (projection)		Noise reduction (Volume space)			Ring artifact reduction			Bad pixel reduction			Median filter
		Filter	Material analysed		Range sigma	Spatial sigma	Iterations	P1	P2	Ring artifact reduction	Filter size	Global threshold	Low domain deviation	High domain deviation		
Default	512	2,5mm Copper	Nickel	Active	1.5	3	4	0.7	0.3	3	3	32768	100	100	3	
Reconstruction volume size	ISO voxel	2,5mm Copper	Nickel	Active	1.5	3	4	0.7	0.3	3	3	32768	100	100	3	
32 Bit Volume	512	2,5mm Copper	Nickel	Inactive	1.5	3	4	0.7	0.3	3	3	32768	100	100	3	
Noise reduction (projection space)	512	2,5mm Copper	Nickel	Active	Inactive	Inactive	4	0.7	0.3	3	3	32768	100	100	3	
Noise reduction (Volume space)	512	2,5mm Copper	Nickel	Active	1.5	3	Inactive	In.	In.	3	3	32768	100	100	3	
Ring artifact reduction	512	2,5mm Copper	Nickel	Active	1.5	3	4	0.7	0.3	Inactive	3	32768	100	100	3	
Bad pixel reduction	512	2,5mm Copper	Nickel	Active	1.5	3	4	0.7	0.3	3	In.	Inactive	Inactive	Inactive	3	
Median filter	512	2,5mm Copper	Nickel	Active	1.5	3	4	0.7	0.3	3	3	32768	100	100	Inactive	
All inactive	512	2,5mm Copper	Nickel	Inactive	Inactive	Inactive	Inactive	In.	In.	Inactive	In.	Inactive	Inactive	Inactive	Inactive	

Annex Q - Porosity analysis parameters of cube n°3 with different reconstruction settings.

Cube	Algorithm	Analysis mode	Material definition		Analysis parameters					Filter result				
			Use determined surface	Auto threshold mode	Noise reduction	Probability criterion	Analysis area	Surface sealing	Probability threshold	Min. Size Diameter (mm)	Max. Size Diameter (mm)	Compactness range	Sphericity range	
3	VGDefX	Void	Interpolation	Interpolation factor	1	High	Pore	From surface (as seen)	Off	1	0	20	0 to 1	0 to 1

Annex R - Process window for EBM of Ti-6Al-4V. Blue circles mark samples with more than 1% porosity, while red circles mark pronounced swelling of the top surface [117].

